Aerosol Assisted Chemical Vapour Deposition of Titanium Dioxide and Tungsten Oxide Thin Films

A thesis presentation to the University College London in partial fulfilment of the requirements for the degree of Doctor in Philosophy

Cynthia Edusi

Supervised by Professor Ivan P. Parkin

and Professor Gopinathan Sankar

University College London

2014

Declaration

I, Cynthia Edusi hereby declare that all the work presented in this thesis is my own work, with exceptions acknowledged from other sources.

Abstract

This thesis focuses on the Aerosol Assisted Chemical Vapour deposition (AACVD) of titanium dioxide (TiO_2) thin films using titanum (IV) isopropoxide (TTIP) and also reports the deposition of tungsten oxide via AACVD using tungsten hexacarbonyl [$W(CO)_6$] in different solvents including methanol and ethanol.

Chapter 1 of this thesis gives an overview of TiO_2, including its properties and functions and the motivation for this project. In chapter 2 brief descriptions are provided of the main characterisation techniques used throughout this thesis.

The substrate and solvent effect on the phase of TiO_2 obtained by AACVD is outlined in chapter 3 and 4. TiO_2 was deposited via the AACVD of TTIP in different solvents including methanol, ethanol and other solvents. The films deposited showed some substrate dependent morphology and properties. In particular at 550°C the films on steel show needle and rod like particles. XRD and Raman spectra of the TiO_2 films showed that on steel or titanium substrates only the rutile form could be obtained, whereas on glass either anatase, anatase-rutile mixtures or rutile could be obtained depending on substrate temperature. Using methanol as the carrier solvent produced exclusively the rutile films on steel and predominantly rutile on glass substrates while the use of the other solvents produced exclusively the anatase phase on the steel under the same conditions. TiO_2 was also deposited by AACVD from a mixture of ethanol and methanol solvents. As little as 15% of methanol in ethanol produces rutile as the predominant phase. The photocatalytic properties and the hydrophilicity of the films deposited are also reported.

X-ray absorption spectroscopy (XAS) was used to map across the surface of the TiO_2 films deposited as described in chapter 5. The X-ray absorption near edge structure (XANES) was used to determine the phase of TiO_2 present at each point on the substrate.

The AACVD deposition tungsten oxide using tungsten hexacarbonyl ($W(CO)_6$) in methanol and ethanol is reported in chapter 6. Preferred orientation was observed when using either ethanol or methanol as the carrier solvent.

In chapter 7 *insitu* work was attempted to investigate the mechanism of the deposited titania and tungsten oxide films. A new reactor vessel was designed, constructed and tested to allow synchrotron radiation in and out using a kapton window. The XANES pattern recorded during *in-situ* deposition were not of high enough to resolve the mechanism. The *in-situ* work carried out has great potential in the growth study of thin film deposition and can in the future help control the phase and composition of deposited films to produce more desirable properties.

Table of contents

List of figures

List of tables

List of equations

List of schemes

List of abbreviations

AACVD - Aerosol assisted chemical vapour deposition

APCVD - Atmospheric pressure chemical vapour deposition

CVD - Chemical vapour deposition

eV - electron volts

EXAFS - Extended X-ray absorption fine structure

g – Gram

HEC- Hydroxyethylcellulose

^{i}Pr - Isopropyl

IR - Infra-red

NMR - Nuclear Magnetic Resonance

Ppm - Parts per million

Rz - Resazurin

SEM - Scanning electron microscopy

TTIP - Titanium tetra-isopropoxide

UV - Ultraviolet

XRD - X-ray diffraction

XPS - X-ray photoelectron spectroscopy

µXANES – micro X-ray Absorption Near Edge Structure

Acknowledgements

I would like to thank my supervisors Professor Ivan P. Parkin and Professor Gopinathan Sankar for believing in me from the start and for always been a source of encouragement even when I doubted myself. They have been with me every step of the way, creating time out of their busy schedules to be involved in every aspect of this work. I would like to thank EPRSC for awarding the funds for this research.

I would like to thank Dr Geoffrey Hyett who helped me with the start of the research, very patient and encouraging when I started. Dr Andreas Kafizas, Dr Sanjay Sathasivam and everyone in room 310 material centre have been a great help to me during this journey and I appreciate you all. I would also like to acknowledge Dr Steve Frith, Mr Kevin Reeves all at UCL. I am grateful to everyone at the department of chemistry UCL for all their help and support.

My special thanks to every member of my family and my closest friends for their continual support and I pray that the good lord will always be their strength.

My final and most worthy thanks goes to God Almighty for his strength when I am weak and mostly for his loving kindness that endures forever.

Chapter 1: Introduction

1.1. Introduction to metal oxide materials

Metal oxides have become technologically important and are now used in many fields. They have found various uses in the chemical industry; transition metal oxides display properties such as, catalytic activities and mutiferroic effects. They are are used in electrochemical reactions as electrode materials and also used in conducting and insulating films in the electronics industry.

The use of metal oxides as catalysts has been the focus of much research.[1,2] The improvement in characterisation techniques, instrumentation and experimental techniques has enabled the in-depth study of metal oxides as catalysts.[1]

Metal oxides are used as catalysts in various chemical processes including the oxidation of SO_2 to SO_3, and also used in CO reduction in emission control. Metal oxides are used in the production of hydrogen in the water-gas shift reaction. One of the most researched areas of metal oxides is photocatalysts. The photocatalysts are able to chemically break down dirt on the surface of the material; this property has lead to development of self-cleaning glasses and also in surfaces used to reduce microbial contamination. [1]

The properties of the surface chemistry of metal oxides are very important in their application as catalysts. The surface of a metal oxide catalyst is involved in the reaction of an absorbate on the surface. It has become increasingly important to understand both the physical and the chemical properties of the surfaces of metal oxides. [1]

The presence of dopant cations and anions on the surface of metal oxide catalysts and their stoichiometric ratio has been studied together with the presence of cationic and anionic vacancies. [1,2]

Several metal oxides have found wide spread interest for self-cleaning applications, water-splitting, gas-sensing, waveguides and solar-cell devices. These metal oxides include zinc oxide, tungsten oxide, and titanium dioxide.[2-4] Amongst these metal oxides titanium dioxide is one of the most studied metal oxide materials because of its diverse applications in commercial self-cleaning glasses, in the photo-assisted splitting of water and in gas sensing. TiO_2 has a wide range of desirable functional properties which includes mechanical durability, chemical stability and high refractive index.[5] Titanium dioxide thin films on glass have excellent adhesion and durability. These properties have led to a variety of applications including antireflective coatings and waveguides.[6] One of the most important functional properties of titania is its ability to act as a photo-catalyst[7] which has found widespread commercial application as a self-cleaning coating, for example Pilkington Activ^{TM}.[5] Potentially of greater importance for titanium dioxide is its ability to harness sunlight to split water into hydrogen and oxygen.

It is very important to study the growth of titanium dioxide films because the phases produced have a great effect on properties and the applications of the films. To enhance the functional properties of titania films we have to understand the growth stages of the films.

1.2. Titanium dioxide

1.2.1. History of TiO_2

Titanium dioxide is also referred to as titania (TiO_2) and is a naturally occurring oxide of titanium in its pure state, it is a brilliant white in colour (figure 1.1). TiO_2 is one of the most important materials for forming thin films. Titanium was discovered in 1791 by William Gregor in a black sandy mineral that he named menachanite. Four years later Martin H. Klaproth isolated the new element from the mineral and he named it titanium. He was not able to make it completely pure but was able to produce titanium dioxide from it.[8]

Figure 1.1. TiO_2 in the powder form.

1.2.2. Structure of TiO_2

There are three main polymorphs of TiO_2; rutile, anatase and brookite. The most thermodynamically stable and common is the rutile phase followed by anatase and then brookite.[9] Because of the thermodynamic stability of the rutile and anatase phases, their structures have been extensively studied. In both anatase and rutile the titanium atom is surrounded by six oxygen atoms in a distorted octahedral configuration.

Studies have shown that the rutile form of TiO_2 has three main crystal faces, two that are low in surface energy and are important and desired for practical polycrystalline and powdered materials.[10] The faces are (110) and (100), (001). The (110) has the lowest energy and hence is the most thermally stable and has been the most studied. The (001) face is thermally less stable, and has been reported to change structure at a temperature 475 °C.[11] The rutile structure is made up of edge sharing TiO_6 chains. The Ti is tetragonal and 6-coordinate.

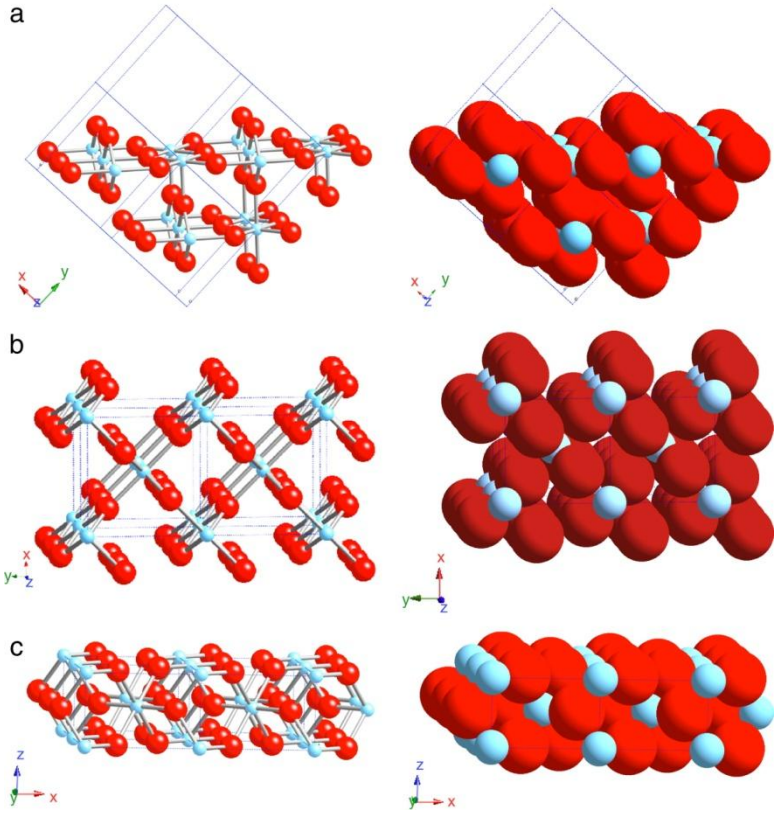

Figure 1.2. Schematic representations of selected low-index faces of rutile: (a) (110); (b) (100); and (C) (001).[10]

Anatase has two low energy surfaces, (101) and (001) which are common for the natural crystal.[12] The (101) surface has alternating rows of 5-coordinate Ti atoms and bridging oxygens, which are at the edges of the corrugations. The (001) surface is rather flat and can be reconstructed into forming another structure. The (100) surface is less common but is observed on rod-like anatase grown hydrothermally under basic conditions.[13] This surface has double rows of 5-coordinate Ti atoms alternating with double rows of bridging oxygen atoms.

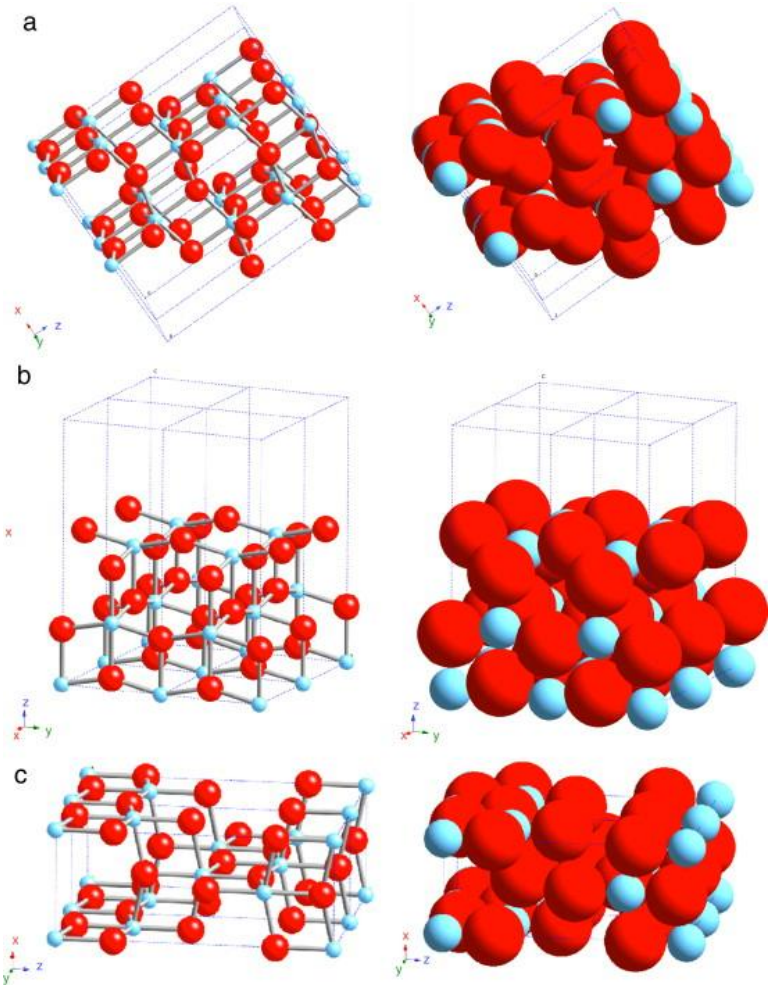

Figure 1.3. Schematic representations of selected low-index faces of anatase: (a) (101); (b) (100); and (C) (001).[10]

Brookite is orthorhombic; the titanium is coordinated to six central oxygen atoms and each oxygen atom to three titanium atoms. In brookite the titanium atoms are displaced from the centres of the TiO_6 octahedral. The brookite phase, is rare and more challenging to prepare, the (100) is most stable crystal face of brookite followed by (110) and (010).[14]

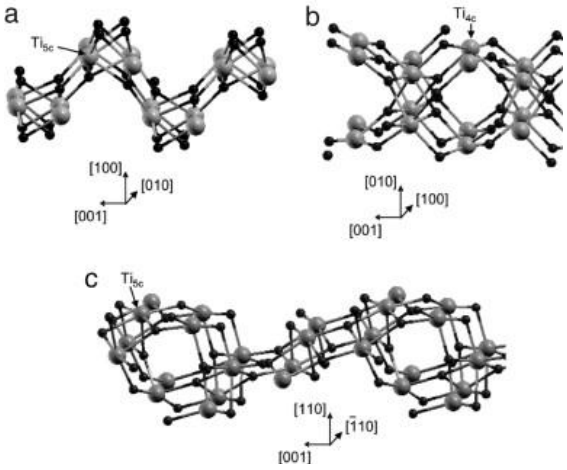

Figure 1.4. Schematic representation of the brookite structure [14]

1.3. Properties and application of TiO_2

1.3.1. Properties

Titanium dioxide is one of the most important materials for forming thin films.[15]It has a variety of desirable functional properties including mechanical durability, chemical stability and high refractive index.[16] Titanium dioxide thin films have excellent adhesion and durability on glass. These properties have led to extensive applications as anti-reflective coatings and waveguides.[17]Table 1.1 shows the shows the properties of TiO_2.

Table 1.1. A table of the properties of TiO_2

Properties	**Ti**
Atomic Number	22
Electron Configuration	$[Ar]3d^2 4s^2$
Appearance	White solid
Density	4.23 g/cm^3
Boiling Point	2972^oC
Melting Point	1843^oC
Refractive Index Anatase (n_D)	2.488
Refractive Index Rutile (n_D)	2.609
Crystal Structure (Anatase and Rutile)	Tetragonal

1.3.2. Application of TiO_2

TiO_2 has a variety of applications; the most important ones are reviewed below.

1.3.3. Pigment

TiO_2 is one of the most widely used white pigments. The reason titania is used as a pigment is because of its brightness and its high refractive index (n = 2.488 for anatase and 2.609 for rutile). The high refractive index of titania determines its opacity.[18] TiO_2 is used as an opacifier in glass, cosmetics, sunscreens, paper, and paints. One of the main advantages of TiO_2 when used as a pigment is its ability to resist discoloration under UV light.[19] The material is also used as a white food colouring; TiO_2 is often used to increase the palatability of skimmed milk.[20]

Both the rutile and anatase polymorphs are suitable as white pigments. The anatase has a better transparency in the UV but rutile is the most preferred pigment, this is because rutile has a higher refractive index and a lower photo-activity hence it is better and has greater durability as a pigment.[21]

1.3.4. Self-cleaning

Self-cleaning glasses are desirable for use as windows and general glazing application. Self-cleaning glasses have been commercialised by various companies. Pilkington activ™ Glass was commercialised in 2001 as the world's first self-cleaning window. TiO_2 is currently the thin film coating on glasses used for this application. TiO_2 thin films are hydrophillic in nature and their photocatalytic ability enables thin film TiO_2 to chemically break down organic dirt.

The self-cleaning ability of TiO_2 coated on glass works by absorbing readily available solar light and ultraviolet light (UV). The band gap of anatase titania is 3.2 eV which corresponds to a wavelength 390 nm in the near UV region. The titania is able to absorb energy that is equal to its band gap or greater, this results in the generation of an electron (e^-) and a positive hole (h^+). A model of this theory is shown in figure 5.[22] Most of the e^- and h^+ generated recombine but some charges migrate to the surface where the h^+ can oxidise adsorbed organic molecules and the e^- can combine with oxygen in the air to produce superoxide radicals and these radicals can also go on to break down nearby organic molecules (dirt). This results in effective "cold combustion" where the organic molecules are converted to carbon dioxide and water and other molecules.[23] When thin film TiO_2 is irradiated with UV light the surface becomes super-hydrophillic,[24] so the water-contact angle of the films on glass becomes very low under the action of sunlight, this causes rain water to form a sheet on the glass surface rather than droplets. These sheets of water are able to wash down the dirt from the surface uniformly. The photocatalysis properties and the processes for titania acting as a photocatalyst have been well studied and reported.[25]

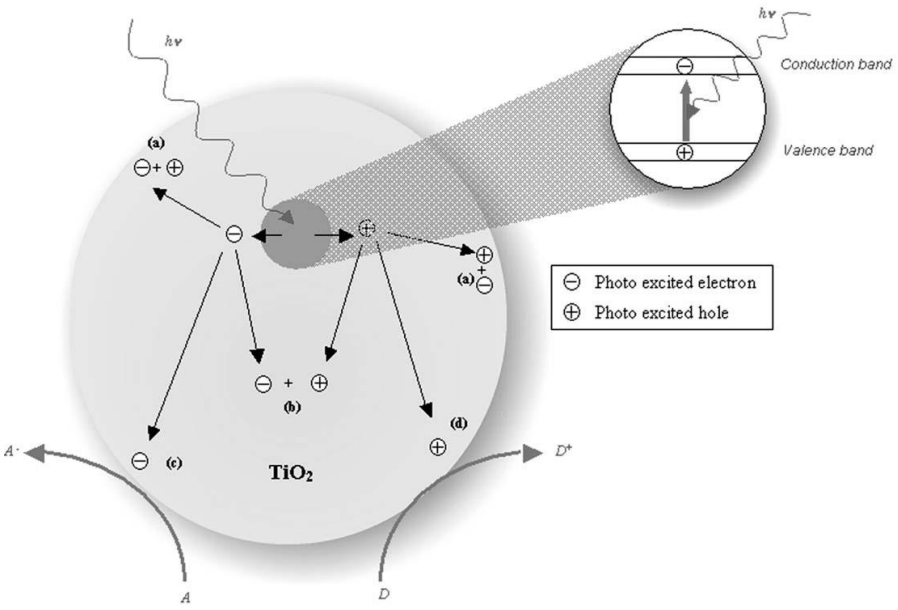

Figure 1.5. Upon irradiation of TiO_2 by ultra band gap light, the semiconductor undergoes photo-excitation. The electron and the hole that result can follow one of several pathways: (a) electron–hole recombination on the surface; (b) electron–hole recombination in the bulk reaction of the semiconductor; (c) electron acceptor A is reduced by photogenerated electrons; and (d) electron donor D is oxidised by photogenerated holes.[24]

The self-cleaning properties of TiO_2 are due to irradiation of the surface using UV-light which is also referred to as photo-induced hydrophilicity (PIH). The photogenerated holes are able to oxidise oxygen on the surface of the material to evolve O_2, this creates oxygen vacancies that can be filled by adsorbed water. This process produces surface hydroxyl groups that makes wetting of the surface easier by bonding with water molecules through hydrogen bonding, lowering the water contact angle to near 0^o after irradiation.[22] The self-cleaning properties of TiO_2 are dependent on the absorption of the ultra band gap light and the generation of electron and hole pairs. The position of the conduction and valance bands are related to key redox potentials.[26]

Researchers have focused on improving the self-cleaning properties of titania by doping and coupling composites. TiO_2 has been coupled with other semiconductors such as tungsten oxide with a lower band gap this increases the charge separation and helps to reduce the recombination of generated holes and electrons.[27] The band gap of TiO_2 lies in the UV region and efforts has been made to change the band structure and to lower so as to shift the absorption into the visible light region of the electromagnetic spectrum. To do this TiO_2 has been doped with a variety of materials including nitrogen, sulphur and carbon. [28]

1.3.5. Photocatalytic water-splitting

Semiconductor photocatalysis was detailed in the review by Mills et al.[24,18] The review shows that one of the most important properties of TiO_2 is its ability to split water and act as a photocatalyst. Fujishima and Honda were the first to report the first photochemical cell for water splitting using rutile TiO_2 photoanode and platinum counter electrode.[29] They reported that in the photoelectochemical cleavage of water, the use of TiO_2 as the anode and platinum at the cathode, when irradiated with light, hydrogen was evolved at the Pt electrode, while oxygen was produced at the TiO_2 electrode. A conventional water splitting photodiode consists of a metal substrate and an oxygen catalyst deposited on the top of the substrate and a hydrogen catalyst deposited on the reverse. The device is then placed between two water sources connected electrically by a photon membrane. The photocatalyst absorbes the light and generates an electron and hole pairs in the semiconductor. The holes can oxidise water to oxygen (equation 1.1), and the electrons are transferred through the substrate to the hydrogen catalyst on the reverse where they reduce water (equation 1.2).[10] The separation of the reduction and oxidation

steps reduces the back reaction and increases the effectiveness of the water splitting device as shown in figure 6.[30]

Equation 1.1. $2H_2O + 4h^+ \longrightarrow O_2 + 4H^+$

Equation 1.2. $2H_2O + 2e^+ \longrightarrow H_2 + 2OH^-$

Titanium dioxide is an n-type extrinsic semiconductor as the oxygen atoms are able to supply extra electrons to the titanium. To activate the semiconductor photocatalyst the material absorps a photon of ultra band gap energy, this results in the promotion of an electron from the valence band to the conduction band. This generates an electron and a hole in the valence band. In the photodiode the holes tend to migrate to the surface of the titania where they can oxidise water and evolve oxygen and the electrons migrate to the reverse metal side where they can reduce water and evolve hydrogen. The photodiode essentially enables vectoral charge separation and could form the basis for hydrogen generation to enable a zero-emission hydrogen economy.

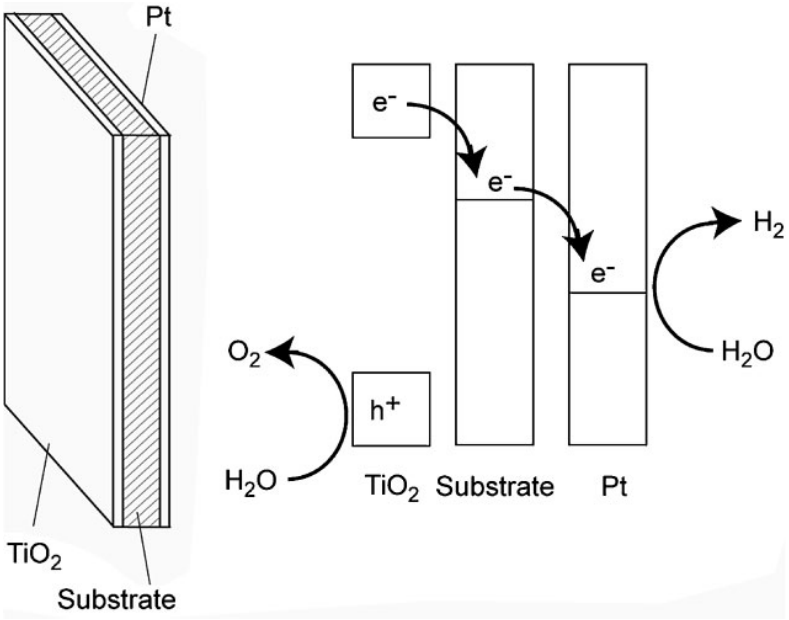

Figure 1.6. Diagram of a TiO_2/Metal/Pt photodiode, and a schematic of the band structure of the device[31, 20]

For TiO_2 to be an effective photocatalyst the recombination of the electron and the hole must be ineffective.[10] TiO_2 has been reported to satisfy the requirement to be an effective semiconductor. [31]

Recombination of the generated positive holes and electrons are also a limitation in water-splitting and the need to block this process is high. Noble metals (Pt, Pd, Ni, Cu and Ag) have been employed to improve the photocatalysis of TiO_2 as they have a lower Fermi-level compared to TiO_2.[32,33] In these systems the photo-excited electrons can be transferred from the conduction band of titania into the metal particles on the surface of the titania and the holes can remain in the titania reducing the electron and hole recombination process. This process results in the effective separation of the holes and electrons and increases the photocatalytic reaction.

1.3.6. Antimicrobial

TiO_2 has been reported to act as a light-activated antimicrobial surface.[34] There has been widespread research and development in antimicrobial surfaces. Antimicrobial surfaces are important in maintaining an acceptable level of hygiene in hospitals and may help reduce hospital-acquired infections.

$$TiO_2 + h\nu \rightarrow e^- + h^+$$
$$h^+ + H_2O_{(ads)} \rightarrow HO^\bullet + H^+$$
$$h^+ + OH^-_{(surface)} \rightarrow HO^\bullet$$
$$e^- + O_2 \rightarrow O_2^{\bullet-}$$
$$2O_2^{\bullet-} + 2H_2O \rightarrow 2HO^\bullet + 2OH^- + O_2$$

Figure 1.7. Reactive radical species generated by TiO_2 photocatalysis[23,33]

Figure 1.7 shows the process where reactive species are produced at the surface of the catalyst. The hydroxyl groups produced are highly reactive and are able to oxidise most organic compounds at the surface. This makes them extremely effective biocides.[34-36]

1.4. TiO_2 thin-film synthesis

The properties of TiO_2 and therefore its uses depend on the form; rutile or anatase and the method of preparation.[16] In this section we will review methods by which TiO_2 has been synthesised and the morphology and phases of the films produced.

TiO_2 has been synthesised by various methods. This includes atmospheric pressure chemical vapour deposition (APCVD), which is one of the most common methods as it allows synthesis of films that are durable and can control the microstructure.[37] Other methods include sol-gel methods, [38] metal-organic chemical vapour deposition (MOCVD) [39], atomic layer deposition (ALD) [40] and chemical spray pyrolysis.[41] The most common routes to synthesise TiO_2 thin films are chemical vapour deposition (CVD) and sol-gel.[42]

1.4.1. Sol gel

The sol-gel method is carried out when the substrate is dipped into a sol of the precursor mixture, left to dry and annealed at different desired temperatures. The sol-gel method is an important method for producing various functional films. [43] This is because of its low processing temperature and the ease of coating large surfaces, it also forms porous films which show good photocatalysis.[44] Sol-gel dip-coating methods have been used to prepare TiO_2 semiconducting oxide films. The properties of the films are affected by the

pore characteristics, surface area, and surface state of the film. The properties of the film produced are dependent on the sol-gel process conditions and this includes the solvent and annealing temperatures. [45]

The variation of structural and optical properties of TiO_2 thin films synthesised by the sol-gel method was studied by Y.U. Ahn et al. They found that the TiO_2 thin films prepared on quartz glass by the sol-gel process are amorphous, and they transform into the anatase phase at 400–600 °C, and into a mixture of anatase–rutile phases at 800 °C, further heating to 1000 °C causes the anatase films to completely transform into the rutile polymorph. The report shows that higher temperatures are required to form the more thermodynamic stable phase of TiO_2 rutile. The SEM of the films produced are typical of what is produced by sol-gel methods. This is shown in figure 1.8.

The SEM results show that the rutile polymorph of TiO_2 is denser than the anatase phase. At lower temperatures the films formed from sol-gel are almost spherical in shape. An increase in temperature results in more dense particles that have non-spherical shape.

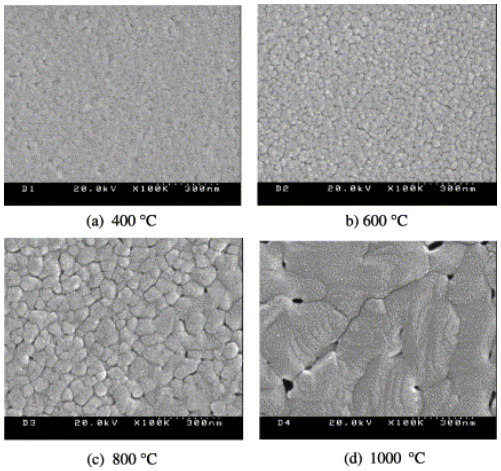

Figure 1.8. SEM of TiO_2 thin films: (a) 400 °C, (b) 600 °C, (c) 800 °C, (d) 1000 °C. [28] *(reproduced with permission)*

Other studies have been carried using sol-gel methods to synthesise TiO_2 films. Rath et al reported that above 400°C anatase is produced via sol gel methods using titanium isopropoxide (TTIP) precursor. They also reported that the conversion of anatase to rutile phase occurs at temperatures between 700–800°C. However the rutile film produced at this temperature still has some anatase phase present. Most studies of sol-gel processes have reported that only above 1000°C is rutile the exclusive phase.[46,47]

1.5. Chemical vapour deposition (CVD)

Chemical vapour deposition (CVD) is one of the most important and most used deposition techniques for the production of thin films in the materials industry. It has been employed for a variety of commercially available products including self-cleaning glasses, gas-sensing materials and optical-coatings. It is a low cost and fast technique and it is suitable for large scale production.

CVD processes involve the transportation of one or more volatile precursors in the gaseous state to a reaction vessel where the precursors react on a heated substrate and in the process deposit films and produce volatile by products. CVD makes use of either a single precursor, where all the elements required to deposit a film comes from one precursor, or it uses dual precursors where the elements required to form the films come from multiple precursors. There are different types of CVD including atmospheric pressure chemical vapour deposition (APCVD) and aerosol assisted chemical vapour deposition (AACVD). These will be referred to and employed throughout this thesis.

The CVD process can be broken down into four important steps as shown in figure 1.10. The first is to provide a pathway for the molecule to be vaporised

into the gaseous phase and transported into the CVD reactor vessel. The second is the precursors in the gas phase undergoing the correct reaction path to form small molecules that will be part of the deposited film and are absorbed onto the surface. The precursor molecules then react on the surface and produce a film with low contamination and the fourth stage is the removal of by products through the exhaust. An efficient production process is when the substrate is fully covered by the deposited film.

In traditional low pressure CVD, the precursors are vaporised by heating to high temperatures where they exhibit a significant vapour pressure. Liquid precursors which are highly volatile are preferred. In CVD depositing a film at lower deposition temperatures is favourable as this allows the use of a wide variety of substrates such as glass substrates and plastics.

Atmospheric pressure chemical vapour deposition (APCVD) is one of the most employed CVD process used in depositing thin films. This is because APCVD depositions are fast and avoid the installation and maintenance of the vacuum systems as required by traditional low pressure CVD. However it does require more volatile precursors than low pressure CVD. Aerosol assisted chemical vapour deposition (AACVD) was employed in the work outlined in this thesis. The main difference between AACVD and other CVD techniques is that AACVD uses a liquid aerosol to transport the precursor to the substrate. AACVD is cost-effective and uses a humidifier to produce the mist of the precursor, removing the need for high vacuum or high precursor volatility. AACVD is a solution based process and allows for the reaction to be monitored *in situ* as the precursors are mixed in solution before reaching the reactor vessel without decomposing before entering the reactor.

1.5.1. Atmospheric pressure CVD (APCVD)

Atmospheric pressure CVD (APCVD) is a technique used in coating thin-films on various substrates, such as glass, steel, and the film thickness is usually in the nanometre to micron range. The APCVD experiment is performed on an apparatus consisting of a horizontal-bed cold-wall reactor connected to an arrangement of stainless-steel heated pipes, valves and bubblers. The apparatus and APCVD technique is well described in various papers. [48]

This technique is currently used to produce the commercialised self- cleaning glasses such as Pilkington Activ,[49] it is also used to synthesise metal nitrides and many other films for a variety of application. This application includes semi-conductors, microelectronic devices and many more. [50]

APCVD has an advantage over other routes of synthesising TiO_2 because it is inexpensive, and is easy to commercialise as it can be incorporated into the float-glass system in industry. APCVD has been used to synthesis TiO_2 and also doped TiO_2. Parkin et al have been one of the major research groups to report on the use of APCVD to synthesise TiO_2 thin films on glass.[51,52]

Parkin at el reported that depositing TiO_2 via APCVD of $TiCl_4$ and an oxygen precursor, an alcohol or water, at 500–650°C on glass produces exclusively anatase films of good quality on glass substrates. They also reported that even though the rutile is thermodynamically the more stable form, the anatase TiO_2 is the most desirable form for self-cleaning purposes as it has the most effective photo-catalytic response and a low water contact angle. The SEM of the films produced from the study shows that the films are uniformed and granular, and the morphology is consistent with an island growth mechanism.

The SEM of the films deposited is shown in figure 1.9 and has a typical morphology of a TiO_2 film deposited via APCVD. The films produced by the APCVD methods are hydrophilic and on irradiation with UV-light they become super-hydrophilic.

The APCVD route produces faster growth rates and under optimum conditions forms uniform films with no contamination. It also produces TiO_2 thin-films that are very mechanically robust and do not have the haze associated with large particle sizes.[52,54]

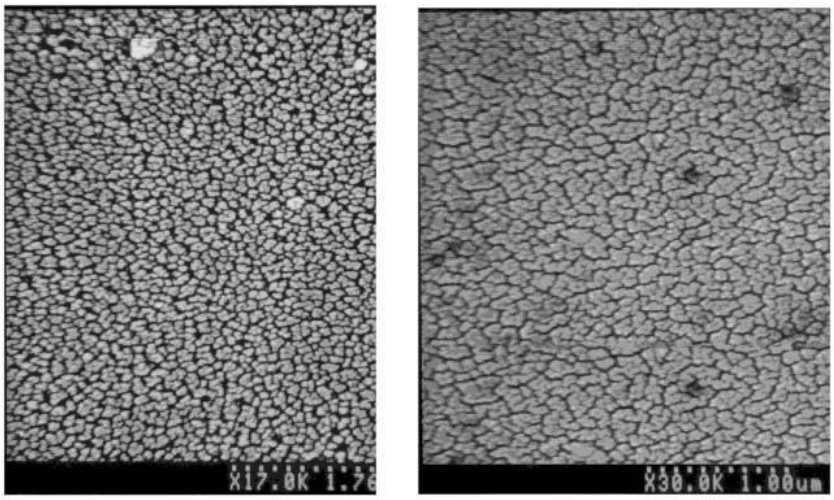

Figure 1.9 SEM micrographs of the films produced from the APCVD of (a) $TiCl_4$ and $^{i}PrOH$ (15 s deposition time at 500 ^{o}C) and (b) $TiCl_4$ and MeOH (15 s deposition time at 500 ^{o}C).[49] (Reproduced with permission)

1.5.2. Aerosol-assisted chemical vapor deposition (AACVD)

AACVD is a method that has been employed when the conventional atmospheric pressure CVD precursor proves involatile or is thermally unstable.[55] In this process the precursor is placed in a nebulizer sitting on an ultrasonic humidifier. The humidifier produces micron and sub-micron sized droplets from the liquid surface. These aerosol particles are then carried by an inert gas to the heated reactor vessel, where evaporation and decomposition occurs and leads to a CVD reaction. AACVD technique does not require precursors to be volatile, but needs them to be soluble in any solvent from which the aerosol can be generated. Figure 1.10 and figure 1.11 show the schematics of an AACVD reactor vessel and the process of AACVD deposition respectively.

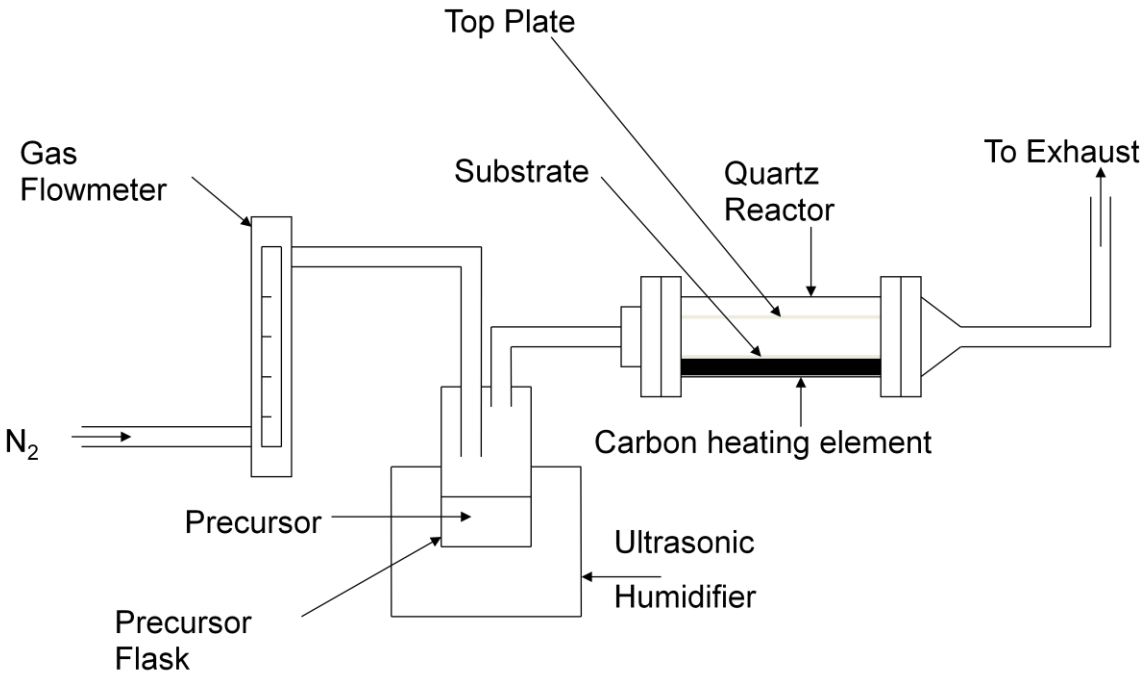

Figure 1.10. AACVD schematic

Figure 1.11. AACVD Process

AACVD has advantages over conventional CVD processes, because it offers better capability and flexibility than the conventional CVD process. The AACVD process is not expensive and relatively environmentally friendly chemicals can be used as precursors in the AACVD process, this is important for large-scale or mass production.[56] Ionic precursors and metal oxide clusters have been used in aerosol assisted depositions as alternative routes to thin films.[57] AACVD has also been used to synthesise nanoparticle precursors as a route to nanocomposite thin films. [57,58]

Synthesis of TiO_2 thin films on glass and metal substrates using AACVD has not been previously reported at the onset of this research. This is a novel idea and this thesis focuses on the synthesis TiO_2 films using aerosol assisted chemical vapor deposition.

1.6. References

1. Transition Metal Oxides: Surface Chemistry and Catalysis by H.H. Kung, Elsvier Science Publishers B.V.**1991**.
2. Ü. Özgür, Y. I. Alivov, C. Liu, A. Teke, M. A. Reshchikov, S. Doğan, V. Avrutin, S.J. Cho, H. Morkoç, *J. App. Phys.*, **2005**, 98, 041301
3. WY. Choi, A. Termin, MR.Hoffman, *J.Phys. Chem.*, **1994**, 98, 13669
4. U.Diebold, *Surface Science Reports*, **2003**, 48, 53
5. A.Fujishima, X. Zhangb, D. Tryk, *Surf. Sci. Reports*, **2003**, 63, 515.
6. A. Mills and S. Le Hunte, *J. Photochem. Photobiol., A Chem.*, **1997**, 108, 1.
7. T. Matsunaga, R. Tomoda, T. Nakajima, N. Nakamura and T. Komine, *Applied and Environmental Microbiology*, **1988**, 54(6), 1330.
8. G. Hyett, A. Mills, J. A. Darr and I. P. Parkin, *Chem. Vap. Depostion* **2010**, 16, 301.
9. Greenwood, Norman N.; Earnshaw, A. **1984**, Chemistry of the Elements, Oxford: Pergamon, 1117.
10. M. Ramamoorthy, D. Vanderbilt and R.D. King-Smith, *Phys. Rev. B,* **1994**, 49**,** 16721.
11. A.Fujishima, X. Zhangb, D. Tryk, *Surf. Sci. Reports*, **2008**, 63, 515.
12. R. Hengerer, B. Bolliger, M. Erbudak and M. Grätzel, *Surf. Sci*., **2000**, 460, 162.
13. S.D. Burnside, V. Shklover, C. Barbe, P. Comte, F. Arendse, K. Brooks and M. Grätzel, *Chem. Mater.*, **1998**, 10, 2419.

14. A. Beltran, L. Gracia and J. Andres, *J. Phys. Chem. B,* **2006**, 110, 2341.
15. I. P. Parkin, R. G. Palgrave, *J. Mater. Chem*., **2005**, 15, 1689.
16. A. Mills and S. Le Hunte, *J. Photochem. Photobiol., A. Chem.,* **1997**, 108, 1.
17. S. Nishimura, A. Shishido, N. Abrams, T. E. Mallouk, *Appl. Phys. Lett.,* **2002**, 81, 4532.
18. Winkler, Jochen, Titanium Dioxide, Hannover: Vincentz Network, **2003**, 5.
19. http://www.pcimag.com/CDA/Archives/3b4a7b83de6a7010VgnVCM100000f932a8c0
20. L. G. Phillips, D. M. Barbano. *J. Dairy Sci*., **1997**, 11, 2726.
21. R.J.H. Clark. The chemistry of Titanium and Vanadium. Amsterdam, Elsevier Pub. Co, **1968.**
22. I. P. Parkin, R. G. Palgrave, *J. Mater. Chem*., **2005**, 15, 1689.
23. A. Mills, A. Lepre, N. Elliot, S. Bhopal, I. P. Parkin, S. A. O'Neill, *J. Photochem. Photobiol., A. Chem.,* **2003**, 160, 213.
24. R. Wang, K. Hashimoto, A. Fujishima, M. Chikuni, E. Kojima, A. Kitamura, M. Shimohigoshi, T. Watanabe, *Nat.*, **1997**, 338, 431.
25. A. Mills and S. Le Hunte, *J. Photochem. Photobiol., A. Chem*., **1997**, 108, 1.
26. B. Sun and P. G. Smirniotis, *Catal. Today*, **2003**, 88, 49.
27. R. Asahi, T. Morikawa, T. Ohwaki, K. Aoki, Y. Taga, **2001**, 293, 269.
28. K.Hashimoto K, H. Irie, A. Fujishima A, *Jpn. J. Appl. Phys*, **2005**, 44, 8269.
29. Fujishima, A.; Honda, K. *Nat.*, **1972**, *238*, 37.

30. G. Hyett, A. Mills, J. A. Darr and I. P. Parkin, *Chem. Vap. Deposition*, **2010**, 16, 301.
31. M.R. Hoffmann, S.T. Martin, W. Choi, D.W. Bahnemann, *Chem. Rev*., **1995**, 95,69.
32. S. Q. Peng, X. Y. Li, F.Y. Jiang, G. X. Lu, S. B. Li , *Phys. Lett.*, **2004**, 398, 235.
33. K. Page, M.Wilson, I. Parkin. *J. Mater. Chem*., **2009**, 19, 3819.
34. A. Mills and S. LeHunte, *J. Photochem. Photobiol., A. Chem*, **1997**, 108, 1
35. W. A. Jacoby, P. C. Maness, E. J. Wolfrum, D. M. Blake and J. A. Fennell, *Environ. Sci. & Technology*, **1998**, 322, 2650.
36. T. Matsunaga, R. Tomoda, T. Nakajima, N. Nakamura and T. Komine, *App. and Environ. Microbiology*, **1988**, 54(6), 1330.
37. A.Mills, N.; Elliott, I.; Parkin, S.; O'Neill, R. J.; Clark, *J. Photochem. Photobiol., A* **2002**, 151, 171.
38. L. Hu, T. Yoko and H. Kozuka. *Thin Solid Films*, **1992,** 219**,** 18.
39. Giovanni A. Battiston, Rosalba Gerbasi and Marina Porchia, *Thin Solid Films*, **1994**, 239**,** 186.
40. V. Sammelselg, A. Rosental, A. Tarre, L. Niinisto, K. Heiskanen, L.S. Johansson, T. Uustare, *App. Surf. Sci.*, **1998**, 134 , 78.
41. M.O. Abou-Helal, W.T. Seeber, *Appl. Surf. Sci.*, **2002**,195, 53.
42. A. Mills, S. K. Lee, A. Lepre, I. P. Parkin and S. A. O'Neill, *Photochem. Photobiol. Sci.*, **2002**, 11, 865.
43. S. Sakka and T. Yoko, in J. C. Jorgensen and R. Reisfeld (eds.),Chemistry, Spectroscopy and Application of Sol Gel Glasses, Springer, Heidelberg, **1991**, 89.

44. Y.Paz, Z. Luo, L.Rabenberg, A.Heller, *J. Mater. Chem.***1995**, 10, 2842.

45. H. Lili, T. Yokot, H. Kozuka, S. Sumio, *Thin Solid Thins*, **1992**, 219, 23

46. H. Rath, S. Anand, M. Mohapatra, P.Dash, T. Som, *Indian J. Phys*., **2009**, 83, 559.

47. X.Z. Ding and X.-H. Liu. *J. Alloys Compd.*, **1997**, 248,143.

48. D. Troy, A. Manning, I. P. Parkin, J.H. Robin, D. Sheel, M. E. Pemble, V. Dimitra, *J. Mater. Chem.,* **2002**, 12, 2936.

49. PilkingtonNSG Group Flat Glass Business, http://www.pilkingtonselfcleaningglass.co.uk/, last accessed 26th February **2009**.

50. H.J. Gysling, A.A. Wernberg, *Chem. Mater*., **1992**, 4, 900.

51. S O'Neill,a P. Parkin, R. Clark,a A. Mills, N. Elliottb, *J. Mater. Chem*., **2003**, 13, 56.

52. A.Mills, N.Elliott, I. Parkin, A.O'Neill, R.J. Clark, *J Photochem. Photobiol., A. Chem.,* **2002**, 151, 171.

53. Chen, Q.; Qian, Y.; Chen,Z.; Wu, W.; Zhou G.; Zhang, Y. *Appl. Phys. Lett*., **1995**, 66, 1608.

54. Kim, E. K.; Son, M. H.; Min, S. K.; Hon, Y. K.; Yom, S. S. *J. Cryst. Growth*, **1997**, 170, 803.

55. I. P. Parkin, R. G. Palgrave. *J. Am. Chem. Soc*., **2006**, 128, 5.

56. K. Choy. Chem. Vap. Deposition, **2006**, 12, 581.

57. W.B. Cross, I.P. Parkin, S. A. O'Neill, D.A.Williams, M. F. Mahon, K. C. Molloy, *Chem. Mater*., **2003**, 15, 2786.

58. Binions, R.; Carmalt, C. J.; Parkin, I. P. *Thin Solid Films*, **2004**, 469-470, 416.

Chapter 2: Characterisation techniques

This research employed different characterization techniques to analyse the deposited films particularly X-ray diffraction (XRD), Raman spectroscopy, and X-ray absorption spectroscopy. A brief introduction of the techniques used in this thesis is provided in this chapter. In particular this chapter describes in some detail a range of synchrotron based techniques. This is because this thesis reports the first application of XANES mapping and CVD growth using central facilities.

2.1. X-ray diffraction (XRD)

XRD is a technique used to characterise materials with long range order. Low angle X-ray diffraction has been widely reported as a technique for the investigation of thin films. XRD is a convenient and effective technique for crystalline phase identification.

The wavelength of X-rays is in the range from 0.5 – 2.5 Å. X-ray scattering generates a unique pattern for each type of crystalline material. The wavelength of X-rays is of a similar degree to the spacing between atoms and so is most suitable wavelength for probing the structural properties of a variety of inorganic materials.

Diffraction is the interference caused by an object in the path of the electromagnetic wave, and occurs when the dimensions of the object are

similar to the wavelength of the radiation. The wavelengths of X-rays are similar to the spacing of atoms/ions in crystals, and are therefore diffracted by them. During diffraction, the waves can interfere either constructively (increasing the wave amplitude) or destructively (decreasing the wave amplitude) and when they are detected, they show up as regions of enhanced or diminished intensity. This is due to the intensity being proportional to the amplitude. Two X-ray beams will interfere constructively if AB + BC (the difference in their path lengths) is equal to an integral number of wavelengths. The pattern of varying intensity as a function of diffracted angle 2θ is called a diffraction pattern. [1] By analysing the diffraction pattern, a detailed picture of the crystal structure can be produced. The way the diffraction works in a crystal system can be explained using the following figure 2.1. [3]

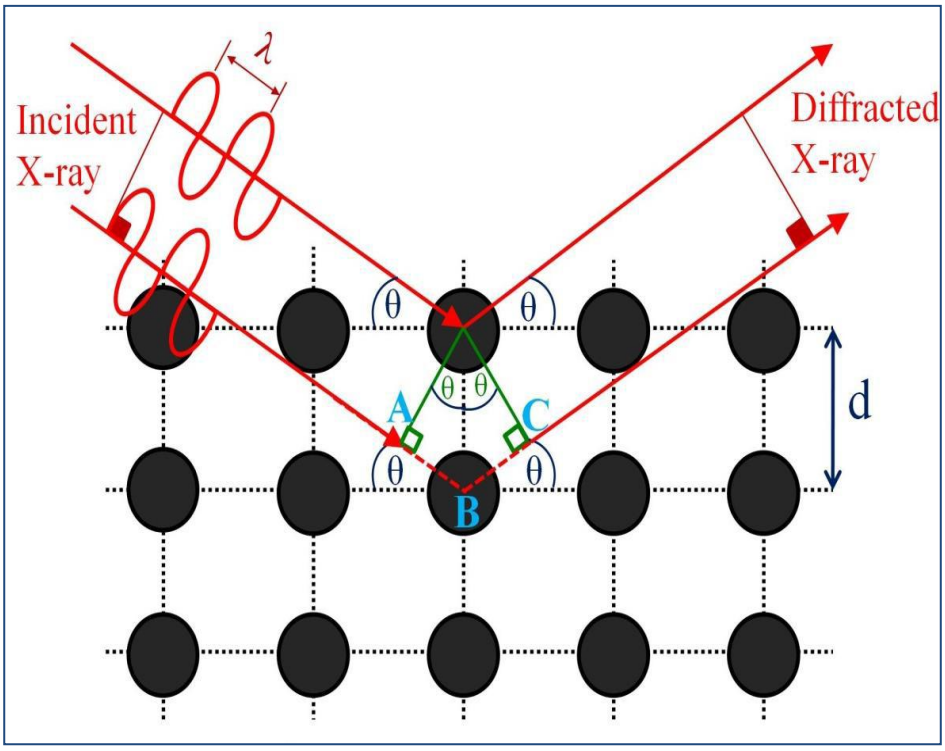

Figure 2.1. Diffraction of an X-ray by an ordered crystal lattice.

The horizontal lines in figure 2.1 represent planes of atoms in a crystal from which the waves are diffracted. The diffracted waves are detected and their glancing angle (2θ (theta)) is recorded. The separations of the planes (d) are calculated using Bragg's Law:

Equation 2.1. $n\lambda = 2dSin\theta$

Equation 2.1. Bragg's law: where λ is the wavelength of the radiation used and n is an integer determined by the order of the diffracted beam.

One of the most used X-ray diffraction techniques for characterizing materials is Powder XRD. The powder is dominated by randomly orientated crystallites of the sample of interest. So in powder XRD a 2-D diffraction pattern is collected that shows concentric rings of reflections related to the different d-spacing in the crystal lattice. The positions of the peaks in the pattern and their intensities are then used to identify the structure or phase of the material. This technique has been used to identify and solve structures of a range of crystalline systems that includes inorganic, organic and biological systems. [4]

Thin film diffraction is a form of XRD technique used to characterise thin films deposited on a substrates.[3] In thin film analysis using XRD the X-ray's penetrate through the layers of the film and are able to measure both the structural properties of the as deposited films and the substrate. The analysis of thin film samples using XRD is usually done at low angles of incidence using glancing angle X-ray diffractometers.

In this study thin film X-ray diffraction was employed to identify the phases of the materials deposited using aerosol assisted chemical vapour deposition (AACVD). Bruker-Axs D8 general area diffraction detector system (GADDS) was used in this project at an incident angle of 5^{o}. GADDS uses a large 2D area X-ray detector. The diffraction data collected with this technique produces a good signal to noise ratio and was collected in a short amount of time. The XRD pattern of a film is determined by the atomic arrangement within its crystal lattice, so the films deposited will have the diffraction pattern that is characteristic of its component compounds or phases which can then be identified by comparing it with the standard patterns available from the ICDD reference database. [2]

2.2. Raman spectroscopy

Raman spectroscopy is one of the most used techniques in analysing molecular motion and fingerprinting of a material. It is concerned with the shift in wavelength of inelastic or Raman scattered radiation from a monochromatic light source, usually from a laser, it provides chemical and structural information of a material. The energy range of Raman spectroscopy is between 200 - 4000 cm^{-1}.[5] The selection rules in Raman spectroscopy complement the selection rules in infra-red spectroscopy. Unlike IR spectroscopy where molecules have to have a dipole moment, vibrational Raman spectra can be recorded for non-polar molecules such as N_2. To be Raman active a molecule needs to have anisotropic polarizability. That means that for a molecule to be Raman active the polarizability of the molecule must change during vibration. When an electric field is applied to a molecule the electron cloud around the molecule is distorted and the extent of the distortion

is termed the polarizability of the molecule. Anisotropic polarizability is when the polarizability is direction dependent. [8]

Laser light interacts with the molecular vibrations in the material. These result in the energy of the laser photons to be shifted up or down and this shift in energy gives information about the vibrational modes present in the material. When a photon excites a molecule it promotes the vibrational ground state to a virtual energy state and when the molecule relaxes it emits a photon and it is returned to a different vibrational state. This is termed the 'Raman effect' and is inelastic. When the emitted photon returns to the same state it is elastic and this state is Rayleigh scattering. The difference between the original state and the final state after absorption causes a shift in the emitted photon's frequency. This shift in frequency is known as the Stokes shift. Figure 2.2 describes the energy level states involved in Raman spectroscopy.

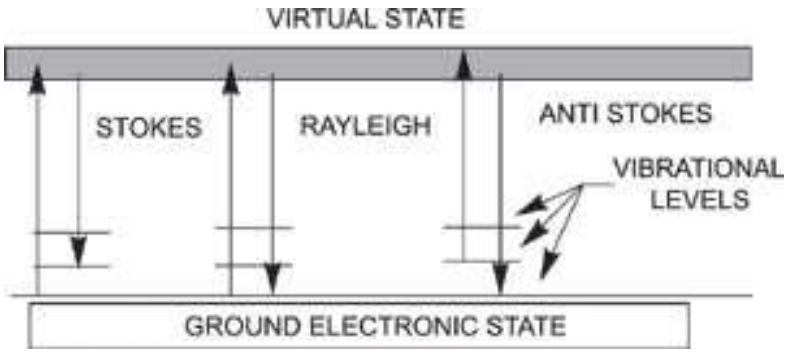

Figure 2.2 Energy level states involved in Raman spectroscopy. [6]

Stokes shifts occur when the final vibrational state of the molecule has more energy than the initial state and the photon is shifted to a lower frequency to balance the total energy of the system. The Anti-Stokes shift occurs when the

final vibrational state of the molecule has less energy than the initial state and a photon is shifted to a higher frequency than the original state. So in other words Stokes radiation happens at lower energy which is at longer wavelength than Rayleigh radiation and anti-Stokes has higher energy which is shorter wavelength that Rayleigh radiation as described in figure 2.3. Because molecular energy levels are quantised this distinct lines can be produced from the molecule.[6]

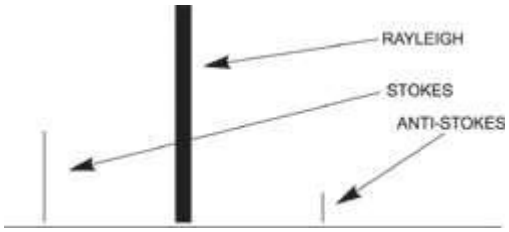

Figure 2.3 describes the Stokes and Anti-stokes phenomenon. [6]

Figure 2.4 shows the selection rules that is allowed in Raman spectroscopy. Raman: $\Delta J = 0, \pm 2$, Stokes is J + 2 and anti-Stokes is J - 2. 7

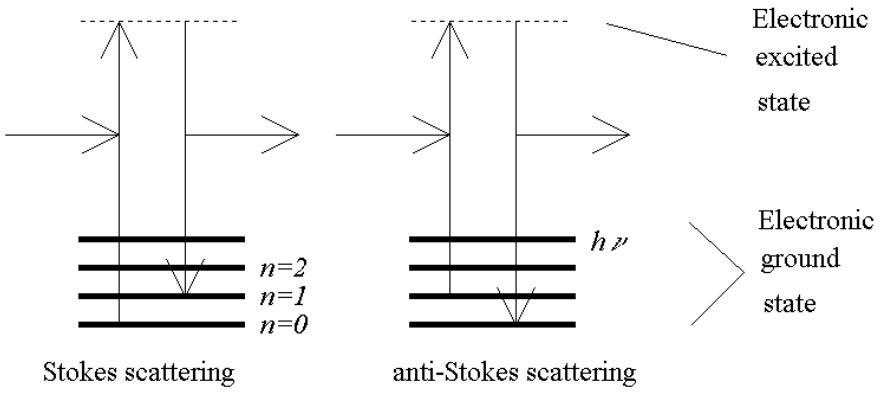

Figure 2.4 The selection rules that is allowed in Raman spectroscopy. [7]

Raman spectroscopy is widely used in chemistry to provide fingerprint identification of materials as the vibrational information corresponds to the chemical bonds and the symmetry of molecules and solids. In this project Raman spectroscopy is mostly used alongside XRD for phase determination of the as deposited thin films.

2.3. Scanning electron microscopy (SEM)

SEM is a type of electron microscopy and is an important characterisation technique and was employed throughout this project. SEM works by using a beam of electrons to illuminate a sample and magnify the surface on the sample upto 250,000 times. In SEM microscopy an image is produced on a particular point on a sample. SEM works by generating an electron beam from an electron gun; the electrons are then accelerated through an electric field and are focused on a single point on the sample using electromagnetic lenses. Deflector plates scan the beam across a rectangular surface of the sample. The electron beam produced causes the emission of secondary electrons from the sample. Back scattered electrons can also occur due to reflected electron beam caused by elastic scattering. These back scattered electrons are higher in energy than the secondary electrons. Secondary electrons gives rise to high resolution images that provide an insight into the morphology of a given sample. Although back-scattered electrons produce lower resolution images, the strong intensity of the back-scattered electron images is related to the atomic number of the sample and is useful in providing information about the distribution of heavier and different elements in a given sample.

2.4. X-ray absorption spectroscopy (XAS)

XAS has been increasingly useful in the study of a wide range of materials including amorphous and liquid state systems and has been used to determine the chemical state of important species mostly those with low concentration. XAS has been recognised as a powerful analytical technique due to the availability of synchrotron radiation.

2.4.1. Synchrotron radiation

Synchrotron radiation occurs when an electric field is applied to accelerate ultrarelativistic particles to near the speed of light in a storage ring. Synchrotron radiation is generated when the magnetic field used in the storage ring causes the accelerated electrons to change direction and lose energy in the form of a 'white' light called synchrotron. The word synchrotron originated from the synchronised way the applied magnetic field is increased in strength in time and the increase in energy of the particles as they accelerate through the circular path in the storage ring. Synchrotron radiation allows different wavelengths to be used because the accelerated electrons emit radiation continuously with various wavelengths and strengths.

An illustration of the synchrotron components is shown in figure 2.5. The Synchrotron includes different features including an electron gun that produces electrons, a linear accelerator (LINAC) where the electrons produced are accelerated to high energy, a booster ring that accelerates the electrons to near ultrarelativistic speed, a storage ring where the electrons with sufficient

energy to produce light are circulated and bending magnets which are present on the curved point in the storage rings are able to focus the electrons round the storage ring.

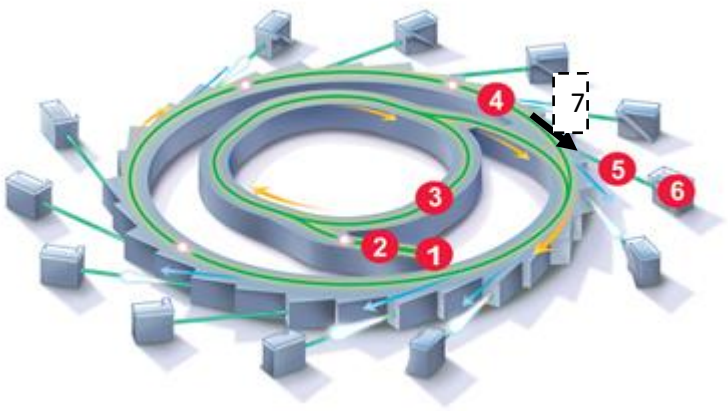

1. Electron gun
2. LINAC
3. Booster ring
4. Storage ring
5. Experimental Hutch
6. Control station
7. Synchrotron radiation

Figure 2.5. A schematic diagram of synchrotron radiation source.

Due to the intensity of the X-rays generated synchrotron radiation has many advantages over conventional X-rays produced by laboratory X-ray tubes. Synchrotron radiation sources are able to produce higher intensity than X-ray tubes and so allow data to be collected at a much faster rate than in the laboratory. This allows chemical processes to be recorded *in situ* whilst an experiment is being conducted. High intensity and tuneable energy are important properties of synchrotron radiation and these properties allow synchrotron radiation to be used for resonant scattering methods and X-ray absorption spectroscopy. Synchrotron radiation has a high degree of collimation allowing more efficient and angularly precise experiments to be carried out with greater resolution. Synchrotron radiation techniques have

been a valuable tool to determine the structure of a range of materials including thin film metal-oxide layers in semiconductors.

2.4.2. X-ray absorption spectroscopy (XAS) technique

XAS characterisation technique is concerned with the study of local environment of an element of interest within a system. XAS has an energy of about 10^4 eV which corresponds to wavelengths of about 1 Angstrom. The wavelength of 1 Angstrom is of a similar order of magnitude as the atom to atom separation in a molecular structure so it is able to provide information on the local environment of the coordinated atom including its coordination number, oxidation state of the element and relative bond distances. XAS has been a useful tool in gaining structural information of non-porous and organometallic materials. XAS unlike XRD is able to provide information on amorphous materials and crystallised materials because long range order is not required in XAS and thus can be used to analyse materials in low concentrations. Data collection using XAS can be done in a very short time allowing for *in situ* studies to be performed.

An X-ray absorption spectrum contains two parts: (1) X-ray absorption near edge structure (XANES) and (2) extended X-ray absorption fine structure (EXAFS). XAS is concerned with the measurement of X-ray absorption of a material as a function of the incident X-ray energy. When an X-ray hits a material, atoms in the material absorbs some of the photon and this decreases the transmitted X-ray beam.

A rise in absorption is caused at a specific energy as a characteristic of each atom type. This edge is called the absorption edge; the absorption indicates the excitation of an electron from the core level into a fully or partially unoccupied level or the continuum. Figure 2.6 shows a representation of the ejection of an electron from the core level into an unoccupied level.

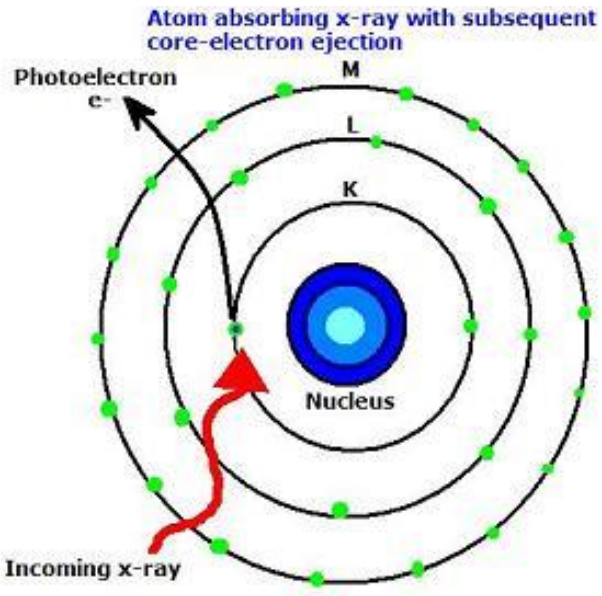

Figure 2.6. An illustration of X-ray absorption. Showing the process when a material is hit with X-ray and an electron is excited from the core level into the continuum.[9]

XAS is a technique concerned with the measurement of the X-ray absorption coefficient μ(E) of a material. μ(E) provides the probability that an X-ray will be absorbed by the material in accordance with Beer's law as shown in equation 2.2 and shown in figure 2.7.

Equation 2.2. $I = I_0 e^{-\mu x}$

In the equation I represents the transmitted intensity (the intensity going through the material), I_0 represents the intensity of the incident X-ray, μ(E) is the absorption coefficient and x is the sample thickness.

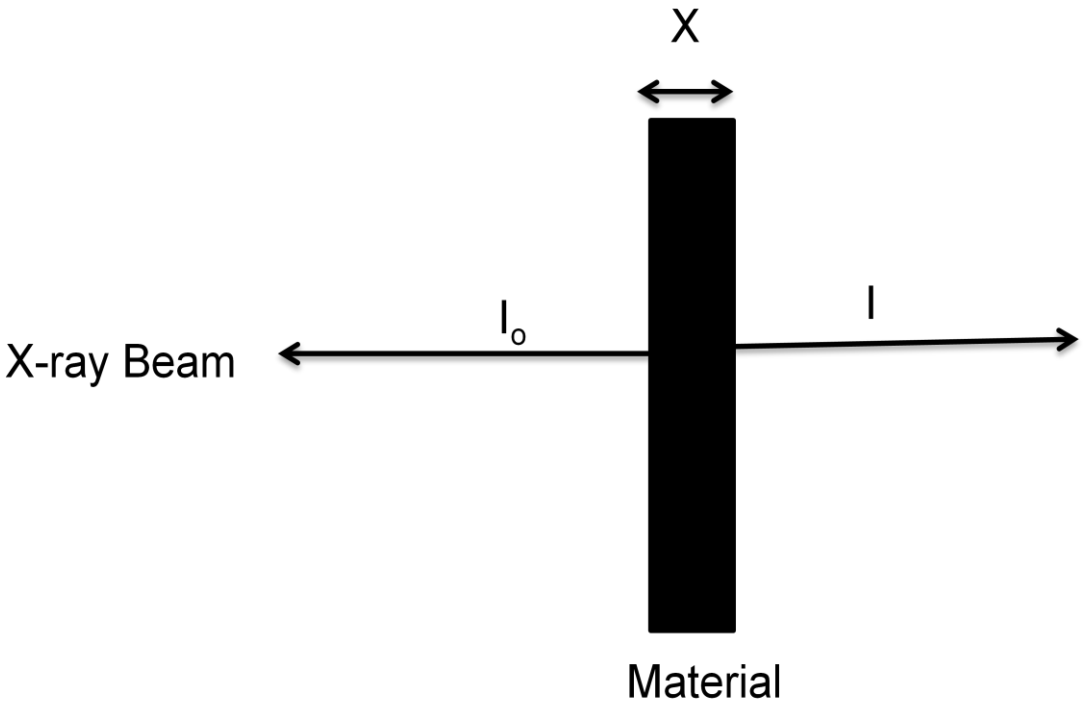

Figure 2.7. Schematic showing the transmission of X-rays through a material where I_0 is the -ray intensity and I represents the transmitted X-ray Intensity.

When the absorption coefficient is plotted against the energy, three interesting features are observed. There is an overall decrease in X-ray absorption with an increase in energy. A sharp increase in the absorption coefficient known as the absorption edge at a specific energy is also observed as the energy increases. Also, just above the edge a series of oscillations is seen. This is shown in figure 2.8.

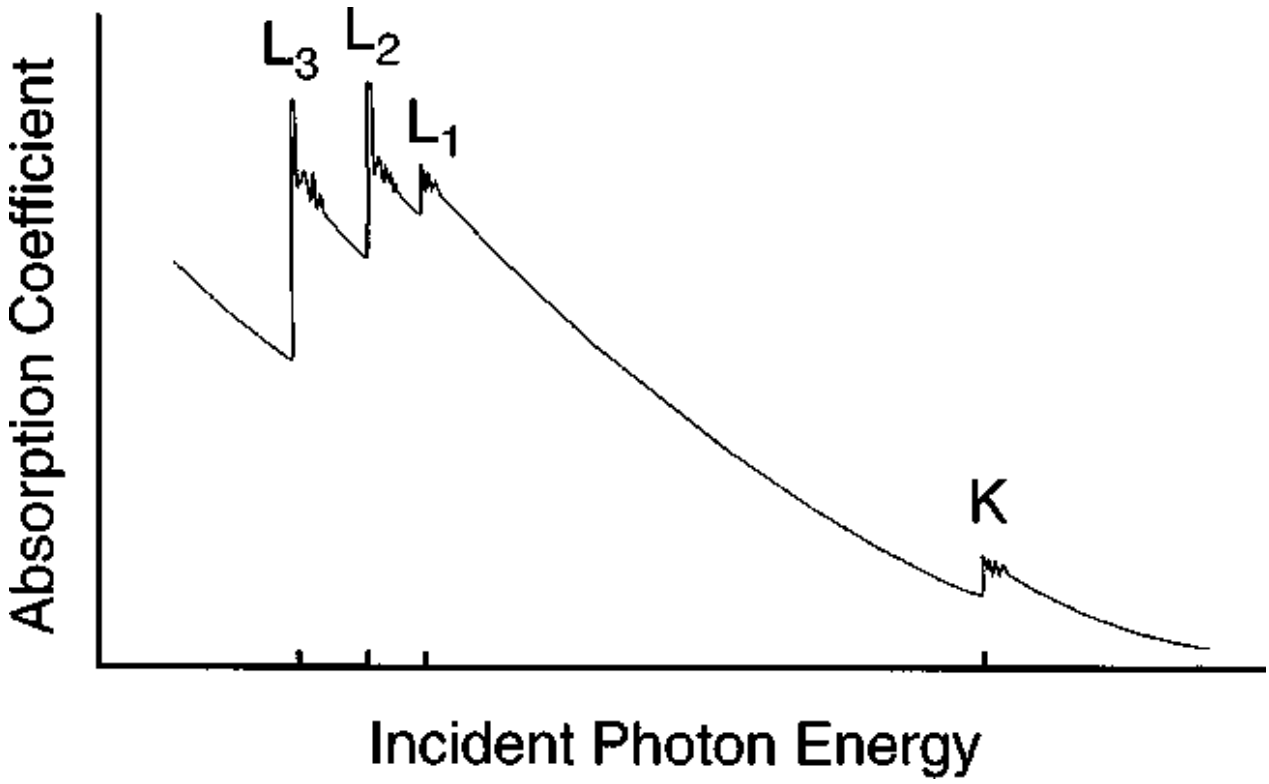

Figure 2.8. The variation in absorption coefficient as a function of X-ray energy, the K and L edges. K represents transitions to Fermi level from1s, L_1 is from the 2s level, L_2 is from the 2p (1/2) level and L3 is from the 2p level (3/2). [10]

The absorption spectrum of an atom consists of three features: the pre-edge and post-edge region of the spectrum is referred to as the X-ray absorption near edge structure (XANES) region and beyond the post edge the series of oscillations observed is termed the extended X-ray absorption fine structure (EXAFS) region as shown in figure 2.9.

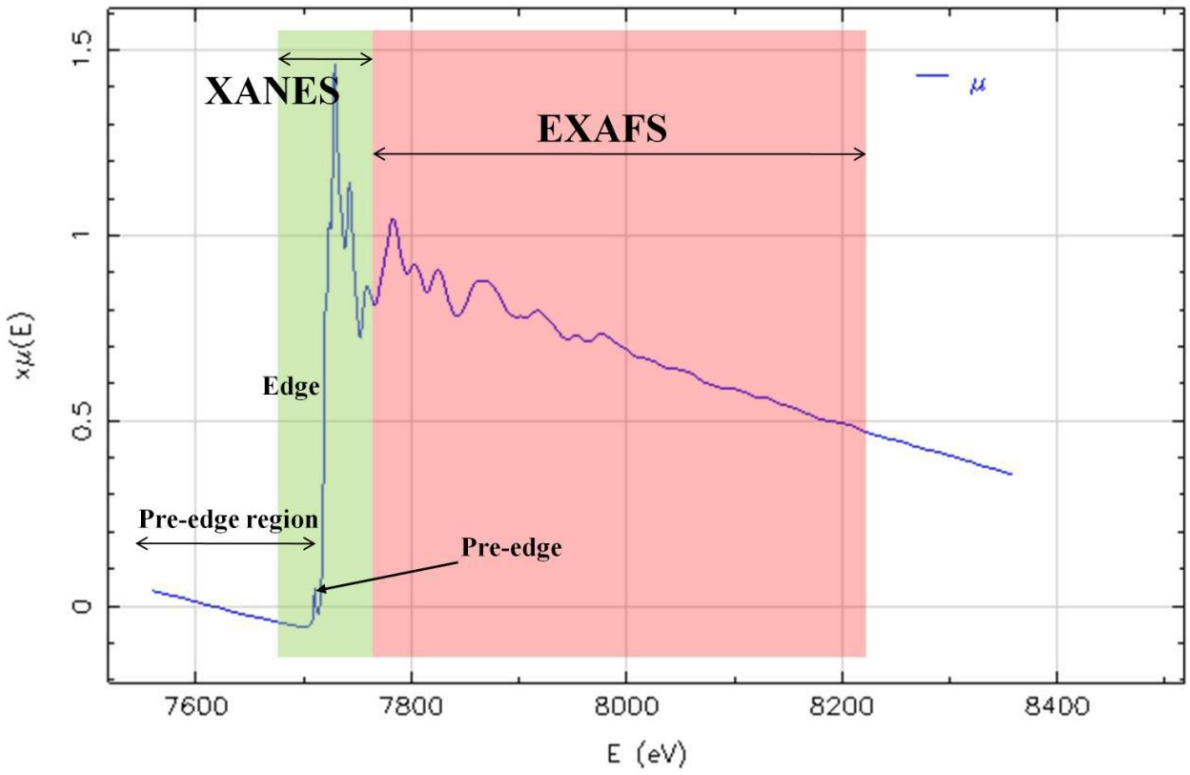

Figure 2.9. Different regions in the X-ray absorption spectrum

The XANES region which is includes any pre-edge is sensitive to the oxidation state and coordination environment of the atom. The EXAFS region gives information of the inter-atomic distances and the details of neighbouring species of an atom.

When an atom absorbs a photon it becomes excited and this means that an electron is promoted to a higher energy level leaving an electron level empty. The empty state can decay either by X-ray fluorescence or Auger emission. If X-ray fluorescence occurs a core electron in a higher energy will fill the core hole and this results in the emission of an X-rays with defined energy levels. When a higher energy level core electron drops to fill the core hole and an

electron is emitted this is referred to an Auger emission. X-ray fluorescence mostly happens when hard X-rays are used and Auger emission occurs when lower energy X-rays are used.

2.4.3. XANES

X-ray absorption near edge structure (XANES) is the region in the absorption spectrum around 50 eV just before the edge (E0) (pre-edge) or just the absorption edge and extends to ca. 100 eV. The peaks in the pre-edge are caused by electronic transitions into partially filled states and these transitions give an indication of the oxidation states in an element. The dipole selection rule $\Delta l = \pm 1$ governs the absorptions in the XANES region. This allows primary K-edge absorption transitions of s → p (1s core electron) and L1 edge (2s core electron) (s → p) and $L_{2,3}$ edges (($2p½$) and L_3 ($2p_{3/2}$) edges) (p → d). Each element has a specific absorption edge that represents the allowed transition and these transitions are very sensitive to the element's oxidation state. For instance an element with higher oxidation state will need more energy to remove the same electron from its core shell. XANES has been employed to provide the oxidation state of redox metals in material science.[11]

2.4.4. EXAFS

Extended X-ray absorption fine structure (EXAFS) is the region in the absorption spectrum where oscillations are seen. The observed oscillations occur due to the scattering of the emitted photoelectron by the neighbouring atoms of the excited atom. The photoelectron is emitted as spherical waves

and backscattering happens when the photoelectron interacts with a neighbouring atom and the wave is bounced back towards the probed absorbing atom. The EXAFS region starts from ca. 50 eV to 1000 eV and beyond above the absorption edge. Figure 2.10 shows an illustration of the excited photoelectron wave and how backscattering occurs.

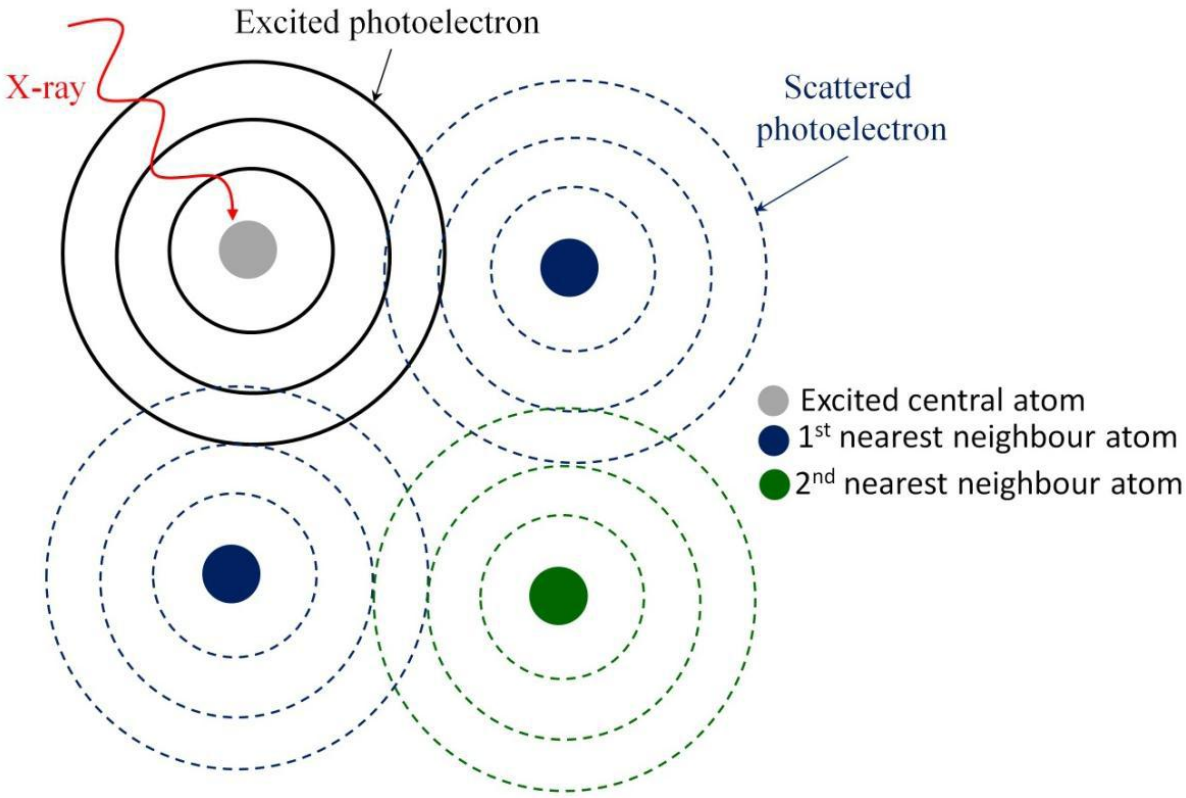

Figure 2.10. Picture showing the outgoing and backscattered photoelectron waves, and the possibility of interference between them.[12]

The sum of the outgoing and backscattered incoming waves $\mu(E)$ is observed in the absorption coefficient variations with energy in an EXAFS spectrum. Equation 2.3 describes EXAFS observations.

Equation 2.3. $\mu_{total} = \mu_0 [1 + X_{EX})$

Where: μ_{total} is the absorption coefficient above the edge, μ_0 represents the atomic background and X_{EX} is the sum of the outgoing and backscattered wave (the EXAFS fine-structure function).

X_{EX} also known as EXAFS fine-structure function is described in terms of a wave vector. The X-ray energy is converted to *k*, the wavenumber of a photoelectron. $\chi(k)$ is therefore used to describe the oscillatory frequencies corresponding to different near neighbour coordination shells and is calculated as shown in the equation 2.4.

Equation 2.4.

$$\chi(k) = \sum_j \frac{N_j}{kR_j^2} e^{\left(-2k^2\sigma_j^2\right)} f_j(k) \sin\left(2R_j k + \delta_j(k)\right)$$

Equation 2.4. Nj =number of neighbouring atoms (the coordination number), Rj = the inter-atomic distance, δ^2 = the mean square displacement from the disorder in the neighbour distances, fj(*k*) and $\delta j(k)$ = scattering properties of the atoms close to the excited central atom.[12]

Although the EXAFS technique is widely used to determine local structure, in this thesis only the XANES part of the data is used to determine the phase compositions of the TiO_2 present in the system.

XANES interpretation is however complicated due to the fact that there is no analytic description presented from XANES, however the XANES signals are much stronger than those of EXAFS, which is an advantage. The challenge in analysing XANES is due to the limitation in the EXAFS equation, as it breaks down at low k due to the 1/k in the equation and the fact there is an increase in the mean free path at low k. Nonetheless the data is recorded in the XANES region is still chemically very useful as XANES provides the oxidation state of atoms which will be very challenging to prove experimentally and it also provides useful coordination environment of an atom.[13] EXAFS data is recorded over a longer period of time compared to XANES making XANES a much quicker technique to use. XANES recording allows fast collection allowing *insitu* recording to be carried out.

The XANES region is also used as a simple phase identification technique (fingerprint) to identify the presence of a specific chemical species. XANES techniques are used extensively in this project to identify the phase of TiO_2 deposited on glass and steel substrates; whether anatase or rutile. The XANES technique was used to map the as-deposited films both on glass and steel substrate in chapter 5 and an *insitu* study of the deposition of TiO_2 and tungsten oxide was also attempted and reported in chapter 7 of this thesis.

2.4.5. Data collection

The XAS data reported in this thesis was collected at Diamond light source in Didcot Oxfordshire beamline I18. A schematic diagram of the beamline is shown in figure 2.11.

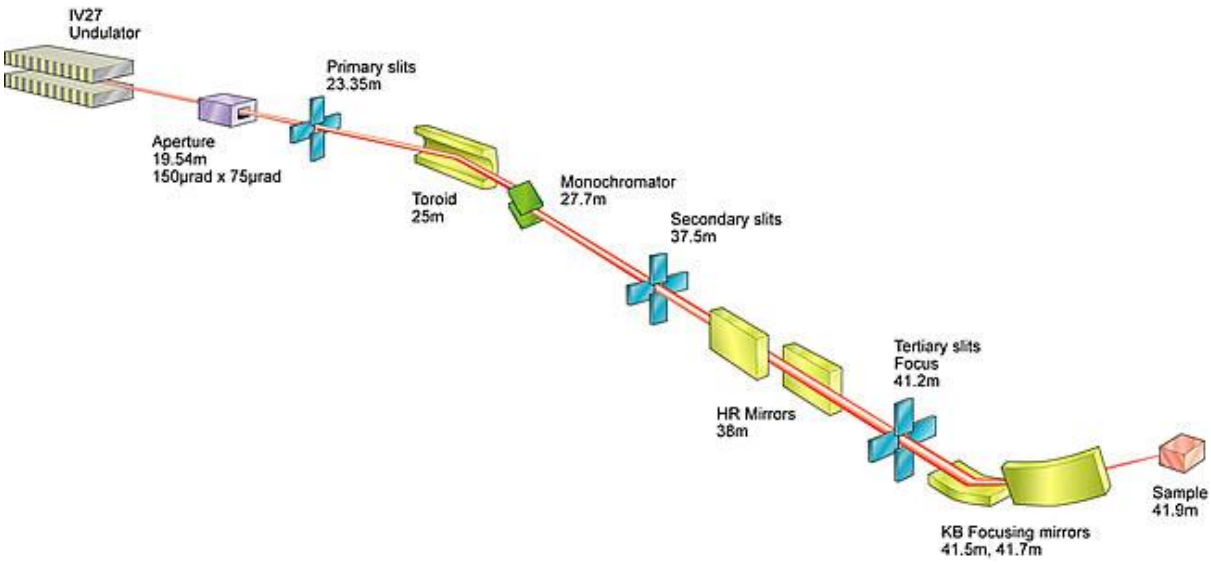

Figure 2.11. Schematic diagram of beamline I18 at Diamond light source.

XANES data can be collected in transmission or fluorescence mode. The absorption coefficient μ(*E*) is measured in the transmission mode by the equation 2.5 shown below.

Equation 2.5. $\mu(E) = \mathrm{Log}\,(I_0/I_t)$

Equation 2.5. The measurement of the absorption coefficient in the transmission mode, where I_t represents the intensity of the transmitted X-ray.

Transmission mode is the measurement of $\mu(E)$ and the data is recorded with the use of ion-chambers which are airtight and contain a carefully measured mixture of inert gases separating two highly (oppositely) charged parallel plates. X-ray transparent windows allow X-rays to enter the chambers. When X-rays enter they ionize the gases causing an ionization current which is then recorded. Ion chambers are placed before the incident X-ray beam and after the sample in the path of the X-ray beam to record the difference in the currents in either side of the sample. This is then related to a change in the X-ray intensity.

Fluorescence data in XAS are collected using highly sensitive detector arrays and in this case a 9 element solid state detector system optimised for energies above 5 keV. These detectors record the X-rays emitted from the sample when a high energy electron fills the core hole. Fluorescence data are particularly used in recording XAS when samples analysed contain dilute amount of the element of interest. The fluorescence mode does not directly measure the absorption coefficient, however the fluorescence yield is proportional to the absorption cross-section as shown in equation 2.6.

Equation 2.6. $\mu(E) \propto \mathrm{Log}\,(I_f/I_0)$

Equation 2.6. The measurement of the absorption coefficient in the fluorescence mode, where If represents the monitored intensity of the fluorescence line.

In this thesis all the data was collected using the fluorescence mode due to the thin nature of the thin films of titania and tungsten oxide studied.

2.4.6. Data analysis

XANES is a very useful technique to analyse the quantity of specific phases in a mixture and it is also very useful to follow *in-situ* experiments. The most used method of analysing XANES is the least squares linear combination analysis and principal component analysis.

The principal component method is the traditional approach that involves choosing a pure model standard and then fitting the edge to the standards. It is a technique based on linear algebra and it aims to find the number of components that can reproduce the experimental spectra. The limitation in using the principal component method is determining the number of standard required and difficulty in knowing a realistic model.[14]

In this thesis the least square linear combination analysis method of analysing XANES spectra was used. In this method a linear combination of reference samples is used which allows the amount of species in a multiple component deposition to be determined from their fingerprint in the XANES region. This method is easy to implement providing good quality spectra of the reference compounds are available and if these were recorded under similar conditions.

The initial step in XAS data analysis is to subtract the pre-edge of the data collected from the background. The background is removed by fitting a smooth line to the pre-edge slope and when subtracted help remove any instrumental background and absorption from other edges. In this work the Athena program is used and an example of data from sample 56457 is shown in figure 2.12a and 2.12b.[15] XANES normalisation is achieved by normalising the edge jump increase $\mu(E)$ from 0 to 1. The maximum derivative of $\mu(E)$ is usually at the mid-point of the edge jump is referred to as the threshold energy E_0.

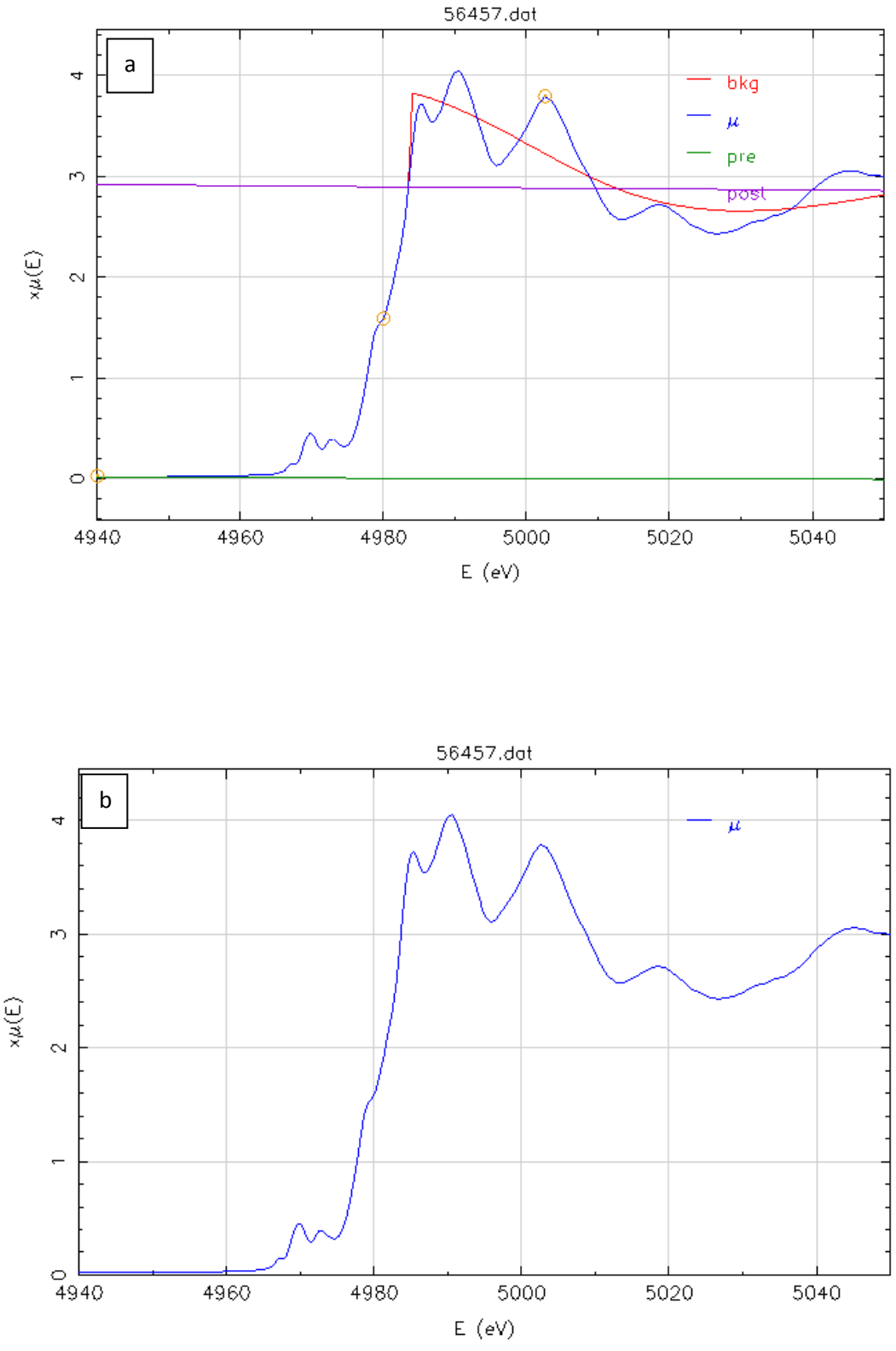

Figure 2.12. Background removal procedure; (a) pre-edge background, post-edge and background, and (b) the normalised data.

In this thesis the XANES data are analysed using linear combination analysis using the Athena software. By carrying out a linear combination fit (LCF) it was possible to determine the phase of TiO_2 present (either anatase or rutile) and quantities of this phases present in the as deposited files using standards of both phases.

Steps to complete a LCF:

- Choose LCF from the Athena menu
- Choose the standards (μ(*E*) of anatase and rutile)
- Select the normalised μ(*E*) of the data and fit marked groups

These steps produce typical spectra as shown in figure 2.13 and also produce a table that can be exported and plotted to show the percentage of each phase present. This procedure is discussed in more detail in chapter 5.

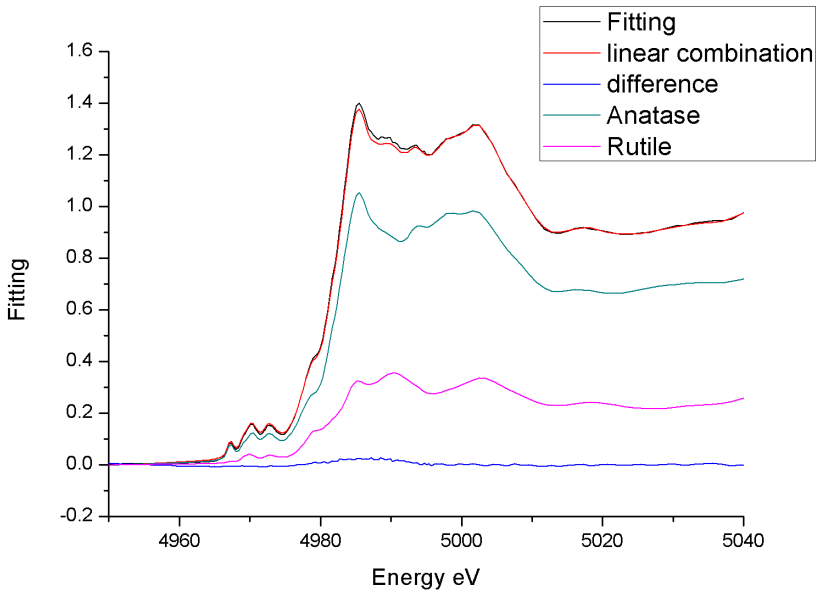

Figure 2.13. An example of the LCF of a μXANES spectra showing best fit, individual components and difference.

While all the techniques described in this chapter were used predominantly to characterise the thin film samples, other routine characterisation methods, in particular FTIR and NMR were also used for specific characterisation and are not described here. Further individual details of the experiments are given in respective chapters.

2.5. References

1. P.W. Atkins, Physical Chemistry, 4th edition, Press, O. U. Ed.**1990**.
2. JCPDS, International Centre for Diffraction Data PDF-2, **1997-2010**.
3. X-ray Diffraction, by B.E. Warren, General Publishing Company, **1969**, **1990**.
4. M. Hartmann, L. Kevan, *Res. Chem. Intermed.*, 2002, **28**, 625.
5. D.J. Gardiner, Practical Raman spectroscopy, **1989**.
6. http://www.andor.com/learning-academy/raman-spectroscopy-an-introduction-to-raman-spectroscopy
7. http://staff.bath.ac.uk/pysdw/newpage11.htm
8. C. E. Housecroft, A. G. Sharpe, Inorg. Chem., 3rd edition, **2008**.
9. http://chemwiki.ucdavis.edu/Physical_Chemistry/Spectroscopy/X-ray_Spectroscopy/XAS%3A_Theory
10. J. Rehr, J. R.C. Albers, *Rev. Modern Phys*., **2000**, 72, 621.
11. A. L. Ankudinov, B. Ravel, J. Rehr, J. J.Conradson, *Phys. Rev. B,* **1998**,58, 7565.
12. Newville, M., Fundamentals of XAFS, In Consortium for Advanced Radiation Sources, University of Chicago: Chicago, **2004**.

13. Nuclear Analytical Techniques for Metallomics and Metalloproteomics, RSC, **2010**.

14. Factor Analysis in Chemistry, 2nd Ed. John Wiley & Sons, NY, **1991**.

15. B. Ravel, M. Newville, *J. Synchrotron Rad*, **2005**, 12, 537.

Chapter 3

Aerosol assisted chemical vapour deposition and characterization of titanium dioxide thin films

3.1. Chapter overview

This chapter details the AACVD and characterisation of as deposited TiO_2 thin films on different substrates at a range of deposition temperatures. Titanum (IV) isopropoxide (TTIP) was used as a single source precursor in methanol. This chapter will detail the phase of TiO_2 deposited with both temperature and the substrate type. The properties of the films will also be explored and the focus will be on the hydrophillicity, and photocatalytic activities of the films deposited.

3.2 Introduction

Titanium dioxide thin films have one of the best adhesion and durabilities on glass compared to other materials. These properties have led to extensive applications as antireflective coatings and waveguides.[1] One of the most important functional properties of titanium dioxide is its ability to act as a photocatalyst which has found widespread commercial application as a self-cleaning coating, for example Pilkington Activ.[2] Potentially of greater importance for titanium dioxide is its ability to harness sunlight to split water into hydrogen and oxygen. The latter can be accomplished by a photodiode that consists of a thin layer of titanium dioxide or modified titanium dioxide on a metal surface encased in a water tank.[2] The action of sunlight on the titania surface generates an electron and positive hole.[3] In the photodiode the holes tend to migrate to the surface of the titania where they can oxidise water and evolve oxygen and the electrons migrate to the reverse metal side where

they can reduce water and evolve hydrogen. The photodiode essentially enables vectoral charge separation and could form the basis for hydrogen generation to enable a zero-emission hydrogen economy. What is important for titania to act as a photocatalyst to photomineralise bacteria or viruses[3,4] or to act as the functional layer in a photodiode is that the morphology of the film is controlled and that there is a degree of phase control between the two most common polymorphs of titanium dioxide- anatase and rutile. [5]

TiO_2 thin films have been formed by a wide range of techniques, the most common of which are physical vapour deposition, chemical vapour deposition and sol-gel routes as detailed in chapter 1. The phase of titanium dioxide synthesised has been generally reported to be temperature dependent, with temperatures above 650°C tending to favour the more thermodynamically stable rutile form, whilst lower substrate temperatures favour the deposition of anatase the kinetically formed phase. However precursor chemistry also plays a role, Sheel et al showed that APCVD of titanium tetraisopropoxide on steel substrates at 500°C formed exclusively rutile titanium dioxide yet exclusively anatase from titanium tetrachloride and ethylacetate under comparable conditions.[6,7] Furthermore Hitchman showed that rutile titania could be formed exclusively at temperatures as low as 300°C using titanium tetraisobutoxide.[8] It is probable that the growth rate of the titanium dioxide plays a role in phase formation with very slow growth as observed by Hitchman enabling rutile to be formed at unexpectedly low temperatures. This cross over from anatase to rutile is of key importance for functional properties. Although both common polymorphs of titanium dioxide are photocatalysts, either pure anatase or anatase-rutile mixes, such as the ubiquitous unofficial

comparative standard Degussa P25 (30/70: rutile/anatase) often show the best performance.[9]

The aerosol technique has commonly been used for precursors that have very low vapour pressure but that can be dissolved in a carrier solvent. Hence the volatility requirement transfers to the solvent enabling a much wider range of materials to be used in deposition. The aerosol can also have an effect on the microstructure of the thin films formed, often encouraging films composed of interlocking spheres- indicating that the process has at least partially occurred in the gas phase.

3.2.1 Deposition of TiO_2 using TTIP

Titanum (IV) isopropoxide (TTIP) is an alkoxide of Ti(IV) and has been employed in organic synthesis and material science. In the AACVD deposition of TiO_2 thin films as reported here TTIP is used as the precursor in an excess of methanol solvent. The mechanism of this process is complicated and is not yet fully understood.

3.3 Experimental

TiO_2 thin films were synthesised using aerosol assisted chemical vapour deposition (AACVD) on either glass (SiO_2 coated float-glass of dimensions 45 x 90 mm), titanium foil (Goodmans, 100 μm thickness) or stainless steel substrates (Goodmans, 250 μm thickness) of dimension 25 x 25 mm. Titanum (IV) isopropoxide (TTIP) (97% Aldrich) and methanol (Fisher, reagent grade) were used without any purification. Deposition was carried out on a cold-wall horizontal-bed CVD reactor that contains a graphite block heated by a Whatman cartridge heater. The glass substrate was provided by Pilkington-NSG. Deposition of thin film was carried out on SiO_2 barrier layer to prevent

migration of ions from the glass bulk into the film. A glass top-plate was positioned parallel above the substrate, and the whole set up was contained within a quartz tube. TTIP (0.60 ml) was added to methanol (50 ml) and an aerosol was generated at room temperature using a Pifco ultrasonic humidifier. The aerosol was carried into the reactor with carrier gas flow of oxygen free nitrogen gas at 1 $Lmin^{-1}$ (BOC). The gas flow was continued until the entire precursor was used up. Films were then cooled and stored in air.

A series of depositions on glass-substrates were carried out at substrate temperatures of 400°C, 500°C, and 550°C. Variation in film thickness was achieved by growing the film for 15, 30, 45 or 75 minutes from the same concentration of precursor solution.

Deposition was carried out under an identical set of conditions on steel and titanium foils to investigate the affect of substrate on film phase and morphology. These foils were placed on top of a glass substrate which in turn was placed on top of the carbon heater block.

Atmospheric pressure chemical vapour deposition (CVD) was used to make thin titania films on glass, steel and titanium at 550°C using a cold-walled reactor. Titanium tetra-isopropoxide was used as the single source precursor, heated in a brass bubbler to 108°C and transported using a flow rate of 1 $Lmin^{-1}$ of oxygen free nitrogen gas (BOC). Prior to entry to the reactor the precursor gas stream was diluted with a further 10 $Lmin^{-1}$ of oxygen free N_2. Deposition was carried out for 180 seconds.

3.4 Characterisation of deposited films

Thin film X-ray diffraction (XRD) measurements were carried out using a Bruker D8 Discover instrument fitted with GADDS area detector and Cu $K\alpha_{1+2}$ source. Diffraction patterns were recorded and collected for 30 minutes per sample, using a fixed incident angle of 10^{o} for glass and 5^{o} for steel and titanium plates. Scanning electron microscopic (SEM) measurement was carried out on the films to determine surface morphology using a JEOL JSM-6301F field emission SEM at an accelerating voltage of 5 KeV. Raman spectra were obtained with a Renishaw Invia raman microscope with a wavelength of 515.5 nm and 50x microscope objective

The rate at which the titania films photo-oxidise water in a sacrificial system was measured using a Rank Brothers oxygen electrode. The device includes a 50 mm diameter glass chamber consisting of a water cooling jacket at the base which is a Clark cell consisting of a platinum working electrode. For water splitting measurements on steel and titanium substrates platinum was sputtered on the reverse side to improve performance. This was carried out using a sputter coater with an argon pressure of 0.1 Torr, and a current of 25 mA for 5 minutes.

The FTA 1000 instrument was used to measure the water contact angles of the films. This instrument uses “drop-shape” analysis to make measurements. It captures video images of liquid droplets (water) on the surface to analyse their shape and size to determine the contact angle.

An intelligent ink based on the dye Resazurin (Rz) was prepared in the same way as described previously by Mills et al.[10] The ink is made up of 3 g of a 1.5 wt. % aqueous solution of HEC polymer, 0.3 g of glycerol and 4 mg of Rz. The titania films formed on glass at 400°C and 500°C were sprayed with an aerosol spray-gun which was filled with the indicator ink solution to form an even ink-coating. The films were subsequently irradiated with a 365 nm lamp. The photocatalytic reduction was monitored *via* UV-visible absorption spectroscopy and digital photographic methods. The films change colour from blue to pink in indicating photoreduction of reazurin (blue) to rezofurin (pink). Further degradation of the dye induces a colourless state, showing the complete reduction of rezofurin.

3.5 Results and Discussion

3.5.1 Synthesis and Characterisation- Films formed by AACVD.

TiO_2 thin films were grown on glass, steel and titanium substrates by AACVD using TTIP in methanol at 400-550°C, Table 3.1, Figure 3.1. The films were adhesive, passing the Scotch tape test. They resisted scratching with a 2H pencil and a brass stylus but could be scratched by a stainless steel or diamond tipped scalpel. The films were impervious to common solvents and 2M mineral acid but could be slowly dissolved by 2M NaOH. The films on glass were transparent (>75% transmission over the visible region) but did show a slight white haze when viewed off angle (ca 5% haze measurement dependent

on specific film). Some evidence for interference colours was noted across the film indicating slight variation in film thickness; this is a common phenomenon for high refractive index films and was used to ascertain film thickness. The thicknesses were actually fairly uniform with variations which ranged from ca 300 nm to 500 nm across the majority of the films with the thickest portions formed at the centre of the substrate.

Table 3.1 XRD Results of as deposited TiO_2 on different substrate and at different temperatures

Substrate	**400°C**	**500°C**	**550°C**
Glass	Anatase	mix of both	More rutile + anatase
Steel	Rutile	Rutile	Rutile
Titanium	Rutile	Rutile	Rutile

X-ray diffraction patterns of the films deposited on glass at a substrate temperature of 400°C showed the anatase form of TiO_2, using the AACVD of TTIP in methanol whereas for the films prepared at 500°C both anatase and rutile forms are present (figure 13(a)) and at 550°C the rutile phase is mostly seen (deposition time 75 minutes) this goes to support that higher temperature favours the thermodynamic phase of TiO_2 the rutile phase. XRD patterns of the titania films deposited on titanium and steel plates show only rutile phase formation at all three substrate temperatures, this observation is surprising as it shows that even at low temperatures the rutile phase is still favourable on metal substrates and whilst on glass substrate temperature has a greater effect

on phase deposited. The characteristic bands seen in Raman spectra, shown in Figure 3.2 support the findings by XRD, with only rutile noted for all depositions on steel and titania subtrates. The anatase phase is observed at 400°C, anatase-rutile mixtures at 500°C and purely rutile formation at 550°C on glass; the Raman spectra were identical to those in the literature for the respective polymorphs of titania.[10] The TiO_2 anatase peaks were observed at 143, 396, 516 and 639 cm^{-1} and the rutile TiO_2 peaks at 144, 232, 447 and 609 cm^{-1}.

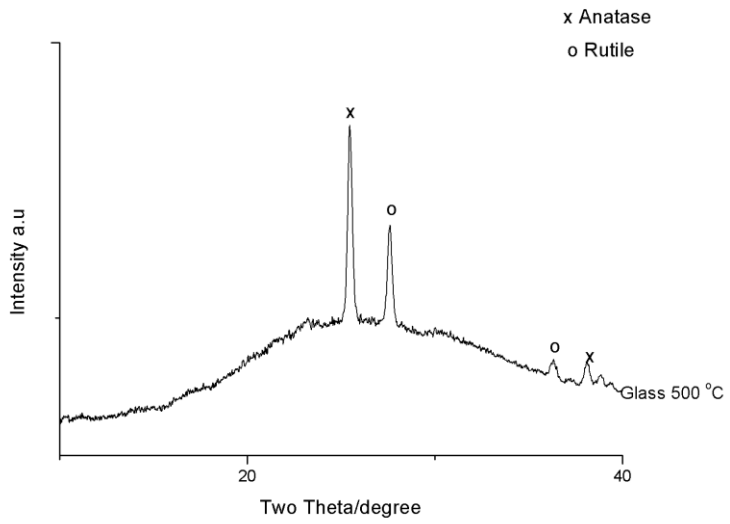

Figure 3.1(a). XRD pattern of as deposited TiO_2 film from the AACVD reaction of TTIP in methanol *on glass substrate at 500°C, showing the peaks that correspond to anatase (x) and rutile (o).*

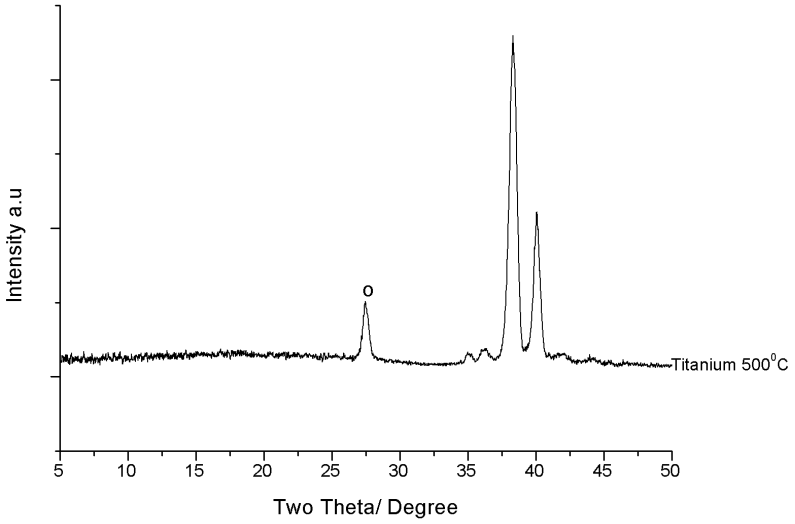

Figure 3.1(b). XRD pattern of as deposited TiO_2 film on titanium substrate from the AACVD reaction of TTIP at 500°C in methanol solvent, showing the peaks that correspond to anatase (x) and rutile (o).

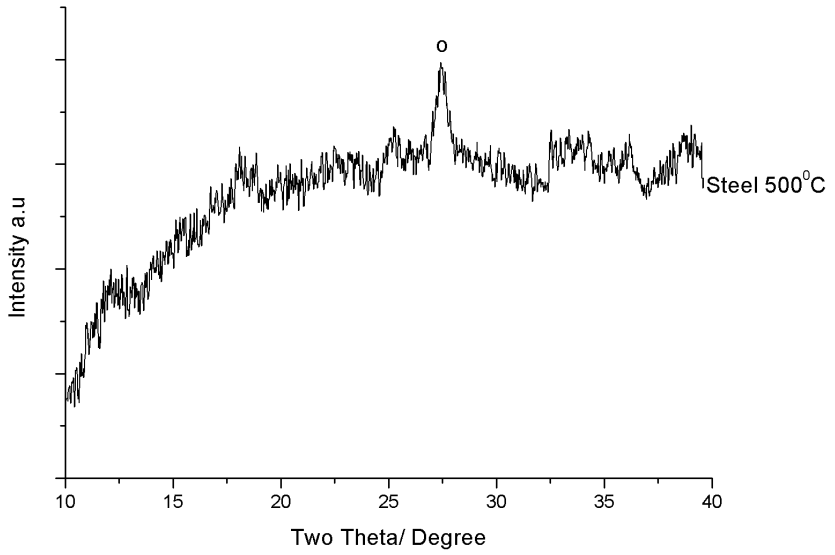

Figure 3.1(c). XRD pattern of as deposited TiO_2 Film on steel substrate from the AACVD reaction of TTIP at *500°C in methanol solvent, showing the peaks that correspond to anatase (x) and rutile (o).*

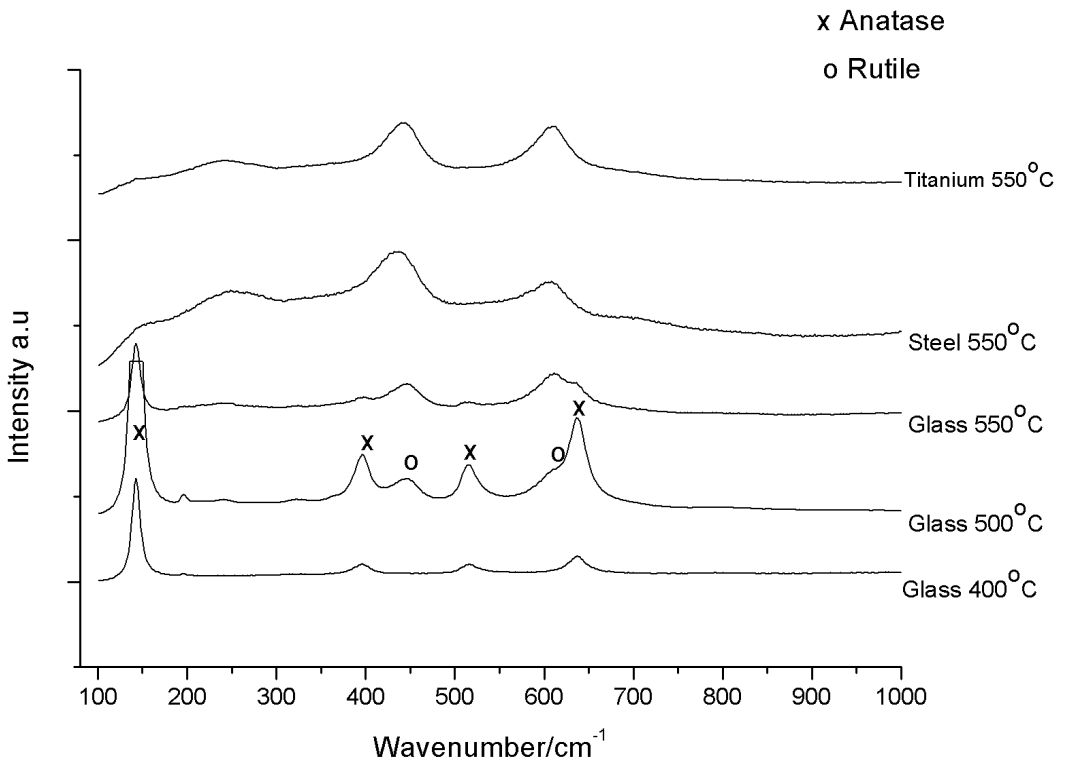

Figure 3.2. Raman spectrum of as deposited TiO_2 film from the AACVD reaction of TTIP in methanol solvent on glass, steel and titanium substrates at different temperature as stated on the figures; (x) is anatase and (0) is rutile.

3.5.2.Variation of thickness

A gross variation in the film thickness was achieved by simply varying the deposition time, deposition rates were fairly uniform at around 5 nm min^{-1} for the central portion of the film.

Growth Rate = Film thickness nm/deposition time minutes

Growth rate = 300 nm/60 minutes = 5 nm/min^{-1}

The Raman spectra of the films produced at 15, 30, 45 and 75 minutes on glass at 550°C is shown in Figure 3.3. Spectra were recorded at different portions of the film and they were all found to be identical confirming the uniformity of

the deposition achieved through this AACVD method. Surprisingly it was observed that the phase changes during deposition with deposition time. For films prepared at 500°C it was observed that at 15 minutes, exclusively the anatase phase was formed. A rutile component was only observed after 45 minutes deposition time, this then became the exclusive form deposited after 75 minutes of deposition. To our knowledge this is the first report of phase control simply by varying the deposition time. Anatase is laid down first as the primary phase, however after a longer deposition time rutile becomes the dominant phase and overlaps the anatase layer. This correlates in part with rutile being the more thermodynamically favoured phase. It should be noted that the heated block was at the correct elevated temperature during all the depositions.

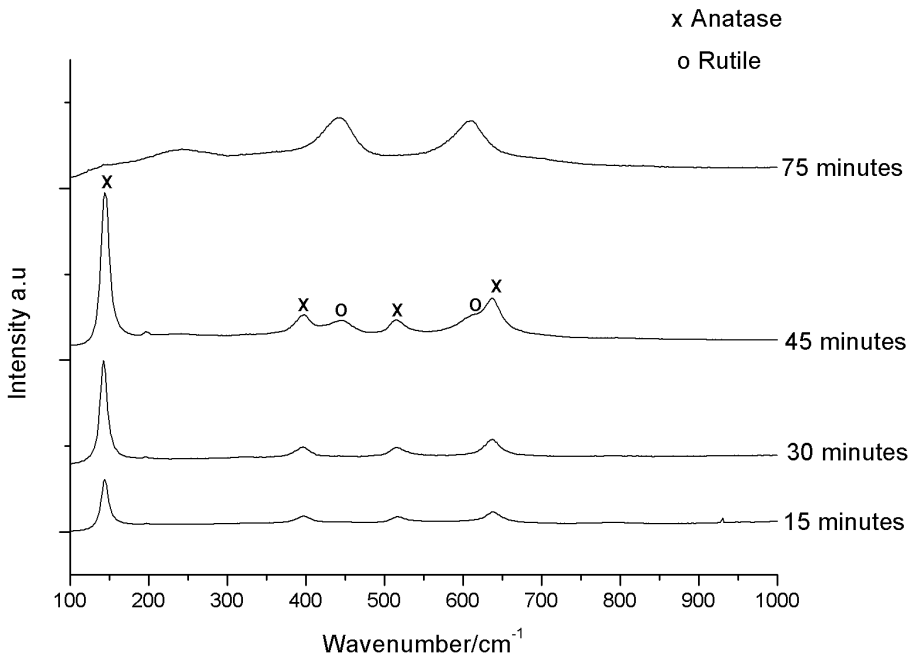

Figure 3.3. Raman pattern of as deposited TiO_2 Films formed by AACVD reaction of TTIP in methanol at 550°C on glass substrate, at different deposition time; (x) is anatase and (0) is rutile.

3.5.3. Film Morphology and Properties

The SEM of the films produced on glass, steel and titanium by AACVD of TTIP are shown in figure 3.4. It was observed that the morphology of the films was radically different from what is expected when using AACVD where spherical particles are common because the reaction often involves a significant gas phase reaction within the aerosol droplet.[12] In these experiments the particle shapes suggest that the reaction must be taking place at the surface. Cross sectional SEM images showed that the surface consisted of angular projections. The depositions on glass showed a largely amorphous film formed at 400°C and that angular crystallites with well defined shapes formed at 500°C and above with the crystallites becoming larger with deposition temperature. The morphology of the films on the metal substrates showed defined block and angular shaped crystallites at 400°C- 500°C. At a deposition temperature of 550°C needle like particles are observed. The shapes of the thin films on the steel are very usual and might be due to the morphology of the substrate interacting with the TiO_2 deposited.

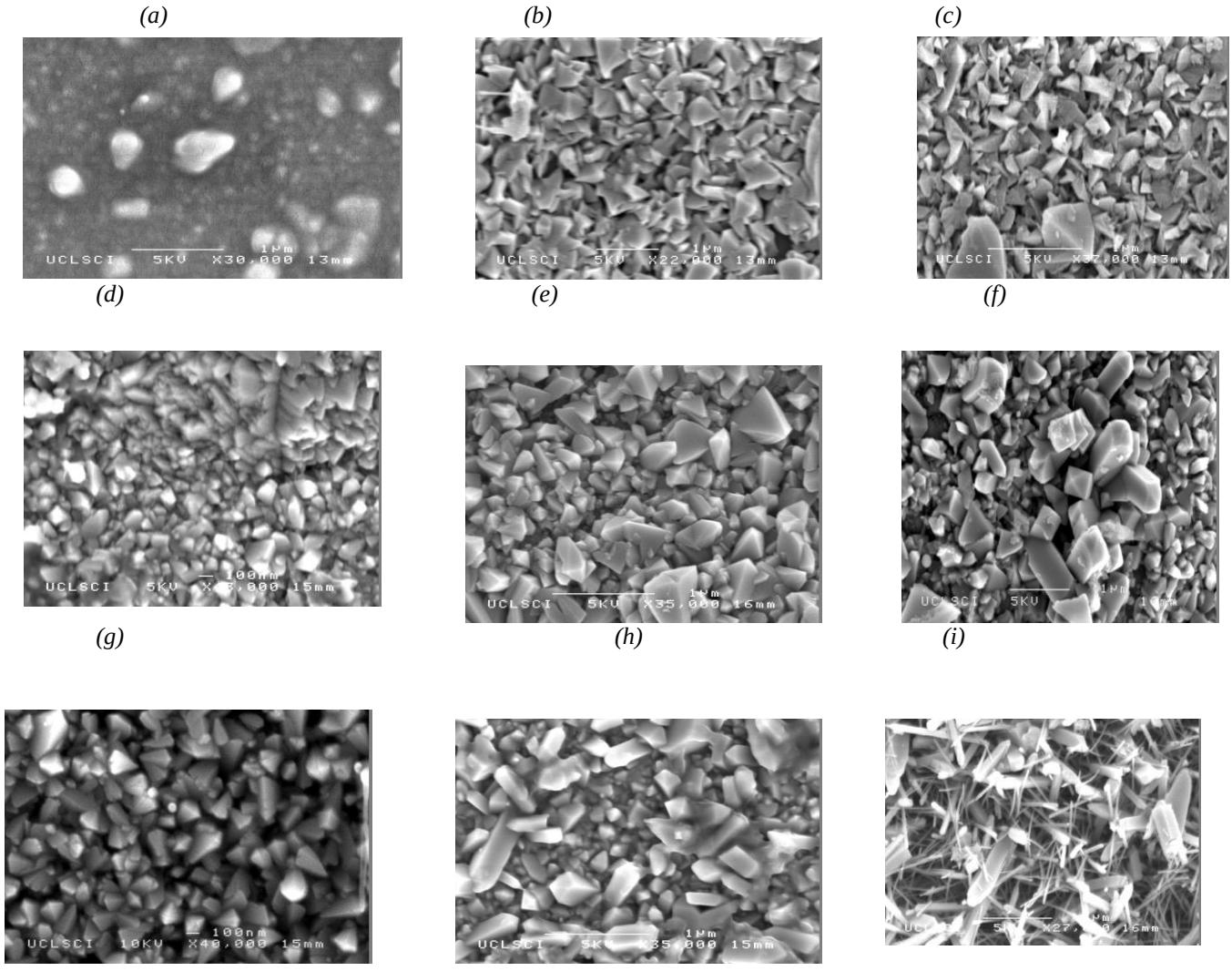

Figure 3.4. Top down SEM of TiO_2 Film as deposited by AACVD reaction of TTIP in methanol solvent *on (a) glass at 400°C, (b) glass at 500°C, (c) glass at 550°C, (d) titanium at 400°C, (e) titanium at 500°C, (f) titanium at 550°C, (g) steel at 400°C, (h) steel at 500°C, and (i) steel at 550°C.*

3.5.4. Photo-activity of the titanium dioxide films

An intelligent ink Resazurin (Rz) was used to monitor the photoactivity of the titania films formed on glass at 400 and 500°C by AACVD of TTIP in methanol. The photocatalytic reduction was monitored via digital photographic methods with the films changing colour from blue to pink to

colourless which follows the complete reduction of the dye induced by the titania photocatalysis. Notably a blank glass slide sprayed with the intelligent ink showed no changes in colour for the duration of the experiment. It took 45 minutes for the films produced at 400°C on glass to completely photodegrade the reazurin dye whilst is took 35 minutes for the films deposited at 500°C to turn colourless. Figure 3.5(a) and 3.5(b) shows the images at recorded 0, 1, 10 and 35 minutes for both films. From the images it can be seen that the rate of photocatalysis scales with film thickness, as the thicker central portion changes colour most rapidly and the thinner edge portions change more slowly. This shows that the thickness of the films has an effect in increasing the photocatalysis of the films as it provides a higher surface area for the reaction.

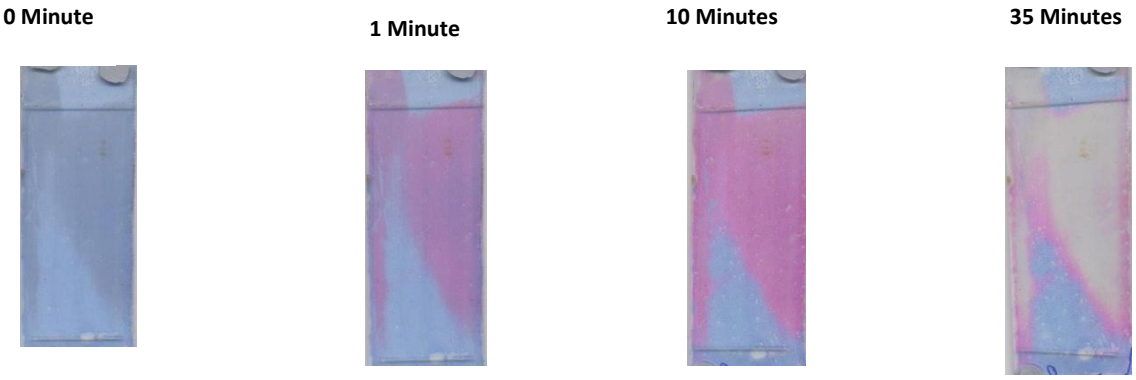

Figure 3.5(a). Photographs of the changes in colour of resazurin intelligent ink sprayed onto a film of anatase/rutile (45 x 90 mm) formed at 400°C by AACVD on glass. The intelligent ink changes from blue →pink→ colourless under irradiation with 365 nm light for 0, 1, 10, and 35 minutes

Figure 3.5(b) . Photographs of the changes in colour of resazurin intelligent ink sprayed onto a film of anatase/rutile (45x90 mm) formed at 500°C by AACVD on glass. The intelligent ink changes from blue → pink → colourless under irradiation with 365 nm light for 0, 1, 10, and 35 minutes.

3.5.5. Water droplets contact angles

Table 3.2 shows the water contact angles measured for the titanium dioxide films that were deposited on three different substrates- glass, steel and titanium metal. Titanium dioxide has been widely reported to be hydrophilic and frequently shows photoinduced superhydrophilicity,[5] especially when irradiated with ultraviolet light.[13] This process is due to both the removal of surface contamination due to photocatalysis and the formation of surface hydroxyl groups. The films produced at 400 and 500°C on all substrates were slightly hydrophilic as they have a water contact angle less than 90^{o}. The unusual films are those produced at 550°C, on both steel and titanium which have water contact angles well above 90^{o} which reflects the hydrophobic character. Figure 3.6 shows the side on SEM images of the films formed on steel and glass at 550°C. It can be seen from the SEM measurements that the surfaces are highly rough with projections that stick up from the substrate.

Table 3.2 water contact angles of as deposited TiO_2 thin films on steel, titanium and glass substrates before and after irradiation with 254 nm light for 30 minutes.

Substrate	**Contact angle before irradiation (^{o})**	**Contact angle After irradiation (^{o})**	**Contact angle 3 days after irradiation (^{o})**	**Contact angle After heating at 100°C for 60 minutes (^{o})**
Steel 400°C	71	7	20	62
Steel 500°C	60	30	60	76
Steel 550°C	109	5	40	80
Titanium 400°C	61	20	41	61
Titanium 500°C	59	23	50	67
Titanium 550°C	110	4	36	78
Glass 400°C	97	6	40	57
Glass 500°C	80	2	35	54
Glass 550°C	101	4	36	65

(a) *(b)*

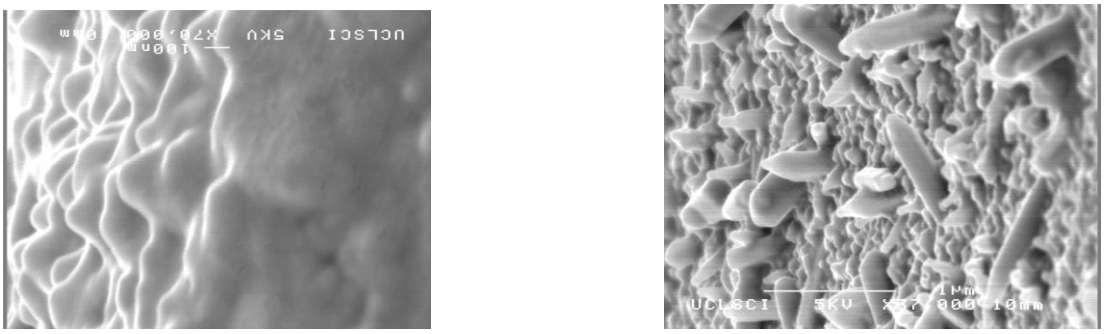

Figure 3.6. Side on SEM pattern of TiO_2 Films as deposited by AACVD reaction of TTIP in methanol *on (a) titanium and (b) steel substrates at 550°C.*

3.5.6. Wenzel or Cassie-Baxter surface

There are two explanations of how a surface can interact with water, the Wenzel and Cassie-Baxter models.[14,15]Both models use the contact angle between the droplet of water and the surface as a measurement of the hydophobicity of the film. In the Cassie Baxter model the water does not completely penetrate the surface porosity, has air trapped under the droplet and the surface is typically slippery for water droplets. In the Wenzel model the water droplet fully penetrates the surface porosity. In both models surface roughness encourages extreme behaviour- with rough surfaces magnifying the underlying hydrophilicity or hydrophobicity. In the case of the films formed at 550°C the Cassie-Baxter model is the probable reason why the surface is hydrophobic as the roughness of the films at this temperature is high and this causes air to be trapped under the water droplet which in turn causes the surface to be slippery and increases the contact angles.[16] After irradiation with UV light of 254 nm for 2 hours the water contact angles of the films formed at 550°C on titanium and steel is typically 5° - superhydrophillic. In this case on irradiation the surface becomes hydroxylated and the water droplets fully wet the surface and the surface becomes water loving. This change over in behaviour has been studied previously and related to structural changes on the surface. The surface Ti^{4+} sites are reduced to Ti^{3+} states by the photogenerated electrons and oxygen vacancies generated. Repeated dissociation of the water adsorbed on the vacancy sites produced hydroxyl groups.

The films formed at 550°C that were rendered superhydrophillic were left in the dark for two days and the measured water contact angle significantly

increased back to the hydrophobic state. This is due to water drying out and the hydroxylated surface is removed. The same samples were also heated at 100°C for an hour and this was also noted to increases the water contact angle. The increase in water contact angle after heating is due to the removal of some surface hydroxyl groups on the titania surface.

This switch from hydrophobic to superhydrophillic is an uncommon phenomenon. Parkin's group have made a wide series of titania films previously by a variety of methods and have not observed this phenomena, the starting water contact angles were never higher than 90° reported in previous studies.[10-16] We attribute this effect to the formation of the highly rough surface, consisting of both needles and projections on the surface formed from the AACVD method – as well as a probable lack of surface hydroxyl group.

3.5.7. Water splitting

Thin films of titania deposited using AACVD onto steel and titanium substrates were tested for their ability to photosplit water in a sacrificial system. The films were coated on the reverse with platinum. The ability of TiO_2 to photocatalyse the oxidation of water to O_2 by persulfate was determined using UV-light. Previous studies have shown that titanium dioxide films can be used to generate oxygen without the need of an additional oxygen catalyst because titania has enough overpotential to produce an effective reaction.[17,18] Table 3.3 shows the rate at which oxygen is produced. From the values shown in Table 3 we see that all the films are photocatalytically active to a great extent with oxygen values as high as 2.02×10^{-4} mol $min^{-1}m^{-2}$ for titania deposited steel and 8.09×10^{-4} mol $min^{-1}m^{-2}$ on titanium.[19] These values

are amongst the highest ever reported and surprisingly are from the rutile polymorphs. Parkin et al.[19] previously reported values between 1.8 – 9.6 mol $min^{-1}m^{-2}$ for films deposited by APCVD (rutile) and Kitano et al.[23] reported a maximum rate of 0.2 $molg^{-1}s^{-1}$ deposited by RF sputtering using a 0.05m $AgNO_3$ sacrificial solution. These rates are close to the rates observed in the films deposited in this thesis.

Anatase has been reported to be more active for the photoreduction of O_2 making it more photoactive in the decomposition of harmful organic materials.[20,21] This can be used to explain the higher rate of oxygen evacuation using the rutile phase as the rutile phase is less active in the photoreduction of O_2.[22] Has discussed in chapter 1 the reduction of O_2 is unwanted in the backward reaction that can happen during photo water-splitting reactions.

Table 3.3, the rate of oxygen generated using as deposited TiO_2 on steel and titanium in mol $min^{-1}m^{-2}$

Steel 400°C	9.48E-05	Titanium 400°C	6.91E-04
Steel 500°C	2.02E-04	Titanium 500°C	6.81E-04
Steel 550°C	1.32E-04	Titanium 550°C	8.09E-04

3.5.8. Anatase vs Rutile cross-over

This work shows that the substrate used in the aerosol assisted chemical vapour deposition has an important role in determining the phase of TiO_2 deposited. On steel substrates at 550°C in the absence of a solvent, TTIP was

shown to form exclusively anatase with the APCVD method. However addition of methanol as a carrier solvent in an AACVD setup allowed only the rutile phase to be formed. It is possible that the use of methanol aerosol causes distinct changes in the precursor, especially during transport into the heated reactor. It would be expected that an alcohol exchange would occur where the methoxide group is coordinated to the metal and ^{i}PrOH is eliminated. This will be explored in chapter 7.

Furthermore the deposition time could also have a major effect. Thin films grown by AACVD have typical growth rates of 100-200 nm min^{-1}, whereas the aerosol process is comparatively slow with growth rates of 5 nm min^{-1}. The faster growth rate forms exclusively anatase whilst the slower growth forms only rutile. The observation correlates with the work of Hitchman who found rutile was favoured by slower growth rates.[8]

3.6. Conclusion

The effect of temperature and substrate on the morphology, phases and properties of TiO_2 thin films formed from TTIP by AACVD was investigated. The substrate had a key role in determining the phase produced in the reaction with metal surfaces producing exclusively rutile whilst glass formed anatase, anatase/rutile mixtures or pure rutile depending on both the susbtrate temperature and the deposition times with the more thermodynamically favoured rutile formed at the longest deposition times and highest temperatures. There was also a great variety in the morphology of the films formed at different temperatures and substrate types. Unusually the very rough microstructure engendered hydrophobic titania surfaces. This work is one of the first examples of using an aerosol to deliver a CVD precursor that is

routinely used at low pressure or atmospheric pressure. It shows that the aerosol has a key role to play in dictating the morphology of the film grown on the surface and that it acts not just as a transport reagent. For example use of TTIP as an APCVD precursor produced exclusively anatase on steel substrates whilst use of the methanol aerosol formed exclusively rutile. It is also reported in this work that the films formed are amongst the best reported for the photosplitting of water and were active photocatalysts.

3.7. References

1. S. Nishimura, A. Shishido, N. Abrams, T. E. Mallouk, *Appl. Phys. Lett.* **2002**, 81, 4532.
2. C. W. Dunnill, G. Hyett and I. P. Parkin, *Edu. in Chem.*, **2010**, 47, 1
3. C. Page, M. Wilson, I. P. Parkin, *J. Mater. Chem*, **2009**, 19, 7381
4. S. Noimark, C. Dunnill, M. Wilson. I. P. Parkin, *Chem. Soc. Rev*. **2009**, 38, 3435.
5. G. Hyett, M. Green. I. P. Parkin, *J. Am. Chem. Soc.*, **2006**, 128, 12147.
6. P. Evans, M. E. Pemble, D. W. Sheel, *Chem. Mater*, **2006**, 18, 5750.
7. M. G. Nolan, M. E. Pemble, D. W. Sheel, Yates, H. M. *Thin Solid Films*, **2006**, 515.
8. M. L. Hitchman, J. Zhao, *J. Phys. IV France* **1999**, 9, 8.
9. I. P. Parkin, R. G. Palgrave, *J. Mater. Chem*, **2005**, 15, 1689.
10. A. Mills, J. Wang, S. K. Lee and M. Simonsen, Chem. Commun., **2005**, 2721.
11. L. Burgio, R .H.J. Clark, *Spectrochimica Acta part A*, **2001**, 57, 1491.
12. A.L. Hector and I. P. Parkin, *J. Mater. Chem*, **1994**, 4, 279.
13. D. Damiriv, A. R. Baily, C. Ballif, P. Holmes, P. E. Scmid, R. Snjines, F. Levy and V. I. Parvulescu, *Appl. Catal*. B, **2000**, 371, 148.

14. S. A. O'Neill, I. P. Parkin, R. J. Clark, A. Mills and N. Elliott, *J. Mater. Chem*, **2003**, 13, 56.

15. X. P. Wang, Y. Yu, X. F. Hu and L. Gao, *Thin Solid Films*, **2000**, 371, 148.

16. L.A. Brook, P. Evans, H. A. Foster, M. E. Pemble, D. W. Sheel, A. Steele, H. M. Yates, *Surf. and Coatings Techn.*, **2007**, 22, 9373.

17. S. Shafiee and E. Topal, *Energy Policy*, **2009**, 37, 181.

18. A. Fujishima, T. N. Rao and D. A. Tryk, *J. Photochem., Photobiol. C. Photochem. Rev*, **2000**, 1, 1.

19. G. Hyett, A. Mills, J. A. Darr and I. P. Parkin, *Europ. J. Chem. in press.*

20. T. Ohno, K. Sarukawa and M. Matsumura, *J. Phys. Chem. B*, **2001**,105, 2417.

21. T. Ohno, K. Tokieda, S. Higashida, M. Matsumura, *Appl. Catal., A*, **2003**, 244, 383

22. Kazuhiko Maeda *Chem. Commun.*, **2013**, 49, 8404.

23. M. Kitano, M. Takeuchi, M. Matsuoka, J. A. Thomas, M. Anpo, *Catal. Today*, **2007**, 120, 133.

Chapter 4

Solvent effect on the phase and morphology of as deposited TiO_2 thin films

4.1 Chapter overview

This chapter details the effect of using different carrier solvents on the aerosol assisted chemical vapour deposition of titanium dioxide and shows a solvent directing effect in controlling the phase of titanium dioxide deposited on a surface. Titanium tetra-isopropoxide (TTIP) is used as the precursor; methanol, ethanol, isopropanol, dichloromethane and hexane were all studied as carrier solvents for titania deposition on glass and steel plates. The effect of methanol as a carrier solvent is reported and with as little as 10% of methanol to 90% ethanol favouring the deposition of the rutile phase. The effect of surface morphology on the water contact angles of the as deposited films is also reported.

4.2 Introduction

A detailed introduction to titanium dioxides, properties and functions is given in chapter 1. One factor that makes this material so important is its ability to act as a photocatalyst. The anatase form has a band gap energy (Eg) of 3.2 eV and irradiation with UV radiation causes promotion of an electron from the valence band to the conduction band. [1,2] These reactive species then participate in oxidation and reduction processes either within the TiO_2 itself (electron and hole recombination), or with adsorbates at the surface. The major reactive

intermediate species in this reaction is the hydroxyl radical, produced by redox reactions between photo-excited TiO_2 and adsorbed water molecules.[3 4,5]

The structural properties and the phase of the titania films (anatase or rutile or a mix) plays a key role in the applications of the films. TiO_2 nanoparticles have been commercialised (Dugussa P25) with a mixture of anatase 80% and rutile 20%; this mixture is a better photocatalyst than the individual phases.[6] The method of synthesis also provides control on the morphology of the films produced. Sol-gel methods have been used to synthesise TiO_2 micro and nonporous thin films that can be used for catalyst support and photo-catalysis.[7,8] Atmospheric pressure chemical vapour deposition has also been used to synthesise titania films with granular structures that can be used for self-cleaning applications.[9] The aerosol assisted chemical vapour deposition (AACVD) method is a technique commonly used for precursors that have very low vapour pressure but that can be dissolved in a carrier solvent. With AACVD the volatility requirement of the precursor is less important as the solvent acts as the carrier medium. [10]

In aerosol deposition, the solvents play a role in the reaction to the extent that the precursor can react differently with various solvent in the gas phase which may lead to the formation of different intermediates and lead to a different phase of TiO_2. There have been a few reports where a variety of solvents have been used to synthesise TiO_2 using a sol-gel approach and spray pyrolysis.[7]All the reports shows that exclusively anatase was formed using ethanol, isopropanol, and toluene and also using supercritical CO_2 solvent.[8]

This chapter shows that the use of different solvents in an aerosol can have a direct effect in controlling the phase of titanium dioxide deposited on a surface.

4.3 Experimental

Thin films of TiO_2 were deposited using aerosol assisted chemical vapour deposition (AACVD) on stainless steel substrates (Goodmans, grade 316, dimension 25 x 25 mm and 0.1 mm thickness). Titanum (IV) isopropoxide (TTIP) (97% Aldrich) and methanol (Fisher, reagent grade) were used without any purification. Deposition was carried out on a cold-wall horizontal-bed CVD reactor that was described in chapter 3, and which contains a graphite block heated by a Whatman cartridge heater. TTIP was used as a single source precursor (0.60 ml) and added to methanol (50 ml) and an aerosol was generated at room temperature using a Pifco ultrasonic humidifier. The aerosol was carried into the reactor with carrier gas flow of oxygen free nitrogen gas at 1 Lmin-1 (BOC). The gas flow was continued until the entire precursor was used up. Films were then cooled and stored in air.

A series of depositions on steel substrates was carried out at a substrate temperature of 550°C using methanol, ethanol, isopropanol, dichloromethane, and hexane solvents. All depositions were subject to the same conditions as stated for methanol.

TiO_2 was deposited using TTIP in a mixture of ethanol and methanol as a solvent. Ethanol and methanol mixture, 99% and 1%, 90% and 10%, 85% and 15%, 75% and 25%, 50% and 50% respectively.

4.4 Characterisation

Thin film X-ray diffraction (XRD) measurements were carried out using a Bruker D8 Discover fitted with General Area Detector Diffraction System (GADDS) area detector and Cu $K\alpha_{1+2}$ source. Diffraction patterns were recorded and collected for 30 minutes per sample, using a fixed incident angle of 5^{o}. Scanning electron microscopic (SEM) measurement was carried out on the films to determine surface morphology using a JEOL JSM-6301F field emission SEM at an accelerating voltage of 5 KeV. Raman spectra were obtained with a Renishaw Invia Raman Microscope with a wavelength of 515.5 nm and 50x microscope objective.

The FTA 1000 instrument was used to determine the water contact angles of the deposited films. This instrument uses "drop-shape" analysis to make measurements. It captures video images of liquid droplets (water) on the surface to analyse their shape and size to determine the contact angle. Preliminary NMR was recorded to monitor the exchange reaction between the isopropoxide group on the TTIP and the methoxyl group on the solvents.

The photocatalytic degradation of methylene blue (MB) was analysed by UV–visible spectroscopy over the 400–800 nm range on a PerkinElmer Lambda 25 UV/VIS spectrometer. The as deposited film was centred at designated positions and were affixed to a 281a plastic cuvette transparent on three sides and holed on the fourth. The hole, centred on the test position, was 25 mm high and 8 mm wide; exposing a 2 cm area to the MB solution. An aluminium frame was used to hold the sample and the cuvette together with a silicon seal providing a water tight boundary. The solution was stirred to ensure a uniform diffusion of the system. This ensured that MB solution was in contact with the

photocatalyst TiO_2 surface. The concentration of MB solution was made up such that the maximum absorbance (≈ 650 nm) was approximately 1 absorption unit. The solution was left to equilibrate for an hour in day light before testing. The solution was subsequently irradiated with a 365 nm lamp. The destruction of MB was then followed as a function of time by the change in height of this absorbance maximum in 30 min intervals for a total of 6 hours and then left for 12 hours. This test was carried out on all the films produced with the different carrier solvents. This reaction was carried out on the TiO_2 films produced using methanol and ethanol as carrier solvents.

4.5 Results and discussion

4.5.1 Deposition of titanium dioxide

Titanium dioxide was deposited on steel substrate by AACVD using titanium (IV) isopropoxide TTIP in methanol, ethanol, isopropanol, chloromethane and hexane solvents at 550°C. The films were adhesive, passing the Scotch tape test. In addition they resisted scratching with a 2H pencil and did not dissolve in common solvents and in 2M (HCl) solution. The films on glass were transparent (>75% transmission over the visible region) but they did show a slight white haze when viewed off angle (ca 5% haze measurement dependent on specific film). The thicknesses of the as deposited thin films were fairly uniform ca 250 nm to 300 nm across the majority of the films with the thickest portions formed at the centre of the substrate as judged by side on SEM. The average growth rates for the films were typical of AACVD at these precursor concentrations at 5–10 nm/min^{-1}. The growth rate was between this 5-10 nm/min^{-1} for all the solvents used.

It has been previously reported that rutile is favoured by slower growth rates and using methanol as the carrier solvents favours rutile.[22] The phase directing effect of methanol to form rutile is probably due to the lack of a beta-hydrogen centre on the methanol, because at least two hydrogen is needed for beta-hydride elimination reaction. Using ethoxide or propoxide as the carrier solvent allows for a beta-hydride elimination decomposition pathway. This is able to explain why methanol favours the rutile phase as methoxide probably causes a lower growth rate compare to the other solvent with more than one carbon. Methyl group is usually used to avoid beta-hydride elimination processes. [23]

4.5.2 Film characterisation and analysis of films deposited using Ethanol, Methanol, Isopropanol, Hexane and chloromethane.

The X-ray diffraction patterns of the films grown using methanol as a solvent, showed reflections exclusively related to the rutile phase when deposited on the steel substrates (figure 4.1). The peaks in X-ray diffraction corresponds to the 1 1 0, 1 0 1 and 2 1 1 reflections. From reference sources we expect the 1 1 0 peak to be the most intense but we observe some preferred orientation for the <1 0 1>and <2 1 1> peaks. [17] Figure 4.3 shows the XRD patterns of the TiO_2 films produced using ethanol as the solvent which indicates the presence of the pure anatase phase. The XRD patterns of films produced on steel substrates using non alcohol solvents; in particular, dichloromethane and hexane also shows exclusively the anatase phase.

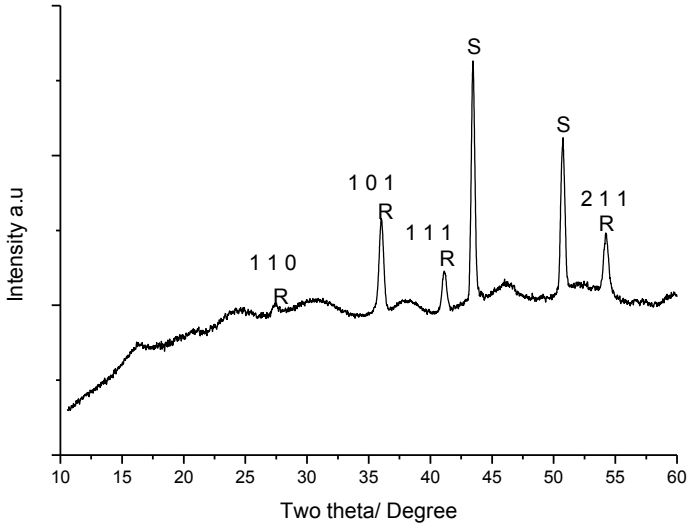

Figure 4.1. XRD pattern of as deposited TiO_2 Film on steel substrate at 550°C, TTIP with methanol carrier solvent, showing the peaks that correspond to anatase A and rutile R.

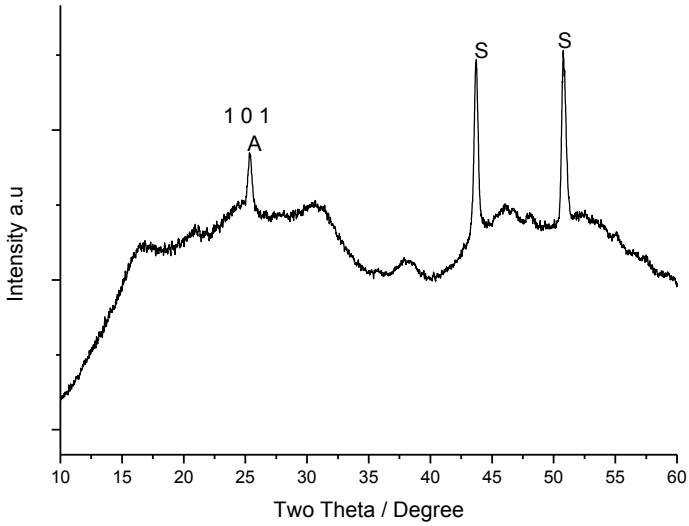

Figure 4.2. XRD pattern of as deposited TiO_2 Film on steel substrate at 550°C, ethanol carrier solvent, showing the peaks that correspond to anatase A and rutile R.

The Raman spectra for the TiO_2 films as deposited on steel using methanol as carrier solvent shows peaks at 144, 232, 447 and 609 cm^{-1} which clearly indicates the presence of the rutile phase and this result is consistent with those reported in the literature [14] (see figure 4.2). These results are consistent with the findings of the XRD analysis. The Raman spectra of TiO_2 deposited on steel at the same temperature using all the other solvents apart from methanol show that only the anatase form is present with peaks at 143, 396, 516 and 639 cm^{-1}, figures 4.3 and 4.4.

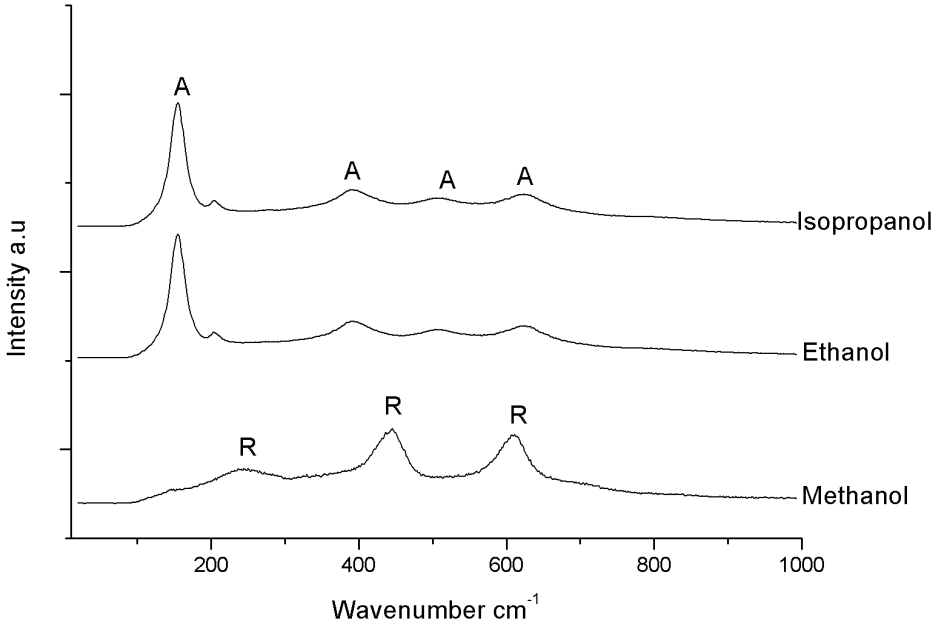

Figure 4.3. Raman pattern of as deposited TiO_2 film by AACVD on steel using TTIP in different solvents (methanol, ethanol and isopropanol) as stated on the figure; anatase A and rutile R.

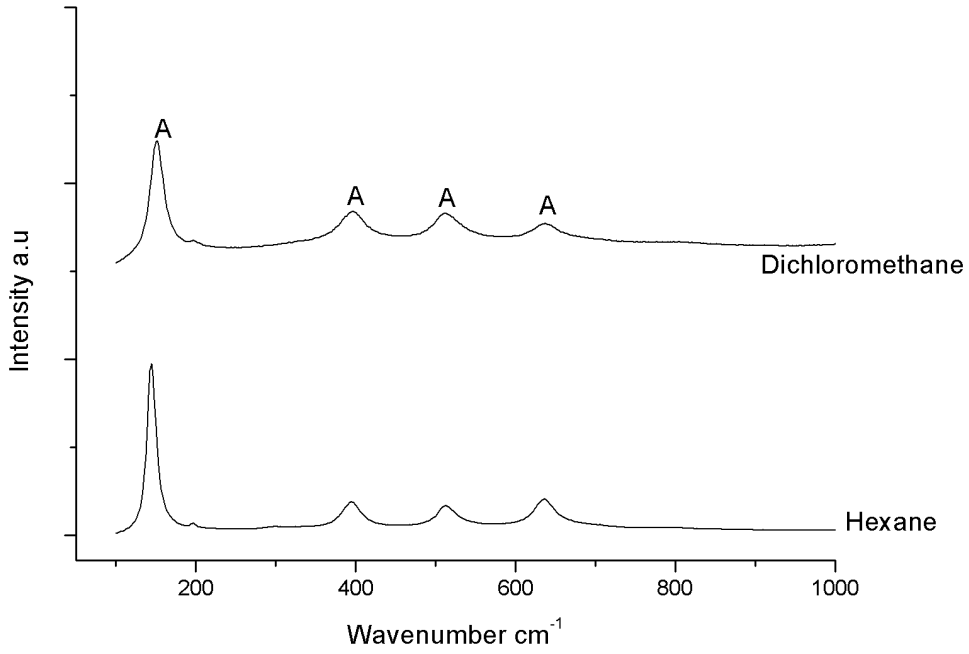

Figure 4.4. Raman pattern of as deposited TiO_2 film by AACVD on steel using TTIP in different non alcohol solvents (hexane and dicloromethane)as stated on the figure; anatase A and rutile R.

Methanol solvent was shown to be unique from this work. It has been reported previously to undergo a breakdown mechanism and can act as a reducing or an oxidising agent. Jackson et al reported that methanol dissociates at elevated temperatures in the presence of a transition metal catalysts to form carbon dioxide and hydrogen.[18]

4.5.3 Film characterisation and analysis of films deposited using a mixture of ethanol and methanol

TiO_2 films deposited from a mixture of ethanol and methanol aerosol droplets showed interesting results. The XRD pattern of films formed from TTIP with 50:50 and 10:90 ratios of methanol and ethanol respectively are shown in figure 4.4 and 4.6. We observe that the use of an equal mixture of solvents in depositing TiO_2 shows that rutile is the major phase with a preferred orientation of the <1 0 1> and <2 1 1> reflections and the one deposited with 10% of methanol shows little anatase but majorly the rutile phase. A systematic study with various ethanol: methanol ratio was carried out and each film was mapped using Raman spectroscopy. It is interesting to note that the films produced with 50:50 and 75:25 mixtures respectively showed the presence of only the rutile phase. When the concentration of methanol was further reduced to 90:10 a mixture of rutile and anatase phase were detected and only when the solvent ratio of 99:1 was used did we see exclusively the anatase phase. The intense background in the pattern is due to the steel substrate. The XRD pattern of the steel is shown in figure 4.8. The XRD pattern also appears noisy and this is because the films are quite thin and the resulting spectrum is not very clear. A typical map of the Raman spectra is shown in figures 4.8. It appears from our results that methanol solvent acts as

a directing agent forcing TiO_2 to form rutile phase, which, to our knowledge, has never been reported previously. Thus it appears from this investigation that a mixture of two phases or their pure forms, with a certain degree of control over the ratio of two phases can be achieved by controlling the solvent mixture ratio, which could be beneficial for the manufacture of specific titanium dioxide films.

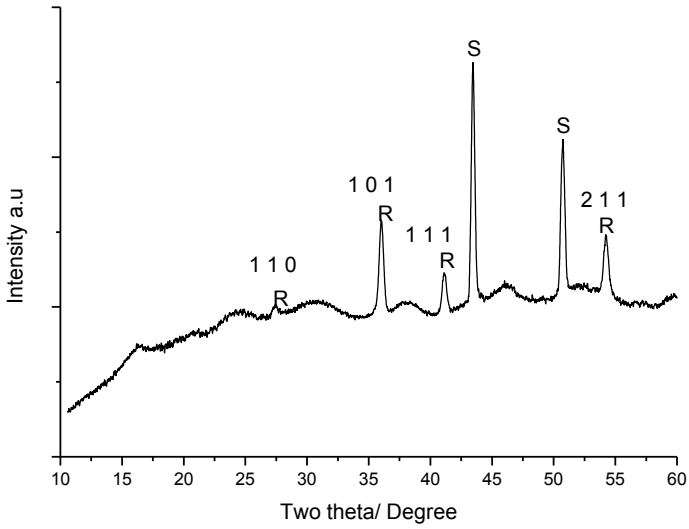

Figure 4.5. XRD pattern of as deposited TiO_2 Film on steel substrate at 550 ° C, TTIP in methanol and ethanol carrier solvent 50:50 ratio, showing the peaks that correspond to anatase A and rutile R.

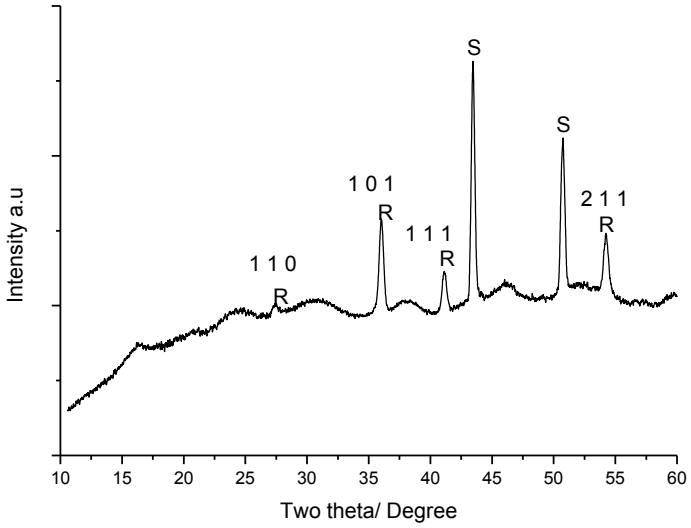

Figure 4.6. XRD pattern of as deposited TiO_2 film on steel substrate at 550°C, TTIP in methanol and ethanol carrier solvent 10:90 ratio, showing the peaks that correspond to anatase A and rutile R.

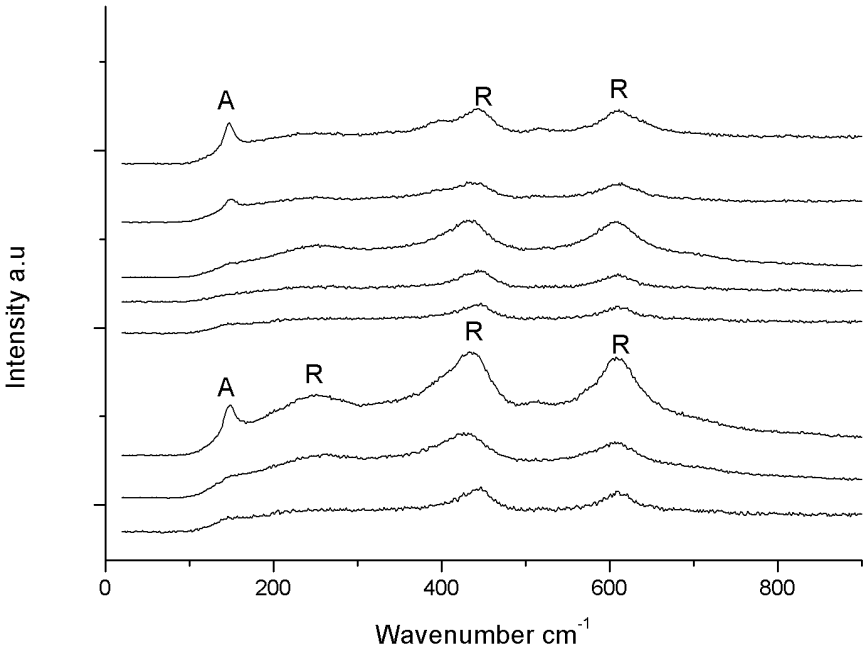

Figure 4.7. Raman pattern of as deposited TiO_2 on steel substrates showing a map across the film deposited. Carrier solvent ratio 10:90 methanol and ethanol with TTIP.

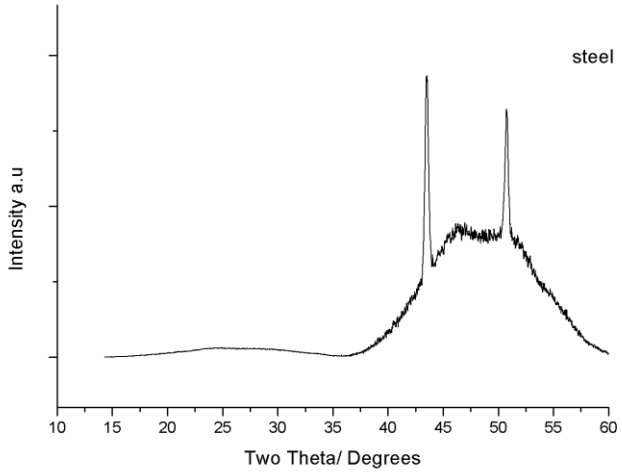

Figure 4.8. XRD pattern of the steel substrate

4.5.4 Preferred orientation

From the XRD data obtained from the as deposited TiO_2 on glass (figures 4.9 and 4.10) on steel substrates at 550^{o}C we observed that there are different orientations with respect to the substrate. TiO_2 deposited on glass has a preferred orientation of 1 1 0 for rutile and 1 0 1 for anatase. This is very interesting because not only can the substrate and the solvent have a combined and an individual effect on the phase deposited whether anatase or rutile. It can also determine the preferred orientation of the deposited film.

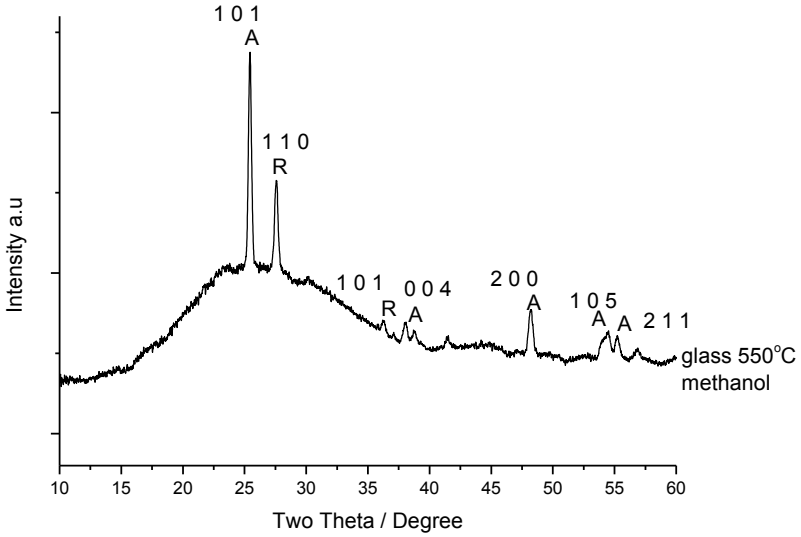

Figure 4.9. XRD pattern of as deposited TiO_2 film on glass substrate at 550°C, TTIP in methanol carrier solvent, showing the peaks that correspond to anatase A and rutile R.

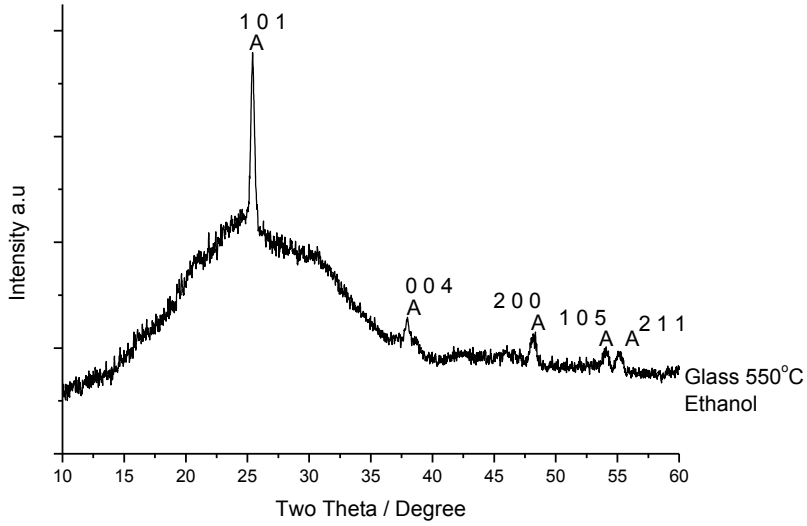

Figure 4.10 . XRD pattern of as deposited TiO_2 film on glass substrate at 550°C, TTIP in ethanol carrier solvent, showing the peaks that correspond to anatase A and rutile R.

4.5.5 SEM analysis and Contact angles

The SEM images of the as deposited TiO_2 thin films are shown in figure 4.11. Block like particles shapes are formed when methanol and ethanol mixtures are used as carrier solvent whilst the films produced using methanol shows needle like particles as seen in SEM of TiO_2 deposited on steel substrates. The water contact angles of all the films shown in Table 1 are all around or above 100^o. This indicates that the hydrophobic nature of the films which is due to the roughness of this structure which enables air to be trapped between the particles and stops water from fully wetting the surface, a typical Cassie-Baxter phenomenon associated with hydrophobic character. [16,19].

(a) (b)

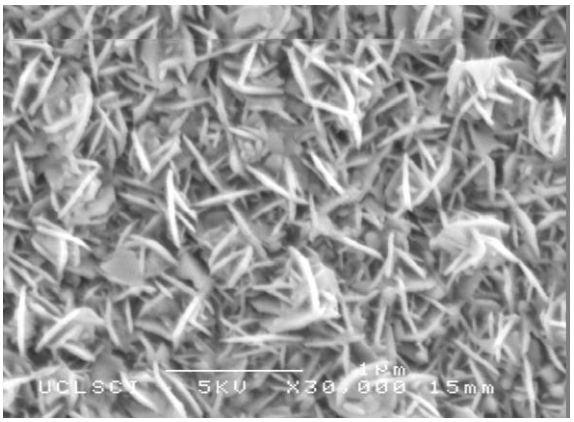

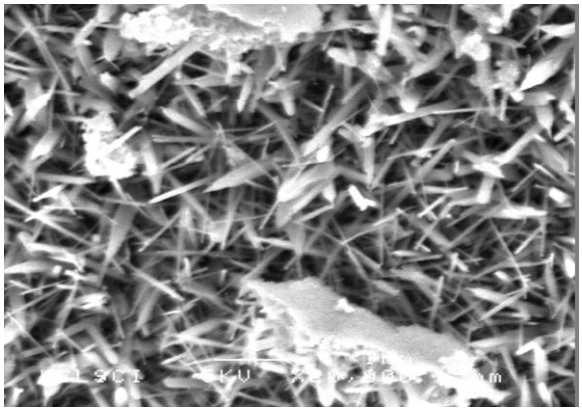

(c) (d)

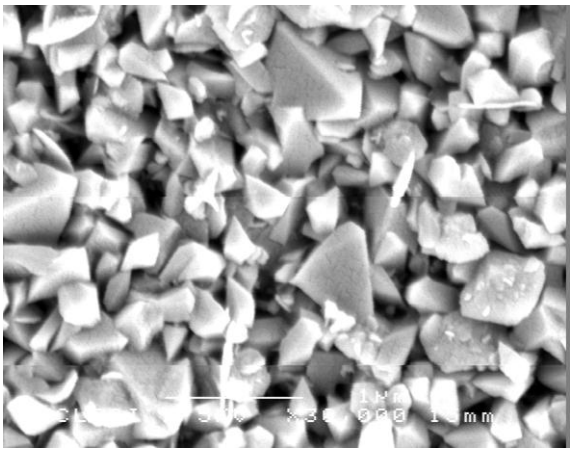

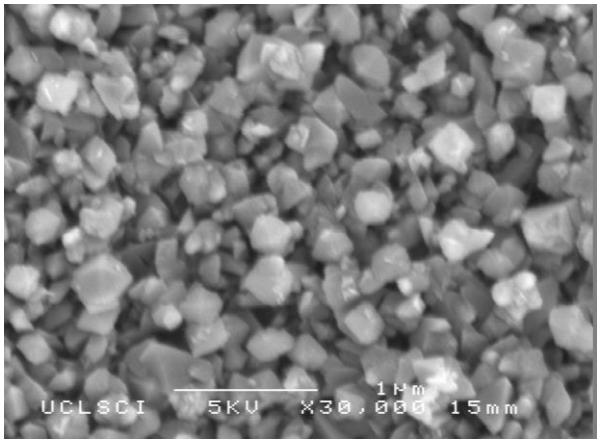

Figure 4.11. Top down SEM of TiO_2 film as deposited on steel by AACVD using different mixture of carrier solvents, (a) ethanol 100%, (b) methanol 100%, (c) 10% methanol and 90% ethanol, (d) 25% methanol and 75% ethanol.

When pre-irradiated with 365 nm light the measured water contact angles is less than 5^{o} and becomes super-hydrophillic this is because the surface becomes hydroxylated and wetting becomes easier.[15] Films that were left after pre-irradiation, in the dark for three days had measured water contact angles of 60^{o} suggesting the reversibility of hydrophobic character of the films. These films could be very useful for self-cleaning applications, since the hydrophilic and hydrophobic natures of the TiO_2 films can be reversible. The contact angles recorded for the TiO_2 thin films deposited with a mixture of ethanol and methanol solvent have a slightly lower contact angle compared to when 100% of both solvents are used. This clearly shows the effect of surface morphology on contact angles as the SEM of the mixtures shows block particles which are less rough compared to the SEM of the films formed from pure methanol and ethanol. The contact angles recorded when mixed carrier solvents are used is slightly lower than when pure methanol or pure ethanol is used. For example when the solvent ratio is 75:25 ethanol and methanol respectively the water contact angle was 99^{o} as shown in Table 1. This correlates with the SEM shown in figure 4.12(d) that shows large blocks compared to when pure methanol or ethanol is used where we observe needle like particles. This clearly shows that the surface roughness has a direct effect on the water contact angle recorded. As already described in chapter 3 the TiO_2 deposited on steel substrate is hydrophobic because it has a Wenze-type surface and the Wenzel model states that an increase in surface roughness will magnify the water-contact angle properties of a material. A hydrophobic surface will increase its water contact angle (above 90^{o}) when the surface roughness

increases and a hydrophillic surface will reduce its water contact angle (below 90^{o}) when surface roughness increases.[24]

Table 4.1 Water contact angles of as deposited TiO_2 on steel substrates using methanol and ethanol as carrier solvents at $550^{o}C$ before and after irradiation with 254 nm light for 60 minutes.

Solvents	**Contact angle before irradiation (^{o})**	**Contact angle After irradiation (^{o})**	**Contact angle 3 days after irradiation (^{o})**
Ethanol	115	0	50
Methanol	120	2	65
50:50 Ethanol and methanol	98	5	50
75:25 Ethanol and methanol	99	7	60
90:10 Ethanol and methanol	98	5	40

4.5.6 Photo-activity analysis

TiO_2 is an active photocatalyst and it is able to oxidise dirt and organic molecules on its surface when exposed to UV radiation. The films deposited with methanol as the carrier solvent exclusively produced the rutile phase which has been previously reported to have a lower photocatalytic activity than the anatase phase.[15] The TiO_2 films deposited with ethanol, isopropanol, dichloromethane and hexane all produce only the anatase phase of TiO_2. The results of the methyl blue test are shown in figures 4.13 (a) and (b). From the graphs showing reactivity, we see that the films produced with ethanol as the carrier solvent (anatase) are almost six times more active in the degradation of the organic dye with a rate of 1.11×10^{12} molecules destroyed per second compared to 3.28×10^{11} molecules destroyed per second with the film deposited using methanol (rutile) as shown in figure 4.14. This result correlates with previous studies of anatase and rutile photocatalysts, where it

has been suggested that rutile is a less active photocatalyst due to its relative instability of photo-generated electrons and holes.[15]

(a)

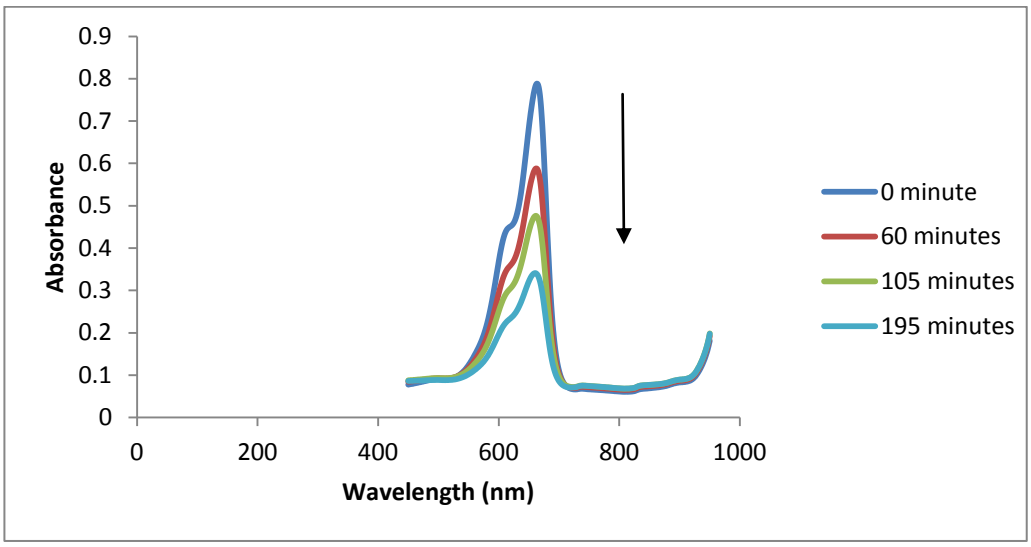

(b)

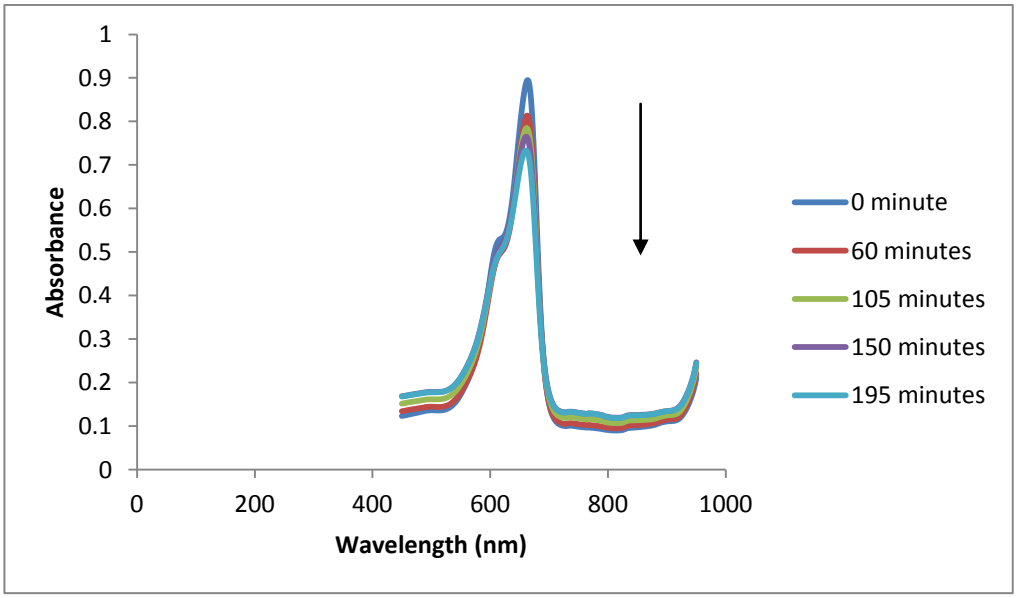

Figure 4.12 (a) and (b). Graph showing the rate of depletion of methylene blue (in minutes) reaction on TiO_2 deposited on steel deposited using ethanol (anatase) and methanol (rutile) respectively.

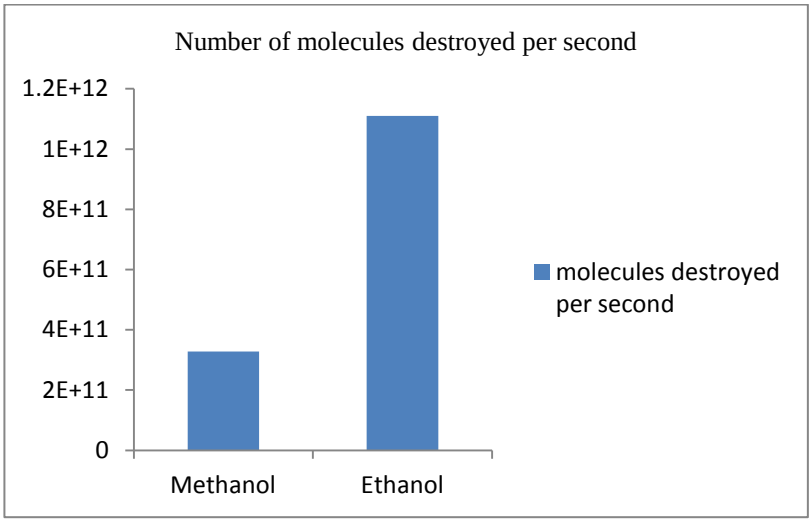

Figure 4.13. Chart of the number of methylene blue molecules destroyed per second on TiO_2 films deposited using methanol and ethanol.

4.6. Conclusion

The effect of solvents on the phase of TiO_2 produced has been studied using AACVD. We have shown here that under identical conditions using methanol as the carrier solvent produces exclusively the rutile phase whilst the other solvents produce only the anatase phase. More interestingly we have shown that a mixture of ethanol and methanol as the carrier solvent produces only the rutile phase at a mixture of as low as 90% ethanol and 10% methanol. This shows that the methanol has a directing effect to produce the rutile phase. We have also shown that the TiO_2 films deposited on steel substrates are photo-catalytically active and the rutile is less photo active than the anatase phase. We have also shown that the deposited TiO_2 films are hydrophobic in nature with water contact angles above 100^0 but can be rendered hydrophillic after irradiation with UV. The contact angles have been shown to be reversible when left in the dark.

4.7. References

1. I. P. Parkin, R. G. Palgrave, *J. Mater. Chem.*, **2005**, 15, 1689.
2. A. Mills and S. LeHunte, *J. of Photochem. and Photobiol. A. Chemistry*, **1997**, 108, 1.
3. K. Page, M.Wilson, I. Parkin. *J. Mater. Chem.*, **2009**, 19, 3819.
4. S. Nishimura, A. Shishido, N. Abrams, T. E. Mallouk, *Appl. Phys. Lett*. **2002**, 81, 4532.
5. A. Mills, N. Elliot, S. Bhopal, I. P. Parkin, S. A. O'Neill, R.J Clark, *J. Photochem. Photobiol, A: Chem*, **2002**, 151, 171.
6. Ohno T, Sarukawa K, Tokieda K, Matsumura M, *J. Catal*, **2001**,203,82.
7. X. Liu, Z. Jin, S. Bu, T. Yin, *J. Sol-Gel Sci. and Techn.*, **2005**, 36, 103.
8. R. Yuan, X. Fu, P. Liu, X.Wang. *Scripta Materialia*., **2006**, 55, 1001.
9. T. D. Manning, I. P. Parkin, R. J. H. Clark, D Sheel, M. E. Pemble, D.Vernadou, *J. Mater. Chem*., **2002**, 12, 2936.
10. X. Hou, K L. Choy, *Chem. Vap. Deposition*, **2006**, 12, 583.
11. C. Edusi, G. Hyett, G. Sankar, I. P. Parkin, *Chem. Vap. Deposition*, **2011**,17, 30.
12. P. Evans, M. E. Pemble and D. W. Sheel, *Chem. Mater*., **2006**, 18, 5750-63; M. G. Nolan, M. E. Pemble, D. W. Sheel, Yates, H. M. *Thin Solid Films*, **2006**, 515.
13. A. Mills, J. Wang, S. K. Lee and M. Simonsen, *Chem. Commun*, **2005**, 2721.
14. L. Burgio, R .H .J. Clark, *Spectrochimica Acta part A*, **2001**, 57, 1491.
15. A. Fujishima, K. Hahimoto, H. Irie, *Jpn. J. Appl. Phys*., **2005**, 44, 8269.

16. B. Sun, P. G. Smirniotis, *Catal. Today*, **2003**, 88, 49.

17. L.A. Brook, P. Evans, H. A. Foster, M. E. Pemble, D. W. Sheel, A. Steele and H. M. Yates, *Surf. and Coatings Techn.*, **2007**, 22-23, 9373.

18. G. Hyett, A. Mills, J. A. Darr and I. P. Parkin, *Chem. Vap. Deposition*, **2010**, 16, 301.

19. S. D. Jackson, D.S. Anderson, G. J. Kelly, T. Lear, D. Lennon and S. R. Segal, *Top. Catal.*, **2003**, 22, 173.

20. C. R. Crick and I. P. Parkin, *Chem. Eur. J,* **2010**, 16, 3568.

21. M. Langlet, J. C. Joubert, *Chem. Adv. Mater*, **1992**, 55.

22. L.Kavan, M. Gratzel, *Electrochim. Acta.*, **1995**, 40, 643.

23. B.K. Bower, H. G. Tennent, *J. Am. Chem. Soc.*, **1972**, 94, 2512.

24. L. Hitchman, J. Zhao, *J. Phys. IV France*, **1999**, 9, 8

25. R. N. Wenzel, *Ind. Eng. Chem.*, **1936**, 28, 988.

Chapter 5. XANES mapping of TiO_2 thin films

5.1. Chapter overview

In this chapter X-ray absorption spectroscopy (XAS) was used to map across the surface of as deposited TiO_2 thin films deposited by the AACVD of titanum (IV) isopropoxide (TTIP) in methanol and ethanol. Deposition was carried out on glass and steel substrates at 550°C. The X-ray absorption near edge structure (XANES) was used to determine the phase of TiO_2 present at each point on the substrate using linear combination analysis.

5.2. Introduction

The deposited phase of TiO_2 thin films of either anatase or rutile has a great effect on its activity making it important to study the growth process of TiO_2.[1,2] Anatase and rutile forms of TiO_2 are great photocatalysts but a mixture of both in 3:1 ratio (P-25 Dugussa) is a much better photocatalyst and has been used in several studies.[5, 6]Studying the growth of TiO_2 thin films will provide evidence in how to vary the ratio of the phase deposited and potentially in improving the effectiveness of TiO_2 as a photocatalyst.

Different characterisation methods were used to derive the structure-function relationships of graded film compositions[15,17] including scanning electron microscopy (SEM), X-ray diffraction (XRD) and Raman spectroscopy. It has been reported in the previous chapter that the phase of titania deposited is affected by the carrier solvent employed in the deposition using AACVD. Methanol in particular deposits exclusively the rutile phase on steel substrates

and ethanol, isopropanol and hexane produces anatase on steel substrates.[12] Although ex-situ characterisation by XRD and Raman spectroscopy revealed the formation of a poorly crystalline TiO_2 phase, these techniques do not provide any evidence of an amorphous titanium dioxide component in the films.

Micro X-ray absorption spectroscopy (μXAS) is an effective characterisation technique to look at complex mixtures because unlike XRD it is not restricted to compounds with long-range order, so it is able to provide information on the local structure in heterogeneous materials either in the crystalline or amorphous systems. X-ray absorption spectroscopy at the Ti K-edge of TiO_2, is well known to be sensitive to the respective phases, although electronic and geometric (first neighbour) interactions are important. Therefore, this technique, in particular X-ray absorption near edge structure (XANES) is ideal to determine the structure and phase composition of titanium dioxide.[18] To our knowledge this is the first application of micro-XANES to a CVD derived film.

5.3. Experimental

Thin films of titanium dioxide were deposited using aerosol assisted chemical vapour deposition (AACVD) on glass (SiO_2 coated float-glass of dimensions 45 x 90 mm) and stainless steel substrates (Goodmans, 250 μm thickness) of dimension 25 x 25 mm. Titanum (IV) isopropoxide (TTIP) (97% Aldrich), methanol (Fisher, reagent grade) and ethanol (AnalaR Normapur) were all used without any purification. The deposition was carried out on a cold-wall horizontal-bed CVD reactor that contains a graphite block heated by a Whatman cartridge heater. The glass substrate was provided by Pilkington-

NSG. Deposition of thin films was carried out on the SiO_2 barrier layer side of the glass to prevent the migration of ions from the glass bulk into the film. The steel foil was placed on top of a glass substrate which was placed on top of the carbon heater block. A glass top-plate was positioned parallel and above the substrate, and the whole set up was contained within a quartz tube. TTIP was (0.60 ml) was added to methanol (50 ml) and an aerosol was generated at room temperature using a Pifco ultrasonic humidifier. The aerosol was carried into the reactor with carrier gas flow of oxygen free nitrogen gas at 1 $Lmin^{-1}$ (BOC). The gas flow was continued until the entire precursor was used up. Films were then cooled and stored in air. The same reaction was repeated with ethanol as the carrier solvent.

5.4. Characterisation of deposited films

µXAS measurements were carried out on the I18 microfocus spectroscopy beam line at Diamond Light Source UK. µXAS (at the Titanium K edge) were recorded in fluorescence mode, in the energy range of 4.94 to 5.04 keV to collect the XANES data, employing a beam size of ca 5 microns and each scan was collected over a ~ 3 min scan time. Figure 5.2 contains the reactor setup highlighting flow direction and the mapping sequence.

The Athena program was used to obtain normalised data and linear combination analysis was performed to determine the phase of TiO_2 present at each point on the substrate using pure anatase and rutile TiO_2 as standards.[14]

Thin film X-ray diffraction (XRD) measurements were carried out using a Bruker D8 Discover diffractometer fitted with a GADDS area detector and Cu

$K\alpha_{1+2}$ source. Diffraction patterns were recorded and collected for 30 minutes per sample, using a fixed incident angle of 10^o for glass and 5^o for steel and titanium plates. Scanning electron microscopic (SEM) measurement was carried out on the films to determine surface morphology using a JEOL JSM-6301F field emission SEM at an accelerating voltage of 5 KeV. Raman spectra were obtained with a Renishaw Invia Raman Microscope with a wavelength of 515.5 nm and 50x microscope objective.

5.5. Results and discussion

5.5.1. Deposition of Titanium dioxide

Titanium dioxide thin films were deposited on glass and steel substrate by AACVD using TTIP in methanol and ethanol solvents at 550°C. The films were adhesive and passed the Scotch tape test. In addition they resisted scratching with a 2H pencil and did not dissolve in common solvents and in 2M (HCl) solution. The films on glass were transparent but they showed a slight white haze when viewed off angle. The film thickness was fairly uniform between 250 – 300 nm as determined using side on SEM. A tilted SEM is shown in figure 3.6 to illustrate the microstructure.

5.5.2. Film characterisation and analysis using µXANES XRD, and Raman on glass substrates

TiO_2 K edge X-ray Absorption Near Edge Structure (µ*XANES*) map was carried out on thin films deposited on glass and steel plates. The mapping was done in an H shape fashion every 2.5 mm to give a good coverage of the films deposited (Figure 5.1).

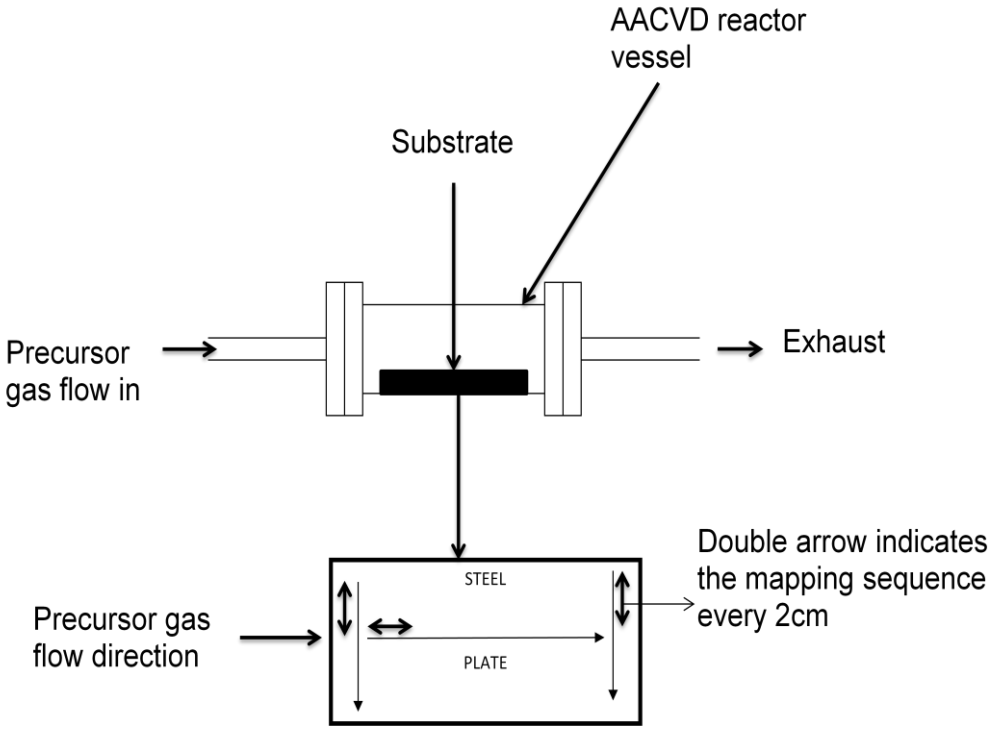

Figure 5.1. The H shape mapping sequence of as deposited TiO_2 films. The arrow ⟶ represents the direction of the mapping, µXANES spectra was recorded every 2.5 mm spacing along the arrow mark using a 50 micron beam. The gas flow direction of the precursor is shown in the setup.

The process to normalise the XANES data has already been discussed in Chapter 2. The normalised standard spectrum of pure anatase and rutile phase is shown in Figure 5.2. The Ti K-edge XANES spectra of the background was subtracted and after normalisation shows that rutile and anatase both have a tetragonal structure and in both, the Ti atom is coordinated to six oxygen atoms. Figure 5.2 shows that there is the transition from 1s to 3d in the pre-edge region. Although both rutile and anatase are tetragonal the major structural difference between them is due to the way the octahedral are deformed and linked together.[8]

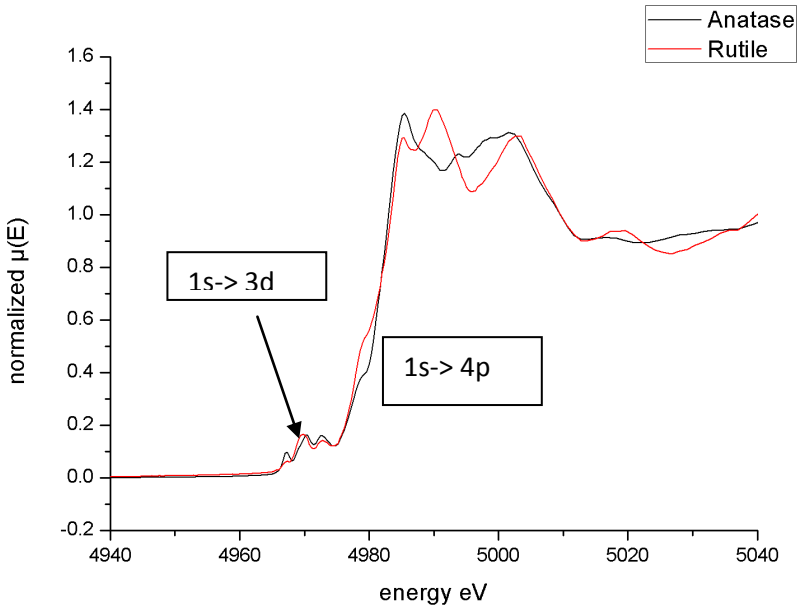

Figure 5.2 normalised XANES standard of anatase powder (Titanium (IV) oxide, anatase 99.8% trace metals basis) and rutile powder (Titanium (IV) oxide, rutile 5 μm, ≥ 99.9% trace metals basis).

The difference in the pre-edge and the edge of anatase and rutile indicates that they both have different long range order.[9] One of the major differences between the anatase and rutile can be seen in the height difference in the 1s-4p transition which has been linked to the difference in crystal structures.[10, 21]

The results of TiO_2 deposited on glass substrate at 550^{o}C using methanol as the carrier solvent are shown in figure 4.9. The XRD shows a mixture of anatase and rutile 5.3(a) and 5.3(b). The Raman spectra also show a mixture of anatase and rutile. The normalised μXANES map shown in figure 5.3c on a 3D line graph further shows a mixture of anatase and rutile.

5.3 (a)

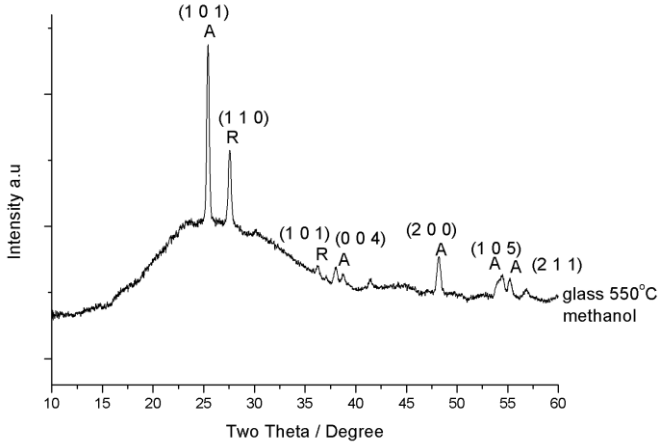

5.3(b)

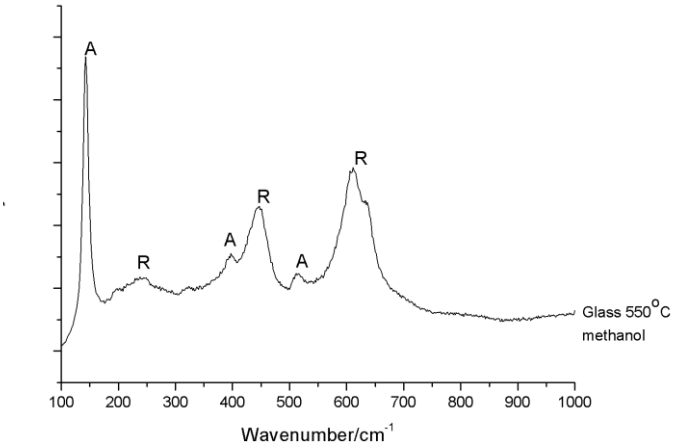

5.3(c)

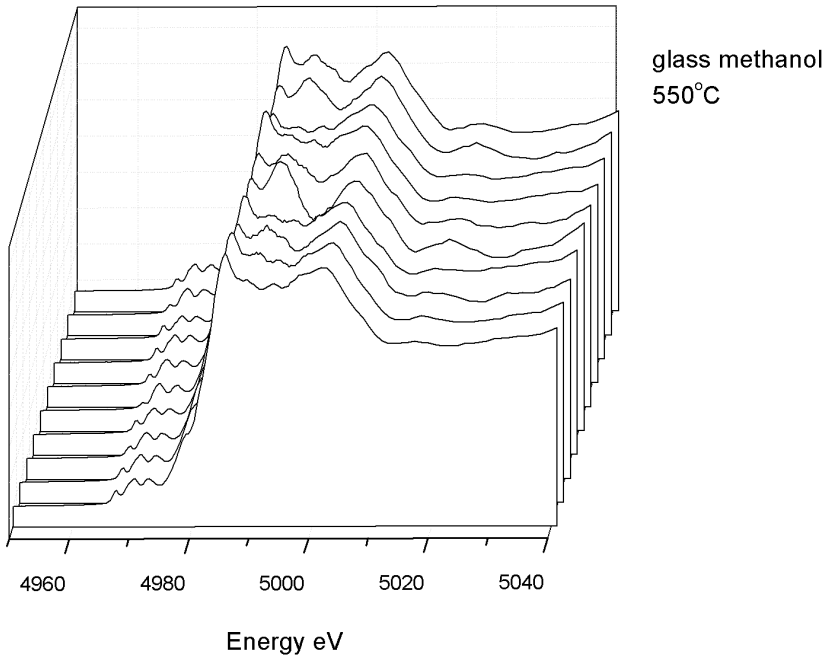

Figure 5.3. (a) XRD pattern, (b) Raman spectra, (c) µXANES mapping of TiO_2 thin film deposited from the AACVD reaction of TTIP in methanol on glass at 550°C.

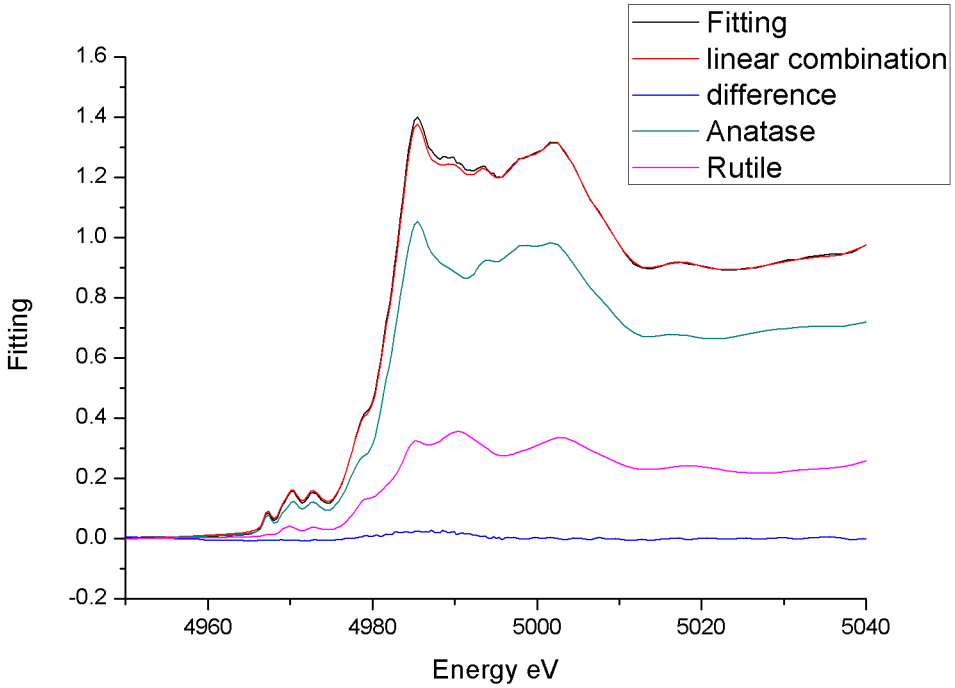

Figure 5.3d. An example of the LCF of a µXANES spectrum of TiO_2 from the AACVD reaction of TTIP in methanol coated on Glass at 550^oC showing best fit and individual components and difference.

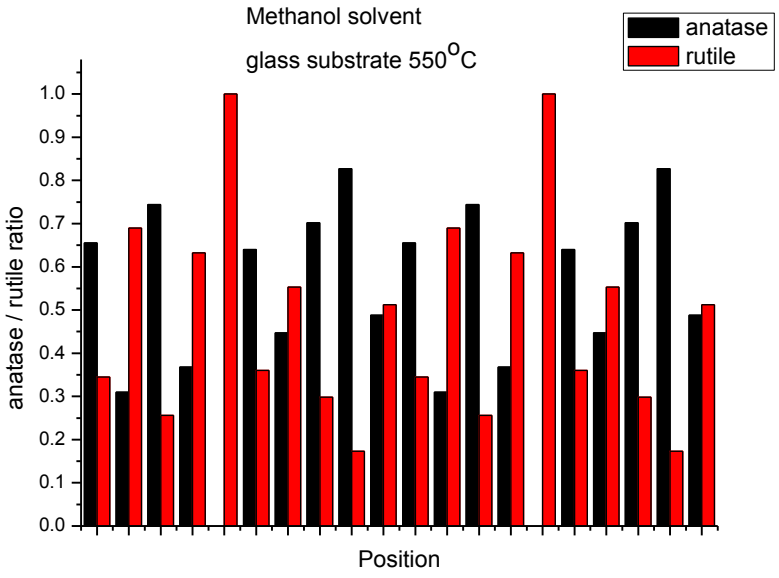

Figure 5.3e. Bar chart of the ratio of anatase and rutile using LCF of the µXANES map of as-deposited TiO_2 thin film deposited from the AACVD reaction of TTIP in methanol on glass at 550^oC.

The linear combination fitting (LCF) analysis of the film was performed using bulk anatase and rutile sample data as references. A typical best fit of one of the spectra is shown in Figure 5.3(d) and a bar graph over the entire film is shown in Figure 4e with an error of +/- 0.01-0.02. This result clearly demonstrates that the deposition produced a heterogeneous distribution of anatase and rutile phases across the film without any identifiable correlation with the gas flow direction. When ethanol was used as a solvent for the deposition of TiO_2 on glass at 550^{o}C, the XRD pattern and Raman spectra shows that the anatase phase is the dominating phase as-deposited, these are shown in Figure 5.3(a) and 5.3(b); the µXANES data also matches that of anatase shown in figure 5.2c. The LCF analysis of the µXANES data of this film is shown in Figure 5.4(d) and indicates that about 90 percent of the deposited material is the anatase form and a small portion to rutile (~ 10 percent). Figure 5.4(e) is an example of how the LCF analysis was carried on each spot on the substrate. The most striking result is the uniformity of the film phase composition with ethanol as the solvent compared to the one produced using methanol as the solvent are shown in figure 4. When methanol is used as the carrier solvent the deposition favours the rutile phase compared to other solvents as already discussed in chapter 4. The methanol solvent has a phase directing effect.

5.4(a)

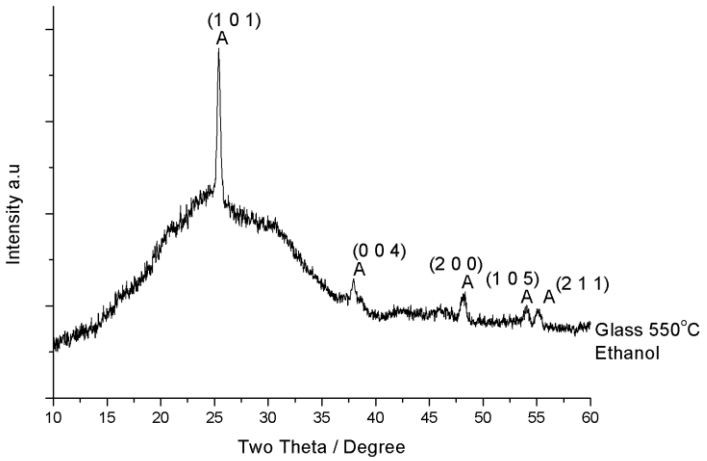

5.4(b)

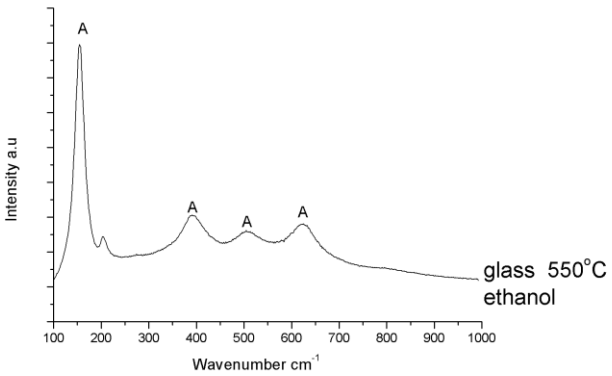

5.4(c)

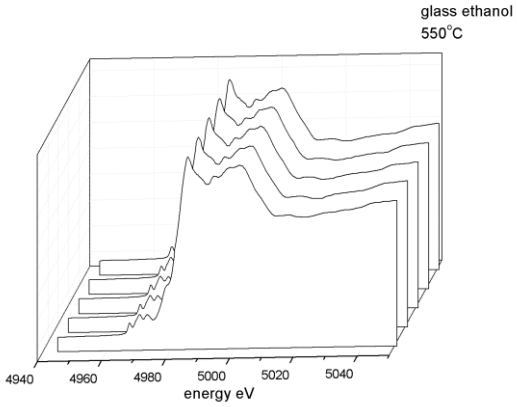

5.4(d)

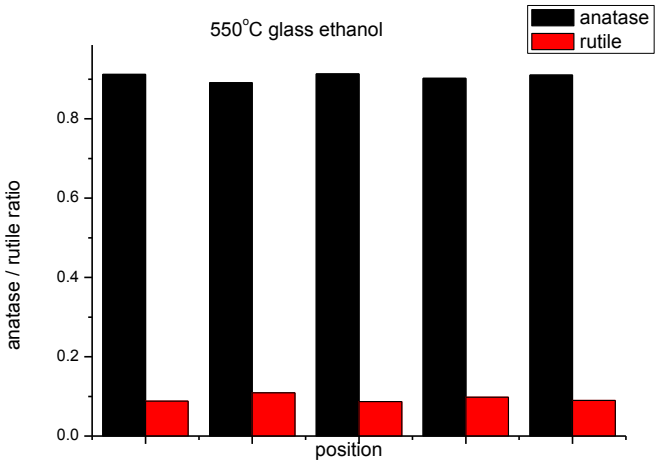

Figure 5.4. (a) XRD pattern, (b) Raman spectra, (c) µXANES mapping (d) LCF bar chart of TiO_2 thin film deposited from the AACVD reaction of TTIP in ethanol on glass at 550°C.

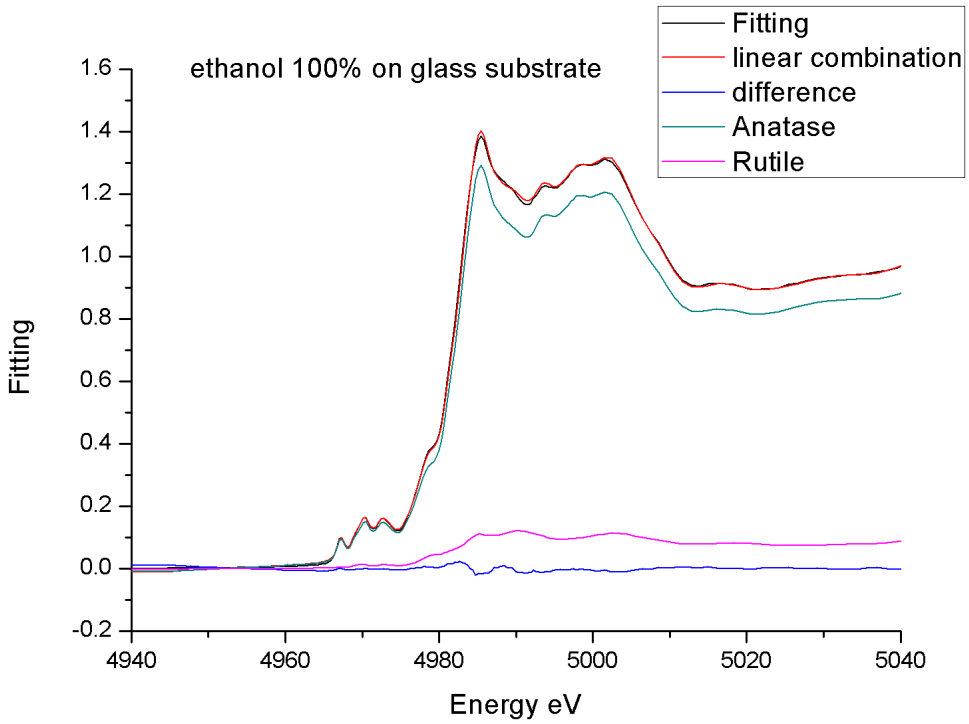

Figure 5.4e. An example of the LCF of a µXANES spectrum of TiO_2 from the AACVD reaction of TTIP in ethanol coated on Glass at 550^oC showing best fit and individual components and difference.

5.5.3. Film characterisation and analysis using µXANES, XRD, and Raman on steel substrates

The X-ray diffraction patterns of as-deposited TiO_2 thin films using methanol as a carrier solvent on steel substrates at 550^oC showed reflections exclusively attributed to the rutile phase as shown in Figure 5.5(a). Figure 5.5(b) shows the Raman spectra recorded for the films using methanol as carrier solvent and it shows peaks at 144, 232, 447 and 609 cm^{-1} which is consistent with those reported in the literature[13] for rutile. These results are consistent with the XRD analysis. The stacked µXANES, shown in Figure 5.5(c) is in agreement with the XRD and Raman results. The linear combination fitting (LCF) analysis of the µXANES data are shown in Figure 5.5(d), using a bar chart of the ratio of anatase and rutile shows the exact ratio of anatase and rutile present in each mapped position. It can be observed from this figure that most of the thin film

is rutile and there is less than 10% anatase present in each mapped position. Thus in contrast to the other characterisation techniques the XAS data indicates the presence of anatase and rutile phase across the film. This implies that XAS is more sensitive for phase analysis in this system.

5.5(a) 5.5(b)

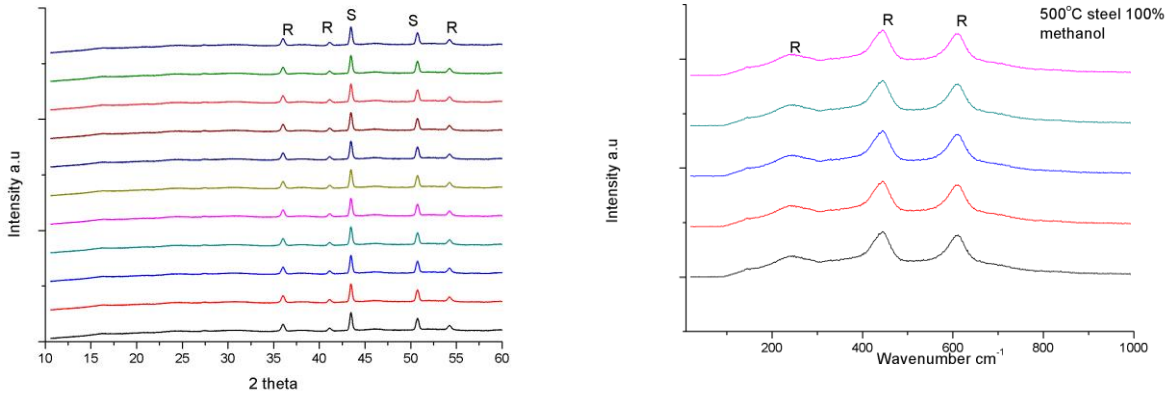

5.5(c) 5.5(d)

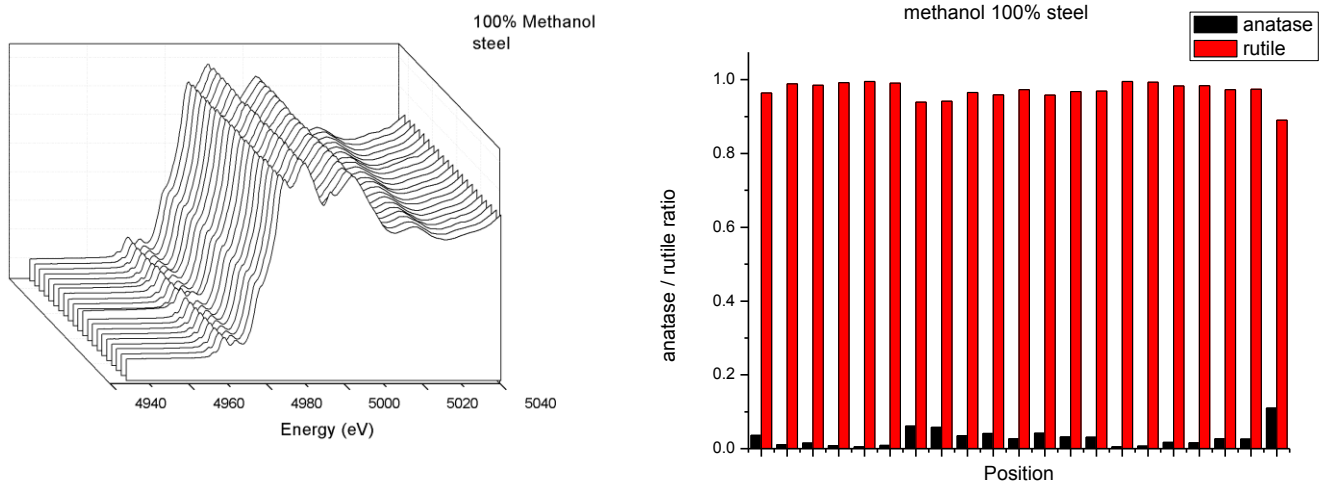

Figure 5.5. (a) XRD pattern, (b) Raman spectra, (c) µXANES mapping, (d) LCF bar chart of TiO_2 thin film deposited from the AACVD reaction of TTIP in 100% methanol on steel at 550°C.

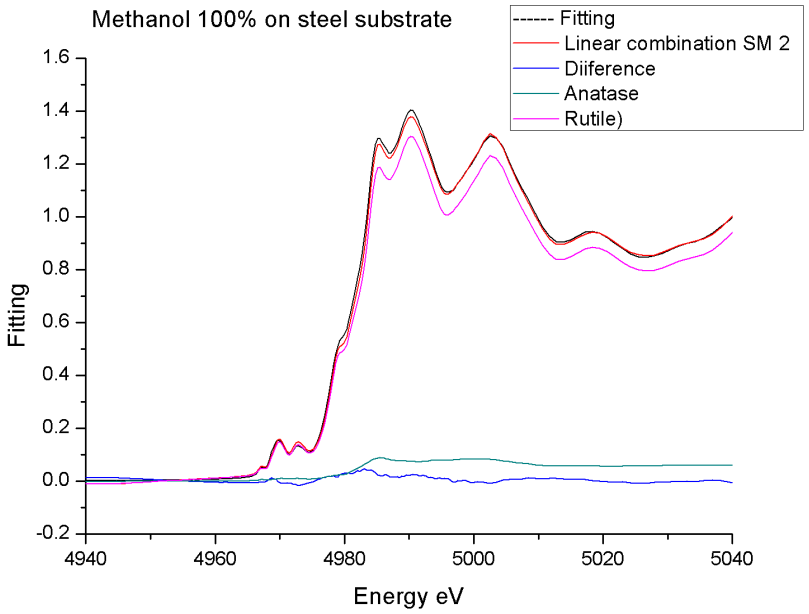

Figure 5.5 e. An example of the LCF of a µXANES spectrum of TiO_2 from the AACVD reaction of TTIP in methanol coated on steel at 550^oC showing best fit and individual components and difference.

The X-ray diffraction pattern and Raman spectra of as deposited TiO_2 thin films using ethanol as a carrier solvent on steel substrates at 550^oC is shown in chapter 4 figure 4.1 and 4.2 respectively and it shows reflections exclusively attributed to the anatase phase however the stacked µXANES, shown in Figure 5.6(a) is in some disagreement with the XRD and Raman results. The linear combination fitting (LCF) analysis of the µXANES data shown in Figure 5.6(b), using a bar chart of the ratio of anatase and rutile shows a mixture of anatase and rutile. An example of how the LCF is achieved is shown in figure 5.6(c). This result was unexpected as several Raman and XRD analysis of TiO_2 films deposited using ethanol as the carrier solvent is dominated by the anatase phase. We attribute this result to an experimental error which might have been due to solvent contamination. It was not possible to carry out another µXANES map of TiO_2 deposited with ethanol carrier solvent on steel substrate because of time limitation on the beamline.

5.6(a) 5.6(b)

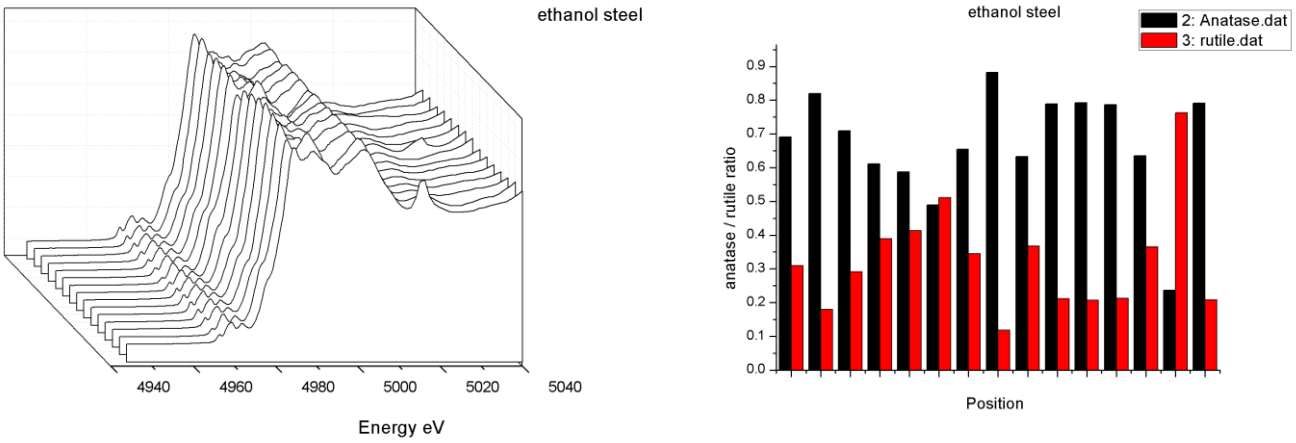

Figure 5.6. (a) µXANES mapping, (b) LCF bar chart of TiO_2 thin film deposited from the AACVD reaction of TTIP in 100% ethanol on steel at 550^oC.

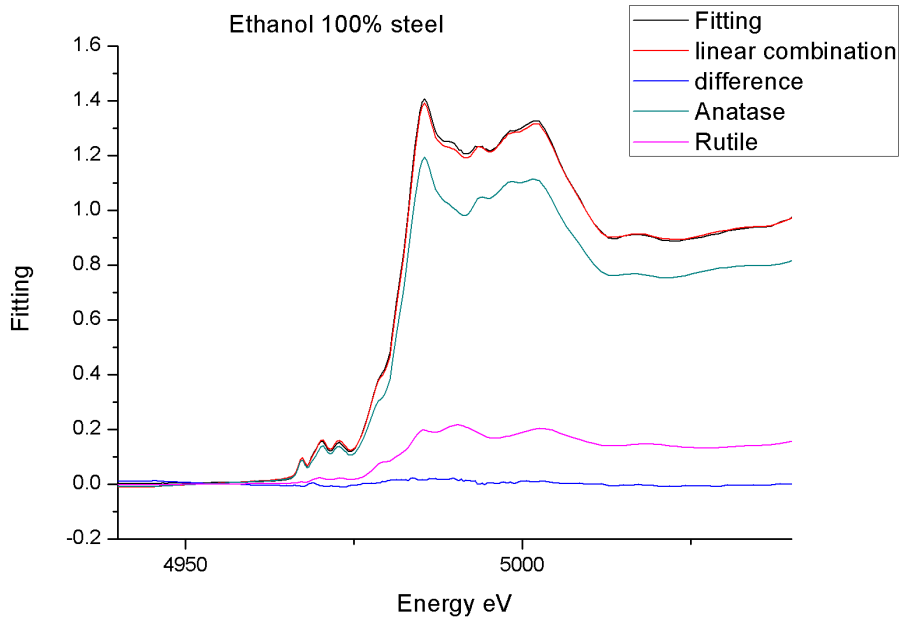

Figure 5.7. An example of the LCF of a µXANES spectrum of TiO_2 from the AACVD reaction of TTIP in ethanol coated on steel at 550^oC showing best fit and individual components and difference.

The solvent effect on the phase of TiO_2 deposited is reported in chapter 4. When methanol is used as a solvent the reaction favours the deposition of rutile compared to other solvents such as ethanol, chloroform and hexane. Figures 5.8 and 5.9 show results from mixtures of methanol and ethanol. It was found that as little as 10% of methanol in a solution of ethanol with TTIP results in more rutile than anatase as shown in Figure 5.9. Figure 5.8 shows the XRD, Raman and µXANES map of a TiO_2 film deposited with 15% methanol and demonstrates that the introduction of methanol clearly favours the deposition of rutile. Using µXANES it has been clearly shown that the deposition of rutile or anatase is independent of the position mapped on the substrate as shown with the glass substrate and that the phase distribution is random.

5.8 (a) 5.8(b)

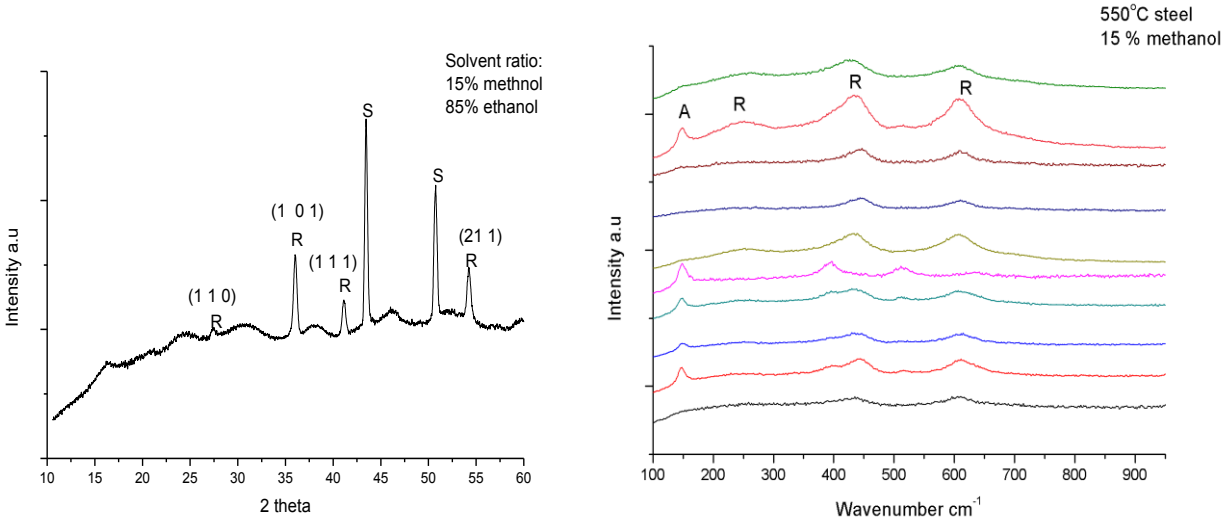

5.8 (c) 5.8(d)

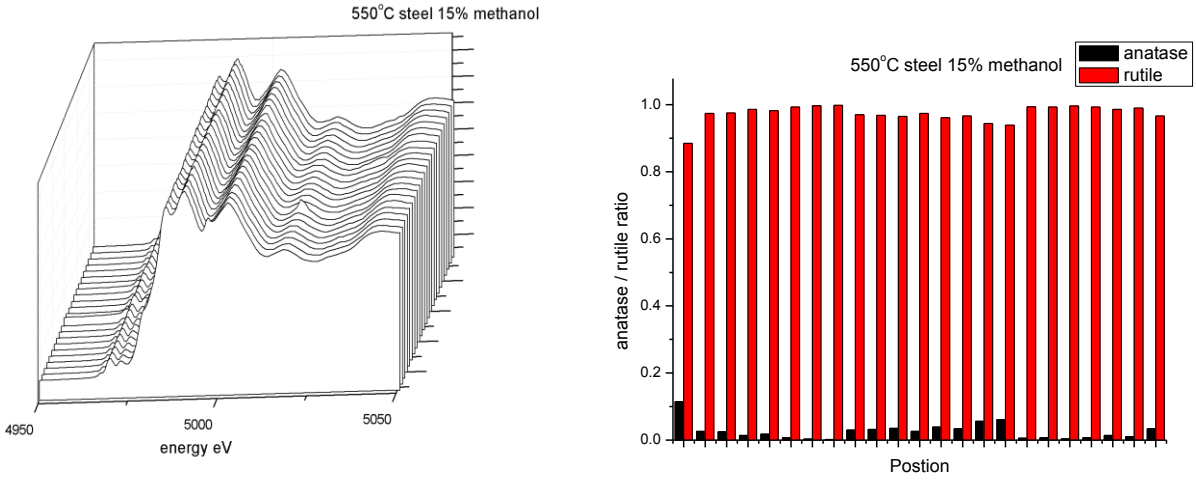

Figure 5.8. (a) XRD pattern, (b) Raman spectra, (c) µXANES mapping, (d) LCF bar chart of TiO_2 thin film deposited from the AACVD reaction of TTIP in 15% methanol and 85% ethanol on steel at 550°C.

5.9 (a) 5.9(b)

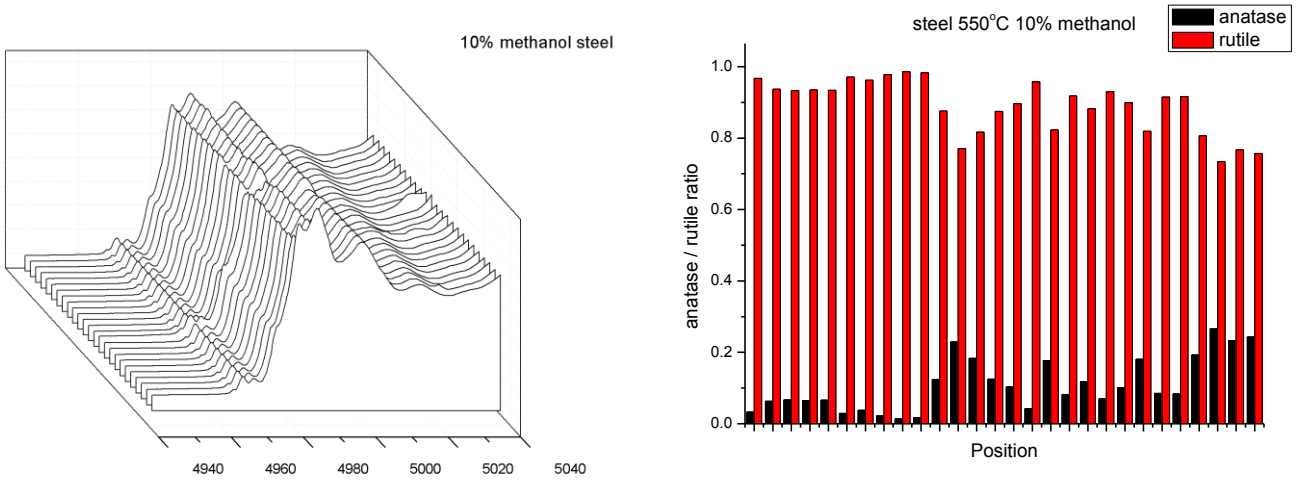

Figure 5.9. (a) µXANES mapping, (b) LCF bar chart of TiO_2 thin film deposited from the AACVD reaction of TTIP in 10% methanol and 90% ethanol on steel at 550°C.

5.6. Conclusion

This chapter shows that μXANES characterisation technique has been effectively used to map as deposited TiO_2 thin films on glass and steel substrates. This chapter shows that the analysis of μXANES data gives clear picture of the percentage ratio of anatase and rutile phase present in the as deposited TiO_2 thin films. It was not possible to correlate the compositional change with gas flow direction as the map shows random deposition of the anatase and rutile phase as particularly on the glass substrates. However, the mapping of the film using Ti K-edge XANES clearly allows us to determine the amount of both phases present at various points of the film, irrespective of the crystalline nature of the system.

To our knowledge this is the first application of XANES mapping on CVD derived films and shows the utility of this technique.

5.7. References

1. A.Mills, N. Elliott, I. Parkin, S.; O'Neill, R. J. Clark, *J. Photochem. Photobiol, A,* **2002**, *151*, 171.

2. A. Mills and S. LeHunte, J. *Photochem.Photobiol A., Chemistry*, **1997**, 108, 1.

3. D'Oliveira, J. C., Minero, C, Pelizzetti, E., and Pichat, P, *J. Photochem. Photobiol. A,* **1993**. 72, 261.

4 C. Edusi, G. Hyett, G. Sankar, I. P. Parkin, *Chem. Vap. Deposition*., **2011**, 17, 30.

5. T. Ohno, K. Sarukawa, K. Tokieda and M. Matsumura, *J. Cataly.*, **2001**, 203, 89.

6. R.I. Bickley, T. Gonzalez-Carreno, J.S. Lees, L. Palmisan, R.D.J. Tilley. *J. Solid State Chem.*, **1991**, 178, 92.

7. G. Tian, Y. Chen, H.-L. Bao, X. Meng, K. Pan, W. Zhou, C. Tian, J.Q. Wang and H. Fu, *J. Mater. Chem.*, **2012**, 22, 2081.

8. L. Bragg and G.F. Claringbu, *Crystal Structures of Minerals*, Bell, London, **1965**.

9. F. Bohr, M.F. Ruiz-Lpez, *Catalysis Letters*, **1993**, 20, 59.

10. L.X. Chen, et al., *J. Phys.Chem. B*, **1997**, 101 .1.

11. S. D. Jackson, D. S. Anderson, G. J. Kelly, T. Lear, D. Lennon, S. R. Segal, *Top. Catal*. **2003**, 22, 173.

12. C. Edusi, G. Sankar and I. P. Parkin, *Chem. Vap. Deposition*, **2012**, 18, 126.

13. L. Burgio, R .H.J Clark, *Spectrochimica Acta part A*, **2001**, 57, 1491.

14. B. Ravel and M. Newville, *J. synchrotron rad.*, **2005**, 12, 537..

15. M. Machida, K. Norimoto, T. Watanabe, K. Hashimoto,,Fujishima, A. *J. Mater. Sci*., **1999**, *34*, 2569.

16. H.Y. Lee, Y. H. Park, K. H. KO., *Langmuir*, **2000**, *16*, 7291.

17. G. Hyett, M. Green, and I. P. Parkin, *J. Am. Chem. Soc.* **2006**, 128, 12147.

18. P.C. Angelomé., *J. Phys. Chem. B*, JP069020Z, in press.

19. J. Stohr, *NEXAFS Spectroscopy*, **1992**.

20. J. F. W. Mosselmans, P. D. Quinn, A. J. Dent, S. A. Cavill, S. D. Moreno, A. Peach, P. J. Leicester, S. J. Keylock, S. R. Gregory, K. D. Atkinson, et al., *J. Synchrotron Rad.*, **2009**, 16, 818.

21. A. Welch, N. R. Shiju, I. D. Watts, G. Sankar, S. Nikitenko, W. Bras, *Catalysis Lett.*, **2005**, 105, 179.

Chapter 6

Aerosol assisted chemical vapour deposition of tungsten oxide thin films

6.1. Chapter overview

This chapter reports on the deposition of tungsten oxide thin films using aerosol assisted chemical vapour deposition (AACVD) on stainless steel and glass substrates using tungsten hexacarbonyl [$W(CO)_6$] in methanol and ethanol solvents. The deposition was carried out at substrate temperatures between 450 and 550°C. The films were characterised by XRD, Raman spectroscopy, XPS and SEM.

6.2. Introduction

Tungsten (VI) oxide, WO_3, also referred as tungsten trioxide occurs naturally in hydrated forms such as $WO_3.H_2O$ anhydrides. Tungsten oxide displays a cubic ReO_3 type structure with corner sharing WO_6. The formal oxidation state of the W in WO_3 is +6 and it has a $5d^0$ electronic configuration. Five structures of WO_3 have been reported at different temperatures: monoclinic (II) phase (ε WO_3) which is stable at room temperature and between 0 - 230K, triclinic (δ-WO_3) stable between 230 – 290 K, monoclinic (I) (γ-WO_3) stable between 290 – 600 K, orthorhombic (β-WO_3) stable between 600 – 1010 K and tetragonal (α-WO_3) stable between 1010 – 1170 K. [1,2]

Tungsten oxide is well known to lose oxygen at high temperatures in reducing environments and therefore can exhibit a wide range of non-stiochiometric phases. Removal of the oxygen atoms from the WO_3 results in formation of lower oxides, so transformation from WO_3 to WO_2 has a number of

intermediates oxides. Partially reduced tungsten oxide is usually written as WO_{3-x} where x varies from 0-0.5.[3] In partially reduced tungsten oxide an oxygen vacancy is generated and the W atoms are in the middle of the octahedral and it is partially reduced from W^{6+} to W^{5+}. The oxygen vacancies occur at specific planes within the crystal and a partial collapse of the structure removes a layer of vacancies and this stabilises the structure and forms sheer planes. A yellow colour is observed when tungsten oxide (WO_3) is fully oxidised and a blue colour for partially reduced tungsten oxide (WO_{3-x}). Hence tungsten oxide is electrochromic in nature. The change in colour of tungsten oxide can be reversible upon irradiation and this has lead to a wide range of applications.

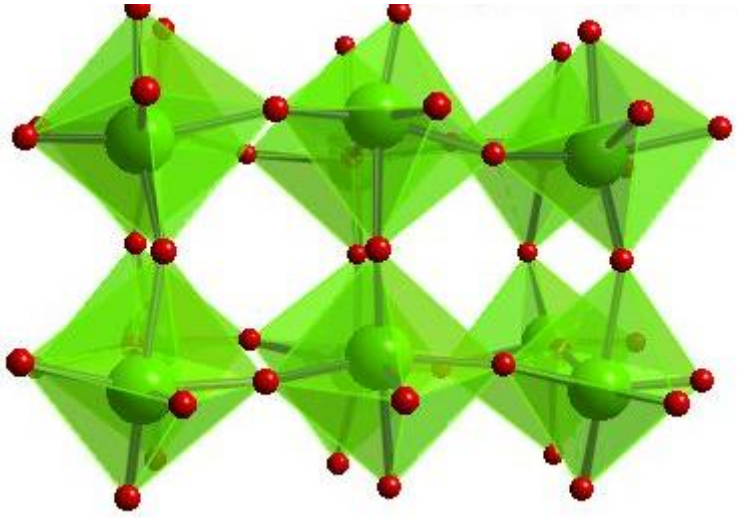

Figure 6.1 The crystal structure of monoclinic WO_3, the green balls represent tungsten metals and the oxygen atoms are shown in red.[2]

6.3. Properties and applications of tungsten oxide

Tungsten oxide displays electrochromism, photochromism and photocatalysis,[1-4] these properties has lead to a diverse range of applications in various industries. It is used in the glazing industry (in electrochromic windows WO_{3-x}) because it is able to control the absorbance of solar radiation as a function intensity and so controlling interior lighting and temperature levels. It has also found uses in gas-sensing because of its conductivity properties. [21]

6.3.1. Electrochromisim

Tungsten oxide is electrochromic because it can change colour reversibly when it undergoes electrochemical redox reactions. Fully oxidised tungsten oxide (WO_3) is transparent to visible light while the partially reduced tungsten oxide (WO_{3-x} (x = 0.5)) is dark blue in colour. The electrochromic property of WO_3 was first observed by S.K. Debs in 1969 and at present WO_3 remains the leading material used in electrochromic devices. The visible change in colour in tungsten oxide has been reported to be due to the generation of W^{5+} sites during electrochemical reduction. The strong absorption of the dark blue state has been reported to be due to intervalence electron transfer between the W^{5+} and the W^{6+} phases when a visible photon is absorbed. Equation 3.1 describes the electrochromic reaction.

$$WO_3 + x\,M^+ + x\,e^- \longleftrightarrow M_xWO_3\ (M^+ = Li^+, H^+, Na^+, K^+)$$

Tungsten oxide finds use as ‘Smart windows’ because it can allow sunlight through glass in cold weather as it works with the transparent WO_3 state and heats up the room and can change to the blue state in hot weather limiting sunlight from coming into a building and keeping the environment inside cool. Figure 4 describes the basic content of an electrochromic design. In the case of the ‘smart window’ two glass layers are coated with a transparent conductive oxide usually fluorine (FTO) or indium (ITO) and sandwiched inside is a layer of electrochromic WO_3 making it an active electrode. An electrolyte is placed in the middle of the layer usually a solid inorganic ion storage layer. A counter electrode that is transparent but not electrochromic is also required and is oxidised as the electrode is reduced. When a voltage is applied to the system, there is instant movement of cations from the counter electrode to the active electrode (WO_3) and this induces the colour change at the active electrode to blue. When the current is positive cations move from the active electrode back to the counter electrode and the active electrode is bleached of the blue colour.

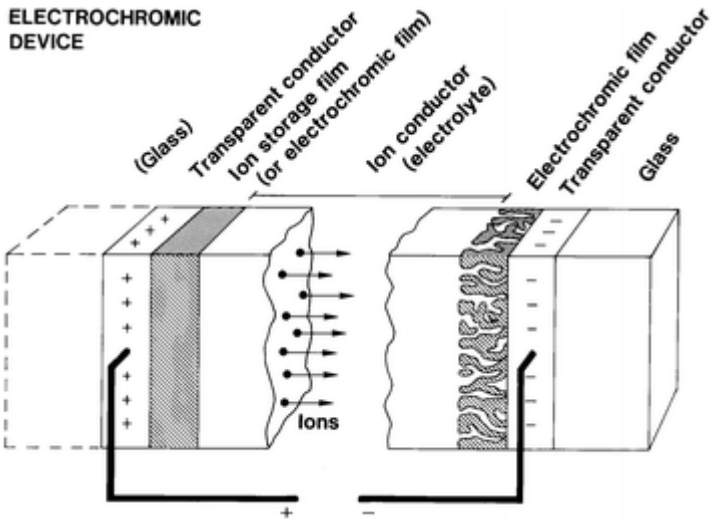

Figure 6.2 Basic design of an electrochromic device including a smart window.

6.3.2. Semiconductor photocatalysis

Self-cleaning glasses have dominated research of semiconductor photocatalysis with the commercially available Pilkington Activ™ produced by chemical vapour deposition of titanium dioxide thin films on glass (chapter 1). TiO_2 has been extensively studied for its hydrophillic properties, photostability and ability to break down organic dirt. TiO_2 with a band gap of 3.2 eV and wavelength λ = 383 nm is considered one of the best photocatalysts but tungsten oxide has potential as it has a band gap of 2.7 eV (460 nm). The conductance band electrons are capable of reducing oxygen to water (E°= −0.5 eV) and its valance valence band holes E° = 3.23 eVA are more oxidizing than titanium oxide E° = 3.0 eV . However the conduction band energy in tungsten oxide is not high enough to reduce oxygen and therefore it is not able to produce oxygen radicals and its ability to break down organic dirt is hence reduced. Research has been reported on increasing the solar absorption ability of TiO_2 by doping the material with a range of materials including zinc oxides, tungsten oxide and others. Figure 2.4 in chapter 1 illustrates the stages involved in the self-cleaning glasses using TiO_2 as a photocatalyst. After the e^- and h^+ are generated at the surface of the semiconductor material, the semiconductor can donate an electron to reduce oxygen (electron acceptor) and the hole h^+ can migrate to the surface and combine with an electron oxidising the organic pollutant. The rate at which this reaction takes place depends on the position of the band edges of the conduction band and valance band and the redox potential of the absorbing compound. To increase the rate of photocatalysis a metal dopant can be is introduced to inhibit the rate of

recombination. Dopants increase the rate of photoactivity by generating isolated energy levels within the band gap of the semiconductor and this level is able to trap the generated holes and electrons preventing e^- and h^+ recombination. It has been reported that a combination of TiO_2 and WO_3 increases the rate of photocatalysis. [15]

6.3.3. Gas sensors

Tungsten oxide (WO_3) is an n-type semiconductor material and most effective at temperatures between 200°C and 500°C because of its high reactivity to many gaseous species. WO_3 is one of the most studied and used metal-oxide gas-detectors used for the detection of NO_x, NH_3, H_2, H_2S, O_3 and SO_2 gases. Gas sensors work by absorption and reaction with molecules on the sensor surface. Depending on if the semiconductor gas sensor is p or n- type the sensor behaviour will be different.[4] Gas sensing in n-type gas sensors can reduce sample gas such as CO or H_2, as the gas can react with oxygen-ions at the semiconductor surface producing neutral molecules. This causes an electron transfer to the sensor material, and then gives rise to a decrease in the electrical resistance, and for an oxidizing gas such as NO_2, the resistivity increases.[6]

WO_3 gas-sensors are very useful for the detection toxic NO and NO_2 that can cause respiratory problems .[5] It is able to effective differentiate between H_2 and CO gases from NO and NO_2. Gas sensors based on WO_3 have already been successfully commercialized.[22]

6.4. Synthesis method of tungsten oxide films

Deposition of tungsten oxide has been accomplished through a number of physical and chemical techniques, these include sol–gel, spray pyrolysis, pulsed laser deposition flash and thermal evaporation, physical vapour deposition (PVD) and chemical vapour deposition (CVD). CVD presents the best potential for large scale depositions; Chapter 1 introduces the process involved in CVD reactions and also outlines the advantages of using CVD. It has been previously reported that the properties of tungsten oxide thin films is strongly dependent on the deposition technique used.

Tungsten hexacarbonyl [$W(CO)_6$] has been widely used in the chemical vapour deposition of tungsten oxide thin films this is because it can be used as a single source precursor. When [$W(CO)_6$] is used as a single source precursor in low pressure CVD black tungsten [$W_{18}O_{49}$] is produced which can then be annealed in air at 500^oC to produced the fully oxidised yellow WO_3.[16,17] $W(CO)_6$ and oxygen in dual-source atmospheric pressure chemical vapour deposition (APCVD) has been reported to deposit thin film fully oxidised yellow tungsten oxide (WO_3) in high oxygen flow and in low oxygen flow rates the partially oxidised blue tungsten oxide (WO_{3-x}) thin films were deposited.

Parkin et el reported the effect of solvent on the phase of WO_3 deposited using WCl_6 with ethanoic acid, water, methanol, ethanol on glass using atmospheric pressure CVD (APCVD) and have reported that most of the solvents produced fully oxidised monoclinic WO_3 at 625^oC except for methanol which deposited

crystalline reduced WO_{3-x} films. [8] It has also been reported that tungsten oxide displays photochromism after irradiation with 254 nm or 365 nm UV light. The change in colour has been widely reported to be reversible when left in the dark and the films return to their previous yellow state. However the use of traditional atmospheric pressure chemical vapour deposition (APCVD) requires precursors to be volatile and thermally stable, the substrate needs to be heated to bring about a reaction of the precursors and then the reaction is carried out under atmospheric pressure. Hence the development of aerosol assisted chemical vapour deposition (APCVD) that removes the limitations on the volatility requirement allows for more precursors to be used.[7] Deposition of WO_3 on metal substrates such as steel has yet to be investigated.

6.5. Experimental

Thin films of tungsten oxide were deposited using aerosol assisted chemical vapour deposition (AACVD) on glass substrate (SiO_2 coated float-glass of dimensions 45 x 90 mm) and stainless steel substrates (Goodmans, 250 mm thickness) of dimension 25 x 25 mm. Tungsten hexacarbonyl [$W(CO)_6$] (97% Aldrich) and methanol (Fisher, reagent grade) were used without any purification. Deposition was carried out on a cold-wall horizontal-bed CVD reactor that contained a graphite block heated by a Whatman cartridge heater. The steel foil was placed on top of a glass substrate which in turn was placed on top of the carbon heater block and the system was set up within a quartz tube. [$W(CO)_6$] was used as a single source precursor (0.37 g, 0.5 mmol) and was added to methanol (50 ml) and an aerosol was generated at room temperature using a Pifco ultrasonic humidifier. The aerosol was then carried into the reactor with carrier gas flow of oxygen free nitrogen gas at 1 L min^{-1} (BOC). The gas flow was continued until the entire precursor was exhausted.

Films were then cooled and stored in air. A series of depositions on glass and steel substrates were carried out at substrate temperatures of 450^{o}C and 550°C using either ethanol or methanol carrier solvent. All depositions were subject to the same conditions as stated for methanol.

6.6. Characterisation

Thin film X-ray diffraction (XRD) measurements were carried out on the deposited films using a Bruker D8 Discover fitted with GADDS area detector and Cu Kα_{1+2} source. Diffraction patterns were recorded and collected for 30 minutes per sample, with a fixed incident angle of 10^{o} for glass and 5^{o} for steel substrates. Scanning electron microscopic (SEM) measurements were carried out on the films to determine the surface morphology using a JEOL JSM-6301F field emission SEM at an accelerating voltage of 5 KeV. Raman spectra were obtained with a Renishaw Invia Raman microscope with a wavelength of 515.5 nm and 50x microscope objective.

6.7. Results and Discussion

6.7.1. Synthesis and characterisation of tungsten oxide thin films deposited on glass substrates

Thin films of tungsten oxide were deposited on glass and steel substrates by AACVD using [$W(CO)_6$] in methanol and ethanol solvent at 450 and 550°C. The films deposited on glass at both temperatures were blue in colour and could not be removed when cleaned with a paper towel. They could not be scratched with a 2H pencil but could be scratched by a stainless steel or diamond tipped scalpel. The films were insoluble to common solvents and 2M mineral acid. The blue films deposited indicat that the reduced form, of tungsten oxide was formed with an oxidation state of WO_{3-x} (x = 0.01 - 0.5)

and indicates the presence of W^{5+} and or W^{4+}centres.[9,10] The films deposited on steel using methanol as the carrier solvent appeared yellow when depositions are carried out at 550^0C and the films deposited using ethanol appeared both blue and yellow at 550^oC. The growth rate of the deposited films were actually fairly uniform with growth rate that ranged from 5 nm min^{-1} to 10 nm min^{-1} across the majority of the films with the thickest portions formed at the centre of the substrate.

The deposition of tungsten oxide on glass at 550^oC forms fully oxidised WO_3 compared to the deposition at 450^oC which showed the deposition of partially reduced WO_{3-x} using methanol and ethanol as carrier solvents. Figure 6.3 shows the Raman spectra of the films deposited on glass at 550^oC using methanol and ethanol as carrier solvents. The spectra shows sharp bands at 257, 318, and 708 cm^{-1} which has previously been identified as the γ-WO_3 monoclinic crystalline phase.[11]The band at 257 cm^{-1} has been assigned to W^{6+} – O –W^{6+} bending modes and the bands at 708 cm^{-1} and 810 cm^{-1} to the W^{6+} O stretching modes.[12] The Raman spectra shows that the yellow WO_3 film formed at 550^oC were fully stiochiometric WO_3. [13]

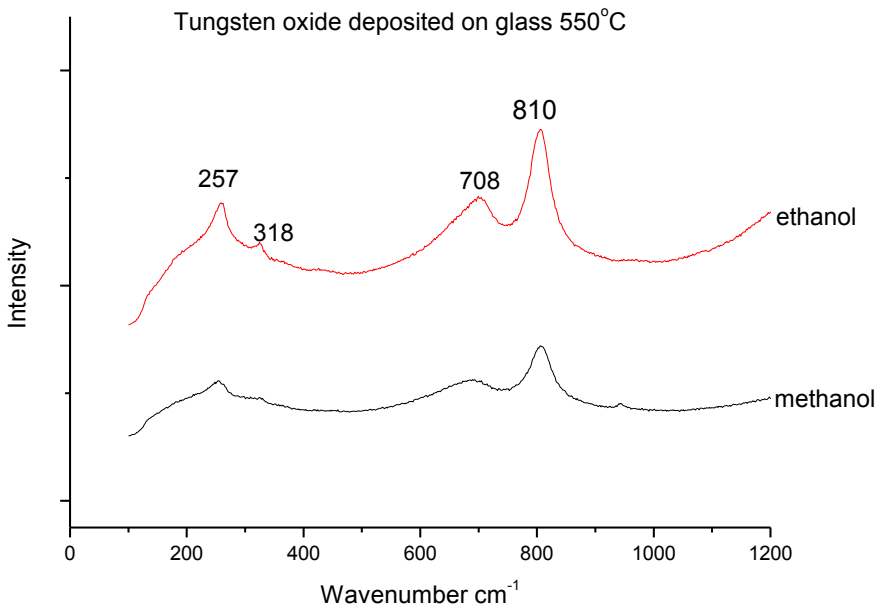

Figure 6.3. Raman spectra of as deposited WO_3 Films by AACVD from $[W(CO)_6]$ on glass using methanol and ethanol as stated on the figure

XRD patterns were also recorded for tungsten oxide thin films deposited at 550°C on glass. The XRD patterns are shown in figure 6.4 which shows reflections corresponding to the (0 2 0), (1 2 0) and (0 4 0) planes for the films deposited using ethanol and methanol. The films deposited using methanol shows an addition preferred orientation peak at <0 0 2>. Previous studies have reported preferred orientations along <0 0 1> and <0 4 0> using APCVD. [18,19]

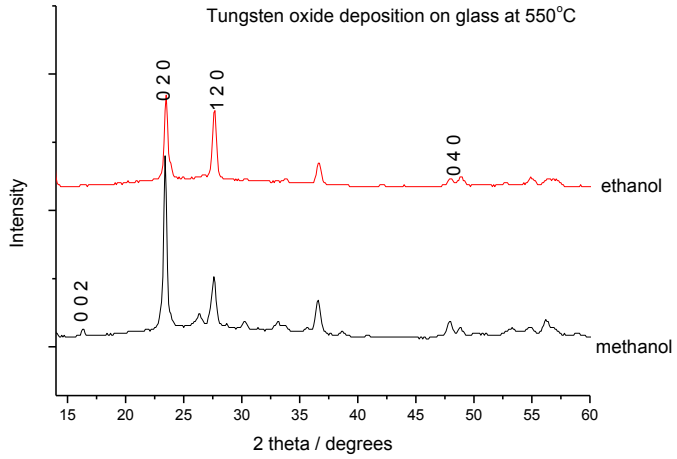

Figure 6.4. XRD pattern of as deposited WO_3 Films by AACVD from $[W(CO)_6]$ on glass using methanol and ethanol as stated on the figure

The scanning electron micrographs (SEM) of the films deposited on glass using methanol and ethanol as carrier solvent are shown in figures 6.5a and 6.5b respectively. The surface morphology of the films shows randomly oriented cone looking particles with a broccoli looking top. This morphology is very different to previously reported surface morphology of tungsten oxide made by APCVD. Agglomerates of spherical particles are normally seen for tungsten oxide thin films on glass at 500°C but in this report cone shaped particles are observed at 550°C.[7] The only difference between the films deposited using methanol and ethanol is that bigger particles are observed using ethanol solvent.

a b

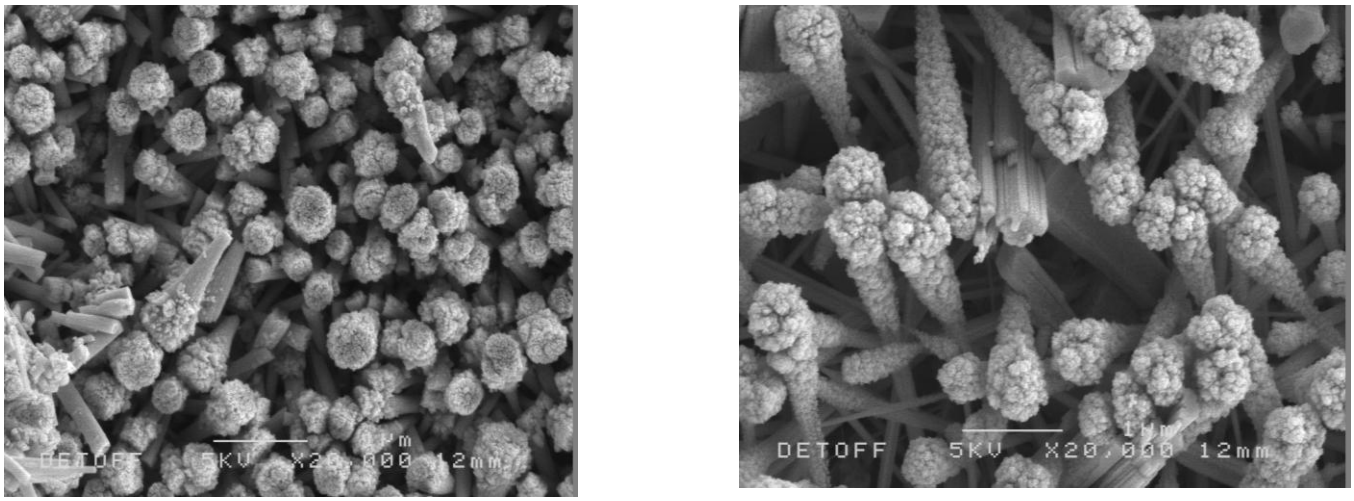

Figure 6.5 SEM of as deposited tungsten oxide thin films from $[W(CO)_6]$ on glass using methanol and ethanol as carrier solvent a and b respectively.

6.7.2. Synthesis and characterisation of tungsten oxide thin films deposited on steel substrates

Tungsten oxide deposited on steel using ethanol as the carrier solvent at 550^{o}C appeared yellow in colour indicating the deposition of fully oxidised WO_3. Figure 6.6 shows the Raman spectra map of the films deposited, the spectra show sharp bands at 273, 715 and 805 cm^{-1} which have been identified as the γ-WO_3 monoclinic crystalline phase. The band at 273 cm^{-1} has been assigned to W^{6+} – O –W^{6+} bending mode and the bands at 715 cm^{-1} and 805 cm^{-1} to the W^{6+} - O stretching modes. Unlike the films deposited on glass the films on steel show a little bit of the amorphous WO_{3-x} with a broad peak at 208 cm^{-1}.

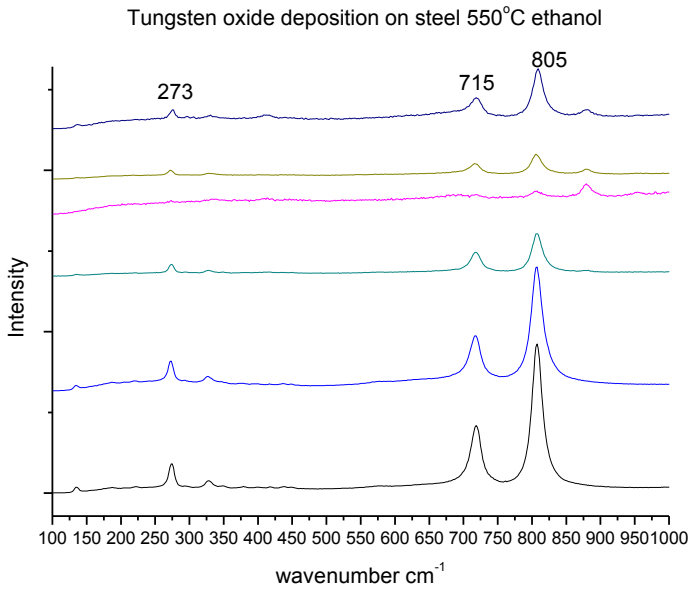

Figure 6.6. Raman spectra map of as deposited WO_3 films from the AACVD of $[W(CO)_6]$ on steel using ethanol as a carrier solvent.

The films deposited with methanol as the carrier solvent at 550°C appeared more dark yellow in colour which also indicates the deposition of fully oxidised WO_3 compared to deposition at lower temperature which formed the blue form at 450°C. The Raman spectra show bands at 271, 708, 805 and 879 cm^{-1}. All these bands are present in the films deposited using ethanol with the only difference being the 333 cm^{-1} and the very sharp 879 cm^{-1} bands from the experiment using methanol. The band at 333 cm^{-1} has been reported to correspond to the stretching mode W-O and 879 cm^{-1} the bending mode O-W-O. These peaks have been previously reported to be due to distorted tetrahedral W-O coordination. [14]

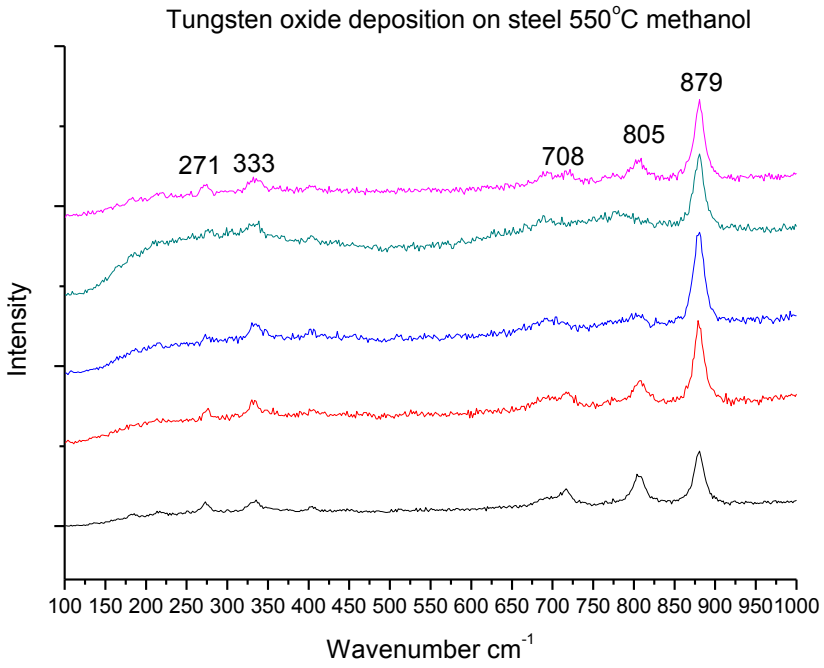

Figure 6.7. Raman spectra map of as deposited WO_3 films from the AACVD of $[W(CO)_6]$ on steel using methanol as a carrier solvent.

The XRD pattern of tungsten oxide thin films deposited at 550°C on steel are shown in figure 6.8. It shows reflections corresponding to the (0 2 2), (0 2 0) and (2 0 2) planes for the films deposited using ethanol. The films deposited using methanol show preferred orientation along <1 2 0> which is not present using ethanol.

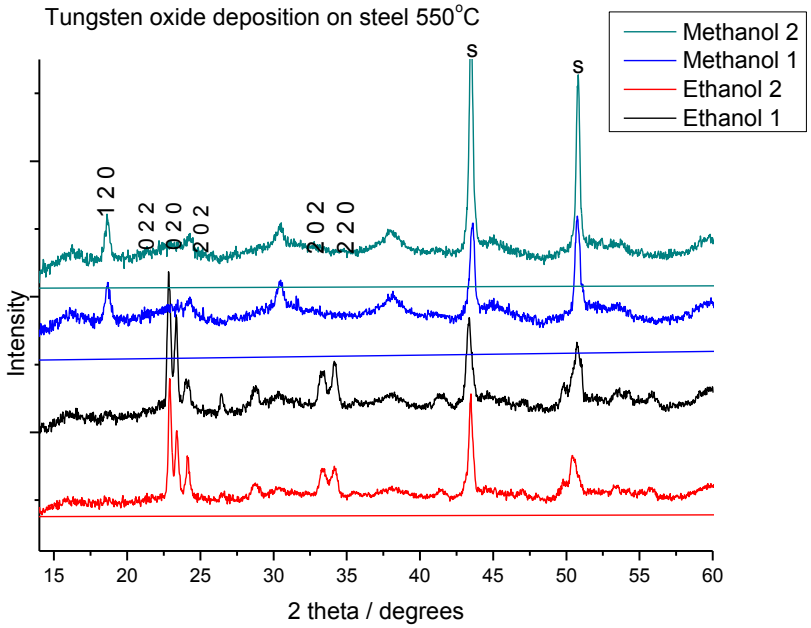

Figure 6.8. XRD pattern map of as deposited WO_3 Films by AACVD from $[W(CO)_6]$ on steel using methanol and ethanol.

SEM of the films deposited on steel using methanol and ethanol as carrier solvent are shown in figures 6.9(a) and 6.9(b) respectively. The surface morphology of the films shows randomly orientations of needle-like particles. The particles appeared bigger using ethanol compared to using methanol. The difference in the morphology of the as deposited tungsten oxide films on glass and on steel is also reflected in the different preferred orientation using each substrate as shown in the XRD pattern. To our knowledge this is the first report of deposition of tungsten oxide on steel substrates.

a b

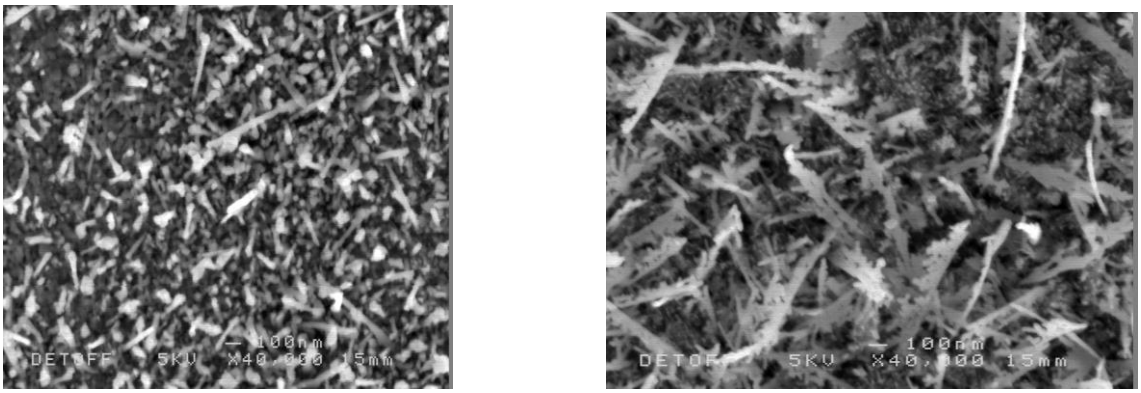

Figure 6.9.SEM of the as deposited tungsten oxide thin films from the AACVD of [$W(CO)_6$] on steel using methanol and ethanol as carrier solvent (a) and (b) respectively.

6.7.3. X-ray photoelectron spectroscopy (XPS) of as deposited films

The as-deposited films were analysed using X-ray photoelectron spectroscopy (XPS). The XPS data were used to determine the amount of carbon contamination present in the films and the W 4f spectra was also used to deduce the oxidation state of tungsten. The carbon content of the as deposited film was less than 1% for all films. The films deposited on glass at 550^{o}C using methanol as the carrier solvent shows tungsten peaks corresponding to the W^{6+} environment, the peaks were at binding energies of 35.9 and 38.2 eV and these energies corresponds to the W $4f_{7/2}$ and W $4f_{5/2}$ photoelectrons[20] as shown in figure 6.10. Binding energies of 35.9 and 38.01 eV are observed when ethanol is used as a carrier solvent on glass substrates as shown in figure 6.11, these energies also correspond to tungsten peaks corresponding to W^{6+} environment. The XPS of fully oxidised WO_3 has been previously reported to exhibit a double peak corresponding to W $4f_{7/2}$ and W $4f_{5/2}$ at binding energies of 35.6 and 37.8 eV respectively, whereas the partially reduced WO_{3-x} has been reported to show a double peak corresponding to W $4f_{7/2}$ and W $4f_{5/2}$ at binding energies of 34.4 and 37.2 eV respectively. [13,23]

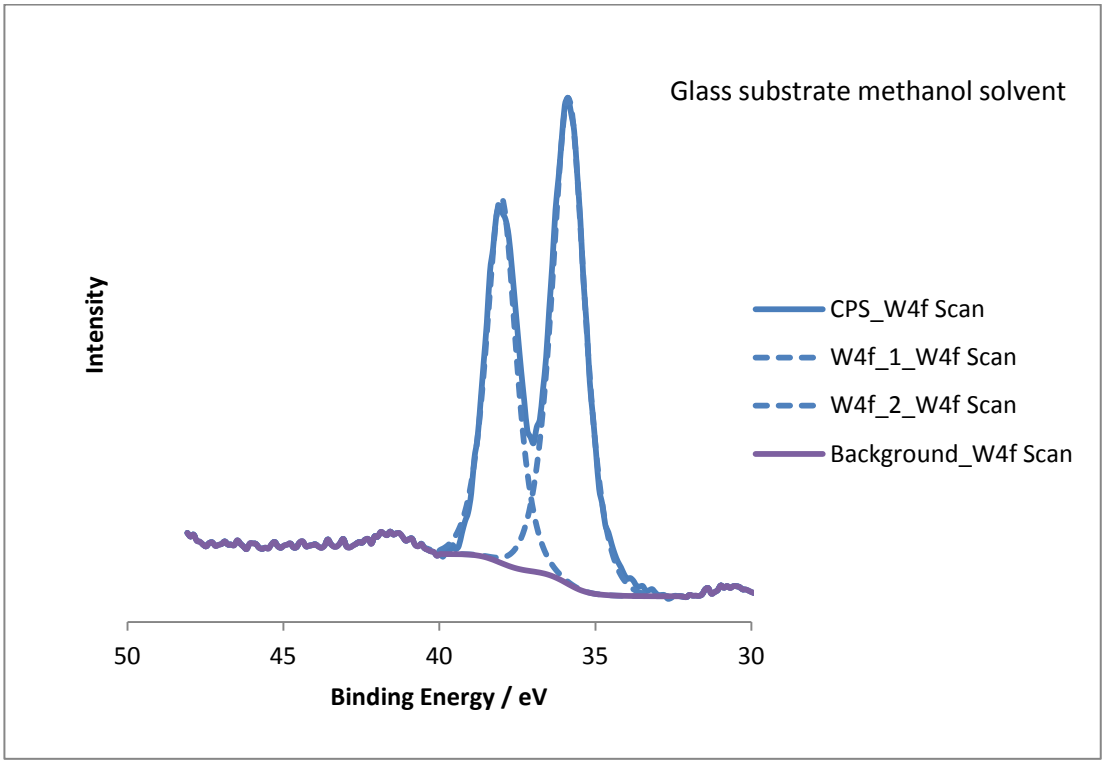

Figure 6.10. XPS of as-deposited tungsten oxide thin films from the AACVD of $[W(CO)_6]$ on glass substrate using methanol as carrier solvent. The experimental data is shown in bold and the fitted peaks are represented by dotted lines.

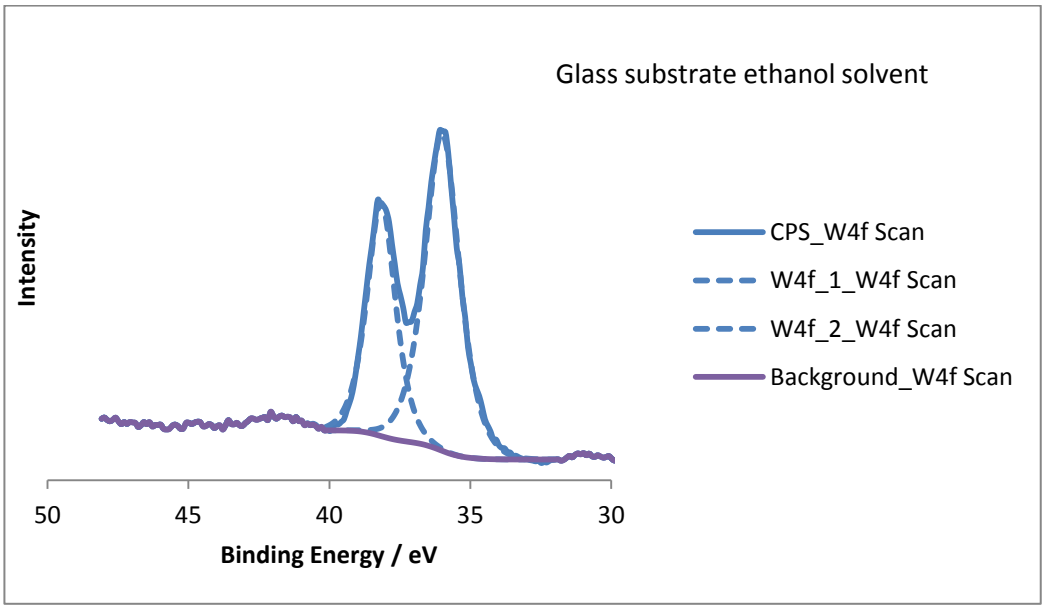

Figure 6.11. XPS of as-deposited tungsten oxide thin films from the AACVD of $[W(CO)_6]$ on glass substrate using ethanol as carrier solvent. The experimental data is shown in bold and the fitted peaks are represented by dotted lines.

The XPS spectra for as-deposited tungsten oxide on steel substrate using methanol and ethanol are shown in figures 6.12 and 6.13 respectively. The films deposited on steel at 550^{o}C using methanol as the carrier solvent shows tungsten peaks corresponding to a W^{6+} environment, the peaks were at binding energies of 35.5 and 37.7 eV. Using ethanol as a carrier solvent also produces peaks corresponding to W^{6+} environment; the peaks were at binding energies of 35.5 and 37.6 eV.

The data collected using XPS does not show any peaks corresponding to the WO_{3-x} stoichiometry even though the films deposited on glass was blue in colour. This probably because the surface of the film was fully oxides WO_3 – yet the bulk primarily WO_{3-x}. Furthermore no shoulders on the main peak were seen that could be modelled to reduce tungsten (+4/+5). The small difference in the values obtained using the steel and glass substrate are probably due to errors in the data collection technique and peak fittings. (Data collected with the help of Dr Sanjay Sathasivam)

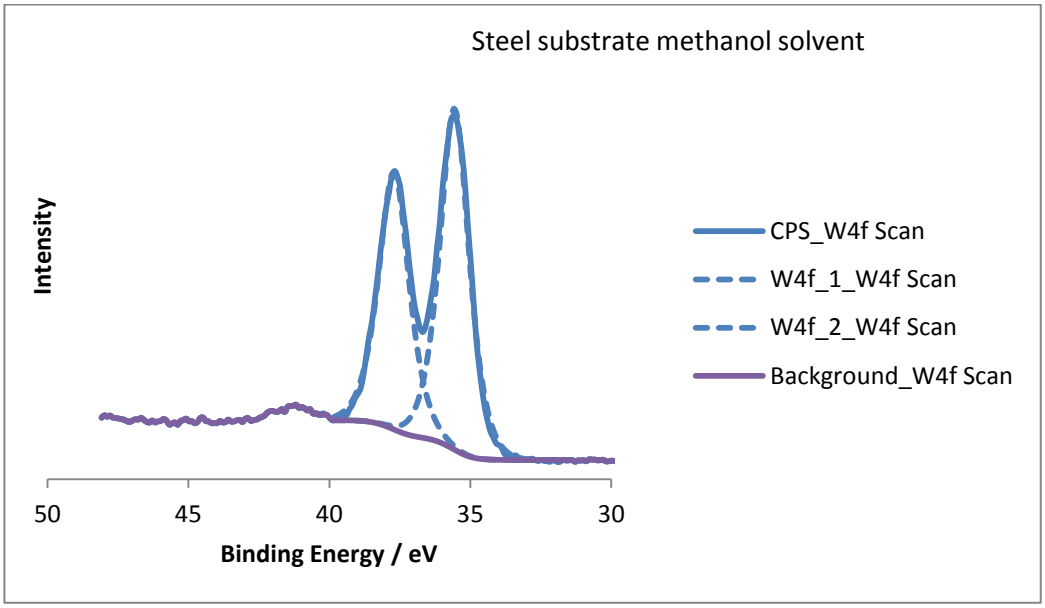

Figure 6.12. XPS of as-deposited tungsten oxide thin films from the AACVD of $[W(CO)_6]$ on steel substrate using methanol as carrier solvent. The experimental data is shown in bold and the fitted peaks are represented by dotted lines.

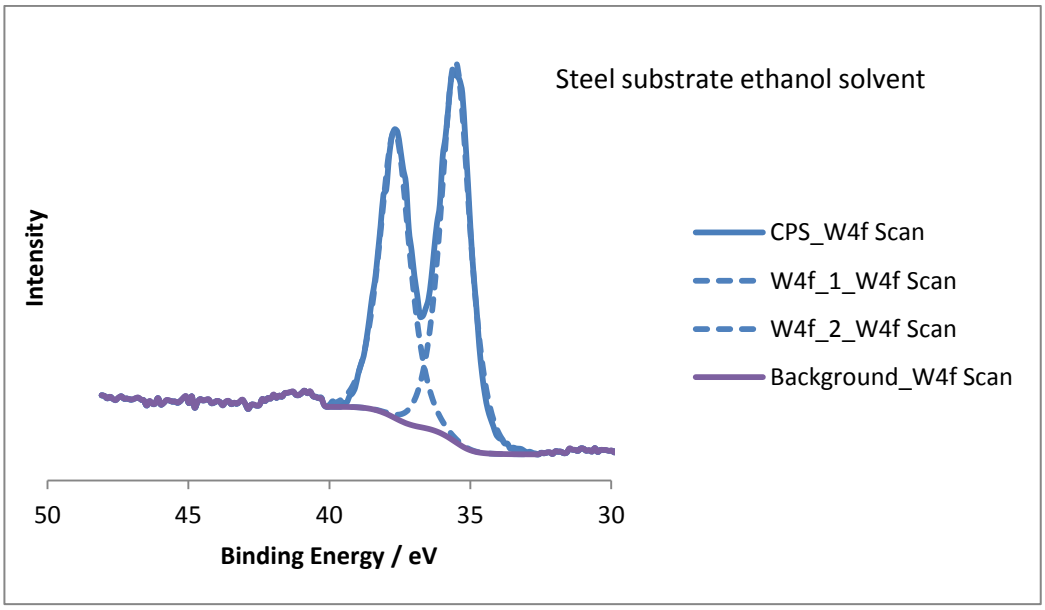

Figure 6.13. XPS of as-deposited tungsten oxide thin films from the AACVD of $[W(CO)_6]$ on steel substrate using ethanol as carrier solvent. The experimental data is shown in bold and the fitted peaks are represented by dotted lines.

6.8. Conclusion

Thin films of tungsten oxide were deposited on glass and steel substrates from the AACVD deposition of $[W(CO)_6]$. The films deposited on glass at 450^oC were blue in colour showing the presence of WO_{3-x}. The films deposited at 550^oC on glass were more yellow in colour but some parts appeared a blue colour. The films deposited on steel substrate appeared dark yellow using either methanol or ethanol as the carrier solvent. The major difference observed using the different substrate either using glass or steel and using different solvents methanol or ethanol is in the morphology of the films, different morphologies are seen using steel and glass substrates and also when methanol or ethanol is used as the carrier solvent.

This chapter shows that the use of different substrate and solvents as a direct effect on the morphology of the films deposited and the preferred orientation of the deposited films.

6.9. Reference

1. D. Bullet, *J. Phys. C: Solid State Phys.*, **1983** 16, 2197.
2. P.M Woodward, A.W Sleight, T. Vogt, *J. Sol. State Chem.*, **1997**, 131, 9.
3. J. P. Bonnet, J. Nowotny, M. Onillon, I. Sikora**,** *Oxid. of Metals,* **1979**, 13, 3.
4. D.E. Williams, P.T. Moseley, B.C. Tofield, *Solid state gas sensors*, **1987**.
5. A. Ponka, M. Virtanen, *Environ. Res*. **1994**, 65, 1987.

6. J. Tamaki, Z. Zhang, K. Fujimori, M. Akiyama, T. Harada, N. Miura, N. Yamazoe. *J. Electrochem. Soc*., **1994**, 141, 2207.
7. S. Ashraf, C. S. Blackman, R. G. Palgrave, I. P. Parkin, *J. Mater. Chem.*, **2007**, 17**,** 1063.
8. R. G. Palgrave and I. P. Parkin, *New J. Chem*, **2006**, 30, 505
9. G. S. Sandhu, S. G. Meikle and T. T. Doan, *Appl. Phys. Lett.*, 1993, **62**, 240
10. K. T. Rie, A. Gebauer, J. Whole, H. K. Tonshoff, C. Blawit, *Surf. Coat. Technol.*, **1995**, 74, 375
11. C. Santato, M. Odziemkowski, M. Ulmann, J. Augustynski, *J. Am. Chem. Soc.* **2001**, 123, 10639.
12. G. Gogova, G. K. Gesheva, A. Kakanakova-Georgieva, M. Surtchev, *Eur. J. Phys.* **2000**, 11, 167.
13. W. B. Cross, I. P. Parkin, S. A. O'Neill, P. A.Williams, M. F.Mahon and K. C. Molloy, *Chem. Mater*, **2003**, 15, 2786.
14. D. Ouafi, F. Mauge, J. C Lavalley, E. Payen, S. Kasztelan, M. Houari, J. Grimblot, J. P. Bonnelle, *Catal. Today*, **1988**, 4, 23.
15. Y. R Do, W. Lee, K. Dewight, A. World, *J. Solid State Chem*, **1994**, 108, 198.
16. D. Davazoglou, A. Donnadieu, *Thin Solid Films*, **1988**, 164, 369.
17. D. Davazoglou, K. Geougouleas, *J. Electrochem. Soc.*, **1998**, 145, 1346.
18. S. Ashraf, C. S. Blackman, R. G. Palgrave, I. P. Parkin, *J. Mater. Chem.,* **2007**, 17, 3708.
19. W. B. Cross, I. P. Parkin, A. J. P. White, D. J. Williams, *Dalton Trans* , **2005** , 1287.

20. http://srdata.nist.gov/xps/default.aspx

21. Y. S. Lin, Y. L. Chiang and J. Y. Lai, *Solid State Ionics*, **2009**, 180, 99.

22. A. Pnozoni, E. Comini, M. Merroni, G. Sberveglieri, *Thin Solid Films* **2005**, *490*, 81.

23. W. B. Henly, G. J. Sacks, *J. Electrochem*. Soc, **1997**, 144, 1045.

Chapter 7

Insitu studies of titanium dioxide and tungsten oxide thin films

7.1. Chapter overview

This chapter focuses on various characterization techniques used to understand the formation of titanium dioxide and tungsten oxide thin films deposited on glass and steel substrates by AACVD. The characterization techniques used includes NMR, IR spectroscopy and μXAFS. The main focus will be the μXANES of the as-deposited films. The stages involved in designing a new AACVD reactor vessel suitable for *in-situ* synchrotron studies will also be outlined.

Although *ex-situ* Raman and XRD studies have revealed structural information of titanium dioxide and tungsten oxide films formed as discussed in chapter 3 and 5 respectively, it was not possible to fully understand the poorly crystalline forms and the oxidation state of tungsten oxide in the films. By using the XAFS micro beam method, it was possible to map the films and determine metal specific information for tungsten oxide and titanium dioxide films.

This chapter also details the challenges involved in carrying out *in-situ* synchrotron studies in an AACVD system.

7.2. Introduction

The previous chapters of this thesis have reported the effect of solvent and substrates on the phase of TiO_2 deposited by AACVD. The most surprising is the phase directing effect when methanol is used as a carrier solvent. This effect is not observed when ethanol is used as a carrier solvent. Methanol has been previously reported to act differently in a chemical reaction compared to when other solvents are used. Yates et al. reported in their study to modify and control the surface morphology of doped SnO_2 deposited by APCVD that when methanol was used as a solvent the surface of the films produced were modified. They reported that the surface morphology of the films deposited was very rough and had elongated and sharp features compared to when using other alcohols were more rounded particles were observed.[1] This correlates to chapter 3 and 4 of this thesis where needle like particles were observed for TiO_2 films deposited when methanol is used as the carrier solvent. This motivated this section of the thesis to further investigate the reaction path of methanol in the reaction.

The phase of the precursor in the gas state and the by-products during deposition are useful in understanding the reaction mechanism and can also help in altering the reaction and enhance the properties of the films deposited. This chapter focuses on investigating the solvent path in the AACVD reaction of TTIP in forming TiO_2. IR spectroscopy was used to investigate the gases coming out of the exhaust during deposition and also the aerosol composition just before entering the reactor vessel. IR spectroscopy has been previously used to investigate reactions in the gas phase[2] and CVD reactions[3]. IR is an effective way to determine functional groups present during a reaction and this

study aims use IR to determine if the solvent composition changes during reaction or if the solvent goes through the deposition unchanged.

Nuclear magnetic resonance (NMR) spectroscopy was used in this study to study the reaction of TTIP in methanol solvent and to record any exchange reaction between the isopropyl group and the methoxy group. NMR technique is very effective in resolving the ^{1}H environment in a compound giving an insight into any change in environment during a reaction.

XAFS is a very useful technique in studying reactions *in-situ* as it focuses on the metal centre and it is able to determine the coordination environment around a metal, intermediate phase during a reaction and it is able to determine the phase of amorphous and crystalline structures compared to XRD that can only resolve crystalline structures. *In-situ* XAFS studies have been used in different research area including catalysis.[4,5,6] µXANES provides information about the coordination state of the metal and it is also used as a finger print region for each metal. The pre-edge and edge of each metal is unique and gives valuable information of the oxidation state of the metal (see chapter 2). *In-situ* XAFS studies have been well studied in the area of catalysis in zeolites[7,8] but to our knowledge this is the first application of µXANES in chemical vapour deposition (CVD).

This section of the thesis will give brief descriptions of NMR and IR spectroscopy and detail the results obtained from the IR and NMR spectra recorded. The majority of this chapter will focus on the design of the X-ray transparent AACVD cell and the results obtained from the in-situ deposition of TiO_2.

7.3. NMR Studies of the titanium precursor [$Ti(OPr^i)_4$] in solution- does pre-reaction occurs?

7.3.1. NMR Spectroscopy overview

Nuclear magnetic resonance (NMR) spectroscopy is able to give an insight about the environment of the nuclei of atoms found in a molecule and can provide information about the structure, the reaction state, and chemical environment of the molecule. A nucleus in an external magnetic field can align itself either with the external field (positive) or against it (negative). Hydrogen and some other nuclei have a spin about their axis. The nuclei with a spin has a magnetic moment and in the presence of an external magnetic field the nuclei turn to a preferred orientation. Nuclei obey the quantum law and in the presence of an external magnetic field a nuclei with ½ quantum number produces two spin states, one up and one down, one aligns with the magnetic field positive ½ and the other opposes it negative ½ .

When a molecule is at equilibrium with the surroundings then the spin distribution will favour more nuclei in the lower state. If then an electromagnetic radiation of frequency is applied and the frequency is the same as the energy difference between the levels then the population of the higher energy state increases and so radiation will be absorbed. Equilibrium will be established if the nuclei loses the energy applied to its surroundings.

Fourier transform (FT) NMR machines are used in most laboratories. FT instruments works by exciting all the nuclei (protons) at the same time and each will send out radiofrequency when returned to equilibrium. The resulting signal given out by each nuclei is a combination of the frequencies of each

chemically distinct nucleus. The FT instrument is then able to produce the NMR spectrum using the frequency and intensity of each nuclei absorption. The chemical shift is usually measured in parts per million (ppm).

7.3.2. Experimental

Preliminary NMR was recorded to monitor the exchange reaction between the isopropoxide group on the titanum (IV) isopropoxide (TTIP) and the methoxyl group on the solvents. We carried out the NMR of TTIP and methanol in benzene solvent at room temperature, NMR of methanol in benzene, TTIP in benzene and TIP and methanol in benzene after 5 days.

7.3.3. Results and discussion

Preliminary NMR studies were carried out to investigate the reaction of the precursor TTIP with methanol as the carrier solvent. This was done to try and explain the difference seen in chapter 4 on the use of EtOH and MeOH in making either anatase or rutile. Figure 7.1(a) shows the NMR spectra of TTIP in benzene, figure 7.1(c) shows TTIP and methanol in benzene and figure 7.1(b) shows IPA in benzene solvent. Scheme 7.1 shows the proposed reaction mechanism for the reaction of TTIP and methanol in an AACVD reactor vessel. The proposed scheme shows that there could be an exchange between the isopropoxide group on the TTIP and the methoxy of the methanol or an intermediate with titanium attached to both the isopropoxide group and the methoxy at the same time. The ^{1}H NMR results however shows no exchange reaction between the isopropanol group on the TTIP and the methanol solvent at room temperature, if this exchange had occur we would

expect a peak at 3.65 ppm due to Ti-OMe but this peak is missing in the NMR spectrum.[11] The NMR of ^{1}H NMR shows the same peaks in methanol in IPA and methanol and TTIP in benzene solvent. This indicate that the methanol is unreacted in the solution. The only observable change is in the shift from 4.5 ppm in figure 7(a) to 3.9 ppm in figure 7(d) in NMR of TTIP in benzene and TTIP, methanol in benzene solvent after 5 days. This change shows that the TTIP starts to breakdown but it is still not at a meaningful rate at room temperature. The exchange therefore did not occur at a meaningful rate at room temperature. The NMR spectra are shown figures 7.1(a) – 7.1(d).

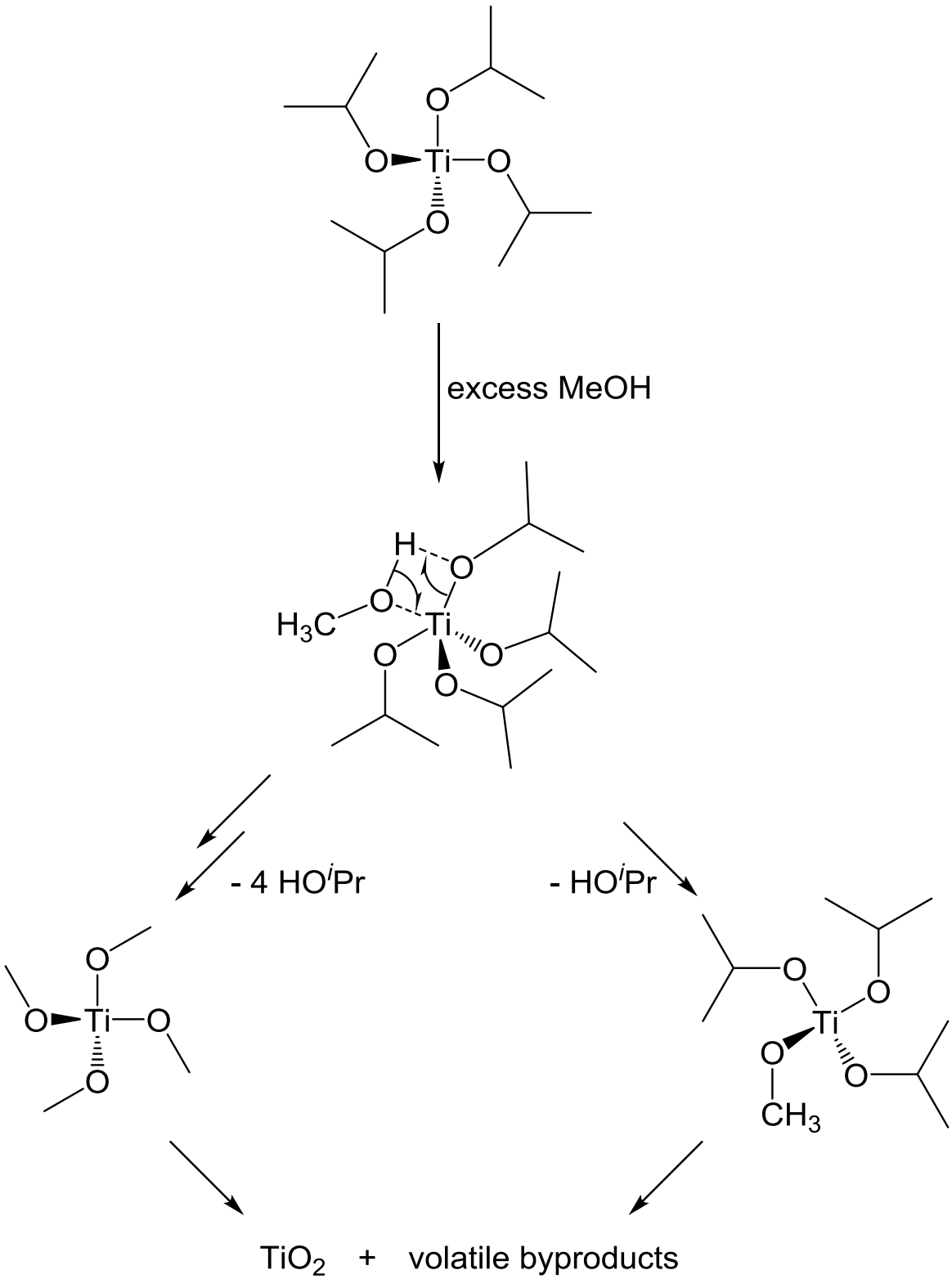

Scheme 7.1. A proposed reaction of TTIP in methanol solvent. ^{1}H NMR at room temperature did not show evidence for reaction: However these procedures are possible at the higher temperature of the aerosol.

(a)

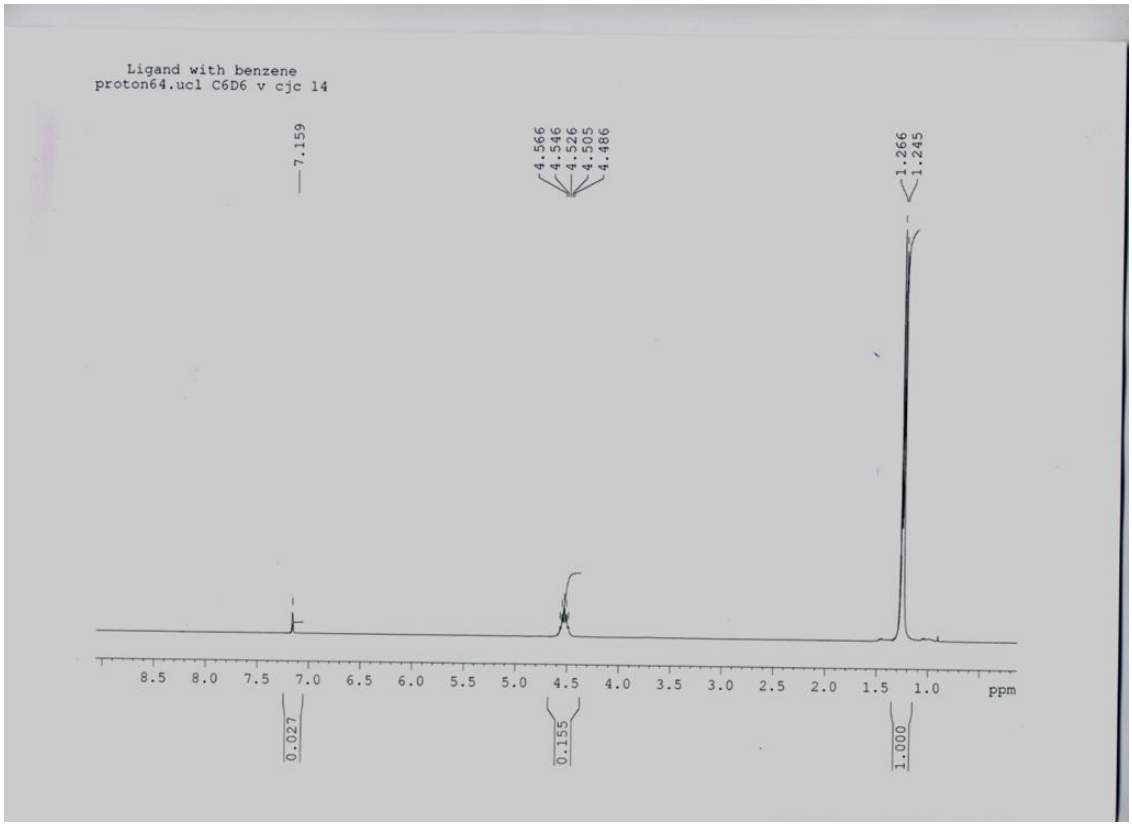
Ligand with benzene
proton64.ucl C6D6 v cjc 14
7.159
4.566
4.546
4.526
4.505
4.486
1.266
1.245
8.5 8.0 7.5 7.0 6.5 6.0 5.5 5.0 4.5 4.0 3.5 3.0 2.5 2.0 1.5 1.0
ppm
0.027
0.155
1.000

(b)

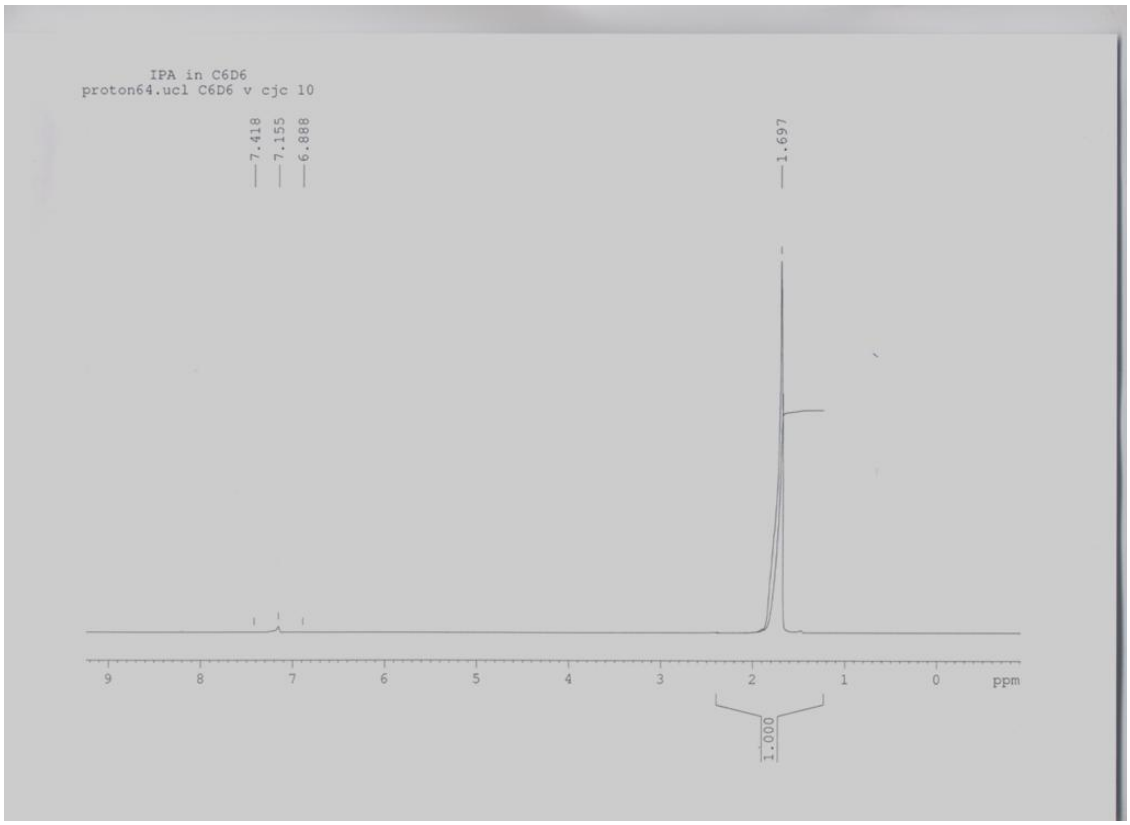
IPA in C6D6
proton64.ucl C6D6 v cjc 10
7.418
7.155
6.888
1.697
9 8 7 6 5 4 3 2 1 0
ppm
1.000

(c)

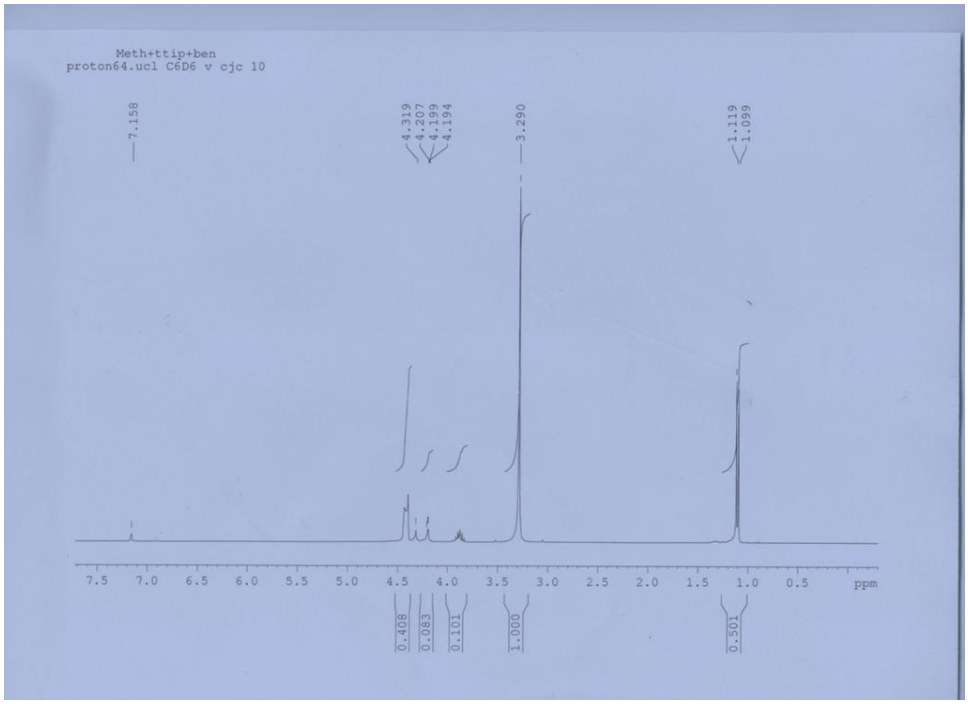

(d)

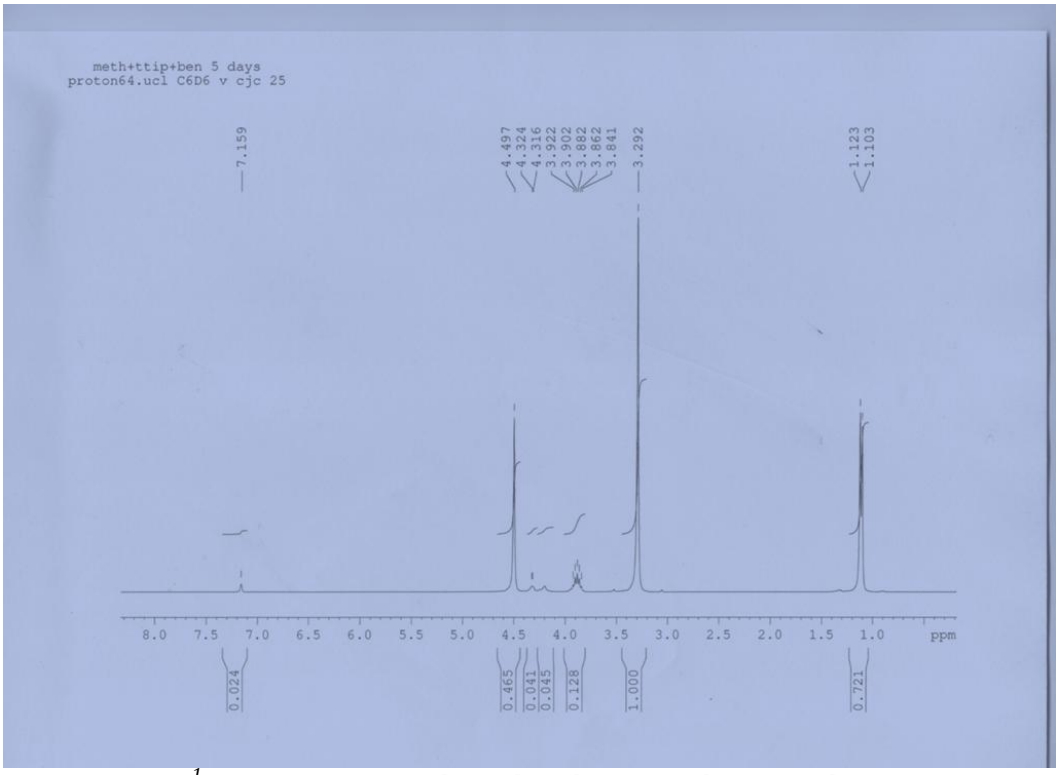

Figure 7.1. [1]H NMR (a) TTIP (ligand) in benzene, (b)IPA in benzene, (c) methanol and TTIP in benzene, (d) methanol and TTIP in benzene after 5 days.

7.4. Insitu IR spectroscopy study of TiO_2

7.4.1 IR overview

Infrared spectroscopy (IR) involves vibrations that result in a change in molecular dipole and have absorption in the infrared region of the spectrum absorb infrared radiation. Atoms in a molecule vibrate about their equilibrium bond distance and their vibrating frequency depends on the mass of the vibrating atoms, the bond length and the strength of its bonds. When electromagnetic radiation of the same or higher than the molecule's natural vibration frequency is applied molecules vibrate at higher frequency and using Fourier transform the frequency of the vibration can be interpreted and an IR spectrum produced. Gases like H_2 and O_2 do not have a dipole moment and so do not absorb in the IR region whilst molecules like CO which has a dipole moment and so has an IR spectra.

The main use of infrared spectroscopy is in resolving molecular structure to characterise the functional groups present in the unidentified molecule.

In chapter 2 we have detailed how the carrier solvent is able to affect the phase of TiO_2 deposited as either as anatase or rutile. We have reported that when methanol is used as a carrier solvent the reaction favours the deposition of the rutile phase and other solvents including ethanol and hexane favour the deposition rutile. Jackson.S.D. et al have reported that the methanol breakdown mechanism involves the production of CO_2 and this is able to create a reactive intermediate that changes the path of the reaction and so changing the end product. Equation 7.1 shows the reaction mechanism as reported by Jackson.S.D. et al.[9]

Equation 7.1. $CH_3OH \longleftrightarrow CO + 2H_2$

The idea of using IR spectroscopy is to test if CO_2 will be produced during AACVD deposition using methanol as a carrier solvent and no CO_2 using methanol or hexane as the carrier solvent.

CO_2 in the IR has a very distinct and strong stretch at 2350 cm^{-1} because it is a linear molecule and is very easy to observe the C=O stretch in the IR region due to the large change in dipole moment associated with the asymmetric stretch. This was attempted by collecting the resulting gas during the AACVD reaction from the gas outlet. This is to our knowledge the first time such an experiment has been conducted.

7.4.2. Experimental

We followed the same procedure detailed in chapter 2.3 and at the outlet of the reactor vessel a tube was attached going into the IR gas chamber. The gas released from the outlet was collected and an IR obtained. We collected the gas of only TTIP, only ethanol and only methanol and also collected the outlet gas during reaction with ethanol and methanol. The aerosol evaporated from the glass containing the reagent before they reach the reactor was also collected and measured.

7.4.3. Results and discussion

The gas IR spectra of the reaction of TTIP were collected during AACVD.

Figure 7.2 shows that the OH band in the IR which is broad in solution is now sharp in the gas phase. This is because of the lack of H-bonding in the gas phase.

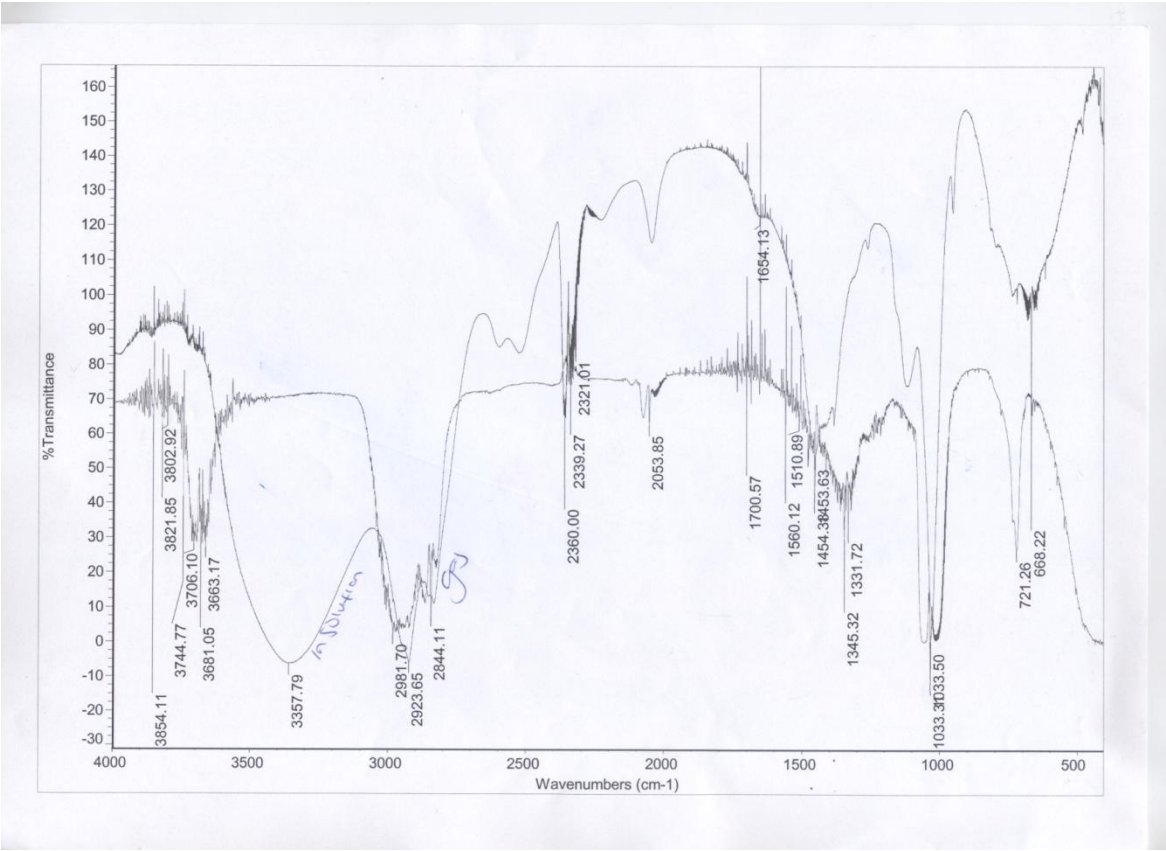

Figure 7.2 . Shows the liquid IR spectra of TTIP in methanol solution and gas phase IR spectra of the gas out of the exhaust during deposition as written on the figure.

Functional Group	Characteristics Absorptions (cm^{-1})
Alcohol broad O-H	3358
Alcohol O-H sharp	3745, 3652
C-H	2924, 2844
C-O	1033
C-H rocking	721
C-H deformation	1345

Figure 7.3-7.5 shows the IR spectra of TTIP, methanol and ethanol respectively, it is observed that the TTIP in the IR does not show sharp absorption due to low concentration. When looking at the IR spectra of methanol and ethanol during the AACVD reaction involving TTIP and methanol or ethanol as the carrier solvent we can see that the IR spectra of the solvents on their own and in reaction with TTIP, this shows exactly the same peaks and we are not able to detect a difference in the solvent peaks. This indicates that the solvent methanol and ethanol go through the reactor as solvents and not as an aerosol (Figures 7.6-7.8). This can be seen this due to the sharp OH peak on both solvent in the IR spectra which indicates that the gas phase MeOH has H bonds in solution and this reduces the O-H frequencies. The spectrum shows P, Q and R branches in the O-H stretch at 3750 cm^{-1}.

CH_2 deformation at 1300 cm^{-1} is present in all the gas phase spectra apart from the TTIP spectra. P, Q and R branches in infrared spectroscopy are the combined rotational and vibrational behaviour of a molecule and can be seen in high resolution gas phase IR spectra.

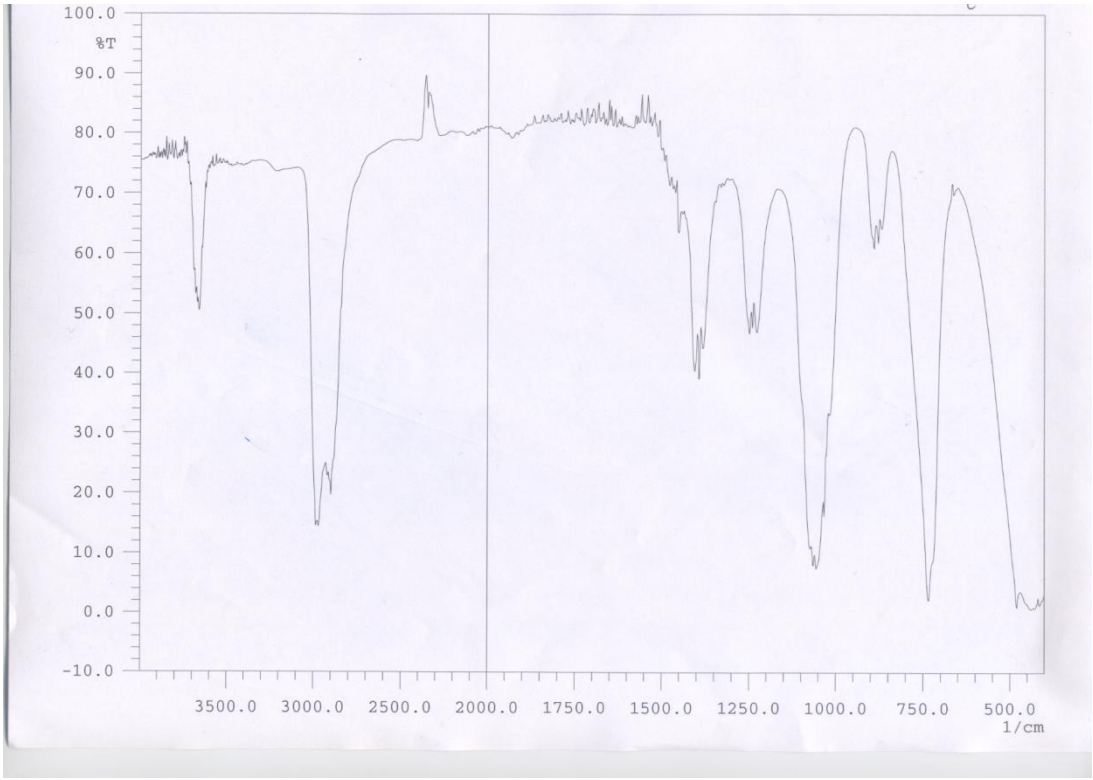

Figure 7.3. The gas phase IR spectra of ethanol

Functional Group	Characteristics Absorptions (cm^{-1})
Alcohol O-H sharp	3700
C-H	2950
C-O	1170
CH_2 rocking	730
CH_2 deformation	1200, 1300

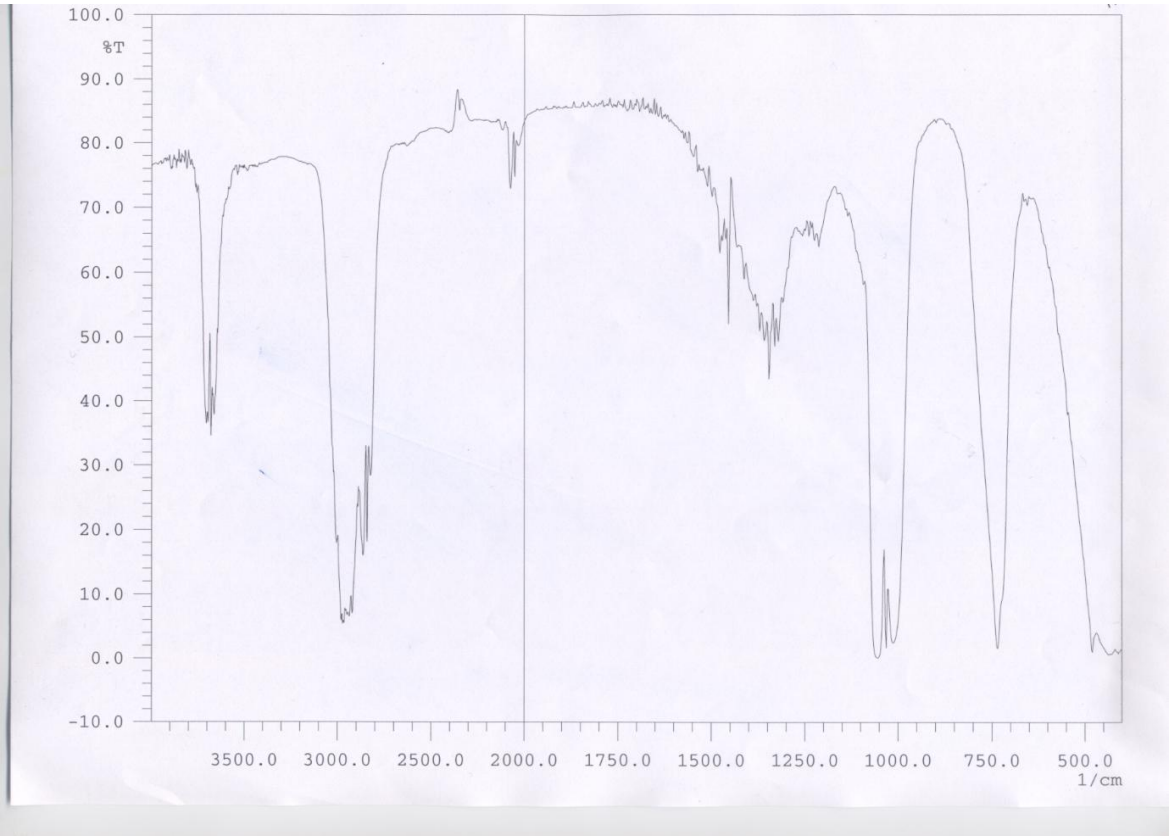

Figure 7.4 . The gas phase IR spectra of methanol

Functional Group methanol	Characteristics Absorptions (cm^{-1})
Alcohol O-H sharp	3750
C-H	2950
C-O	1120
CH_2 deformation	1300
CH_2 rocking	720

Figure 7.5. The gas phase IR spectra of TTIP

Functional Group TTIP	Characteristics Absorptions (cm^{-1})
C-H	2850
C-O	1150
CH_2 rocking	750

CO_2 vibration was not detected in the IR spectra obtained from the exhaust gas during the reaction of TTIP and methanol in the AACVD process. This indicates that the methanol goes through the reaction unreacted or the reaction happens on the surface of the substrate or it happens and could not be detected

from the exhaust gas using IR spectroscopy at the quantities formed. An overlap of TTIP, methanol and ethanol in the IR spectra was not able to give any information because the peaks from TTIP are overlapping with the peaks from the solvent. The only observation is that the TTIP peak is not detected in the IR spectra shown in figure 4 and 5 from the exhaust gas using methanol or ethanol as the carrier solvent, indicating it has decomposed during the reaction or is at a concentration that could not be detected.

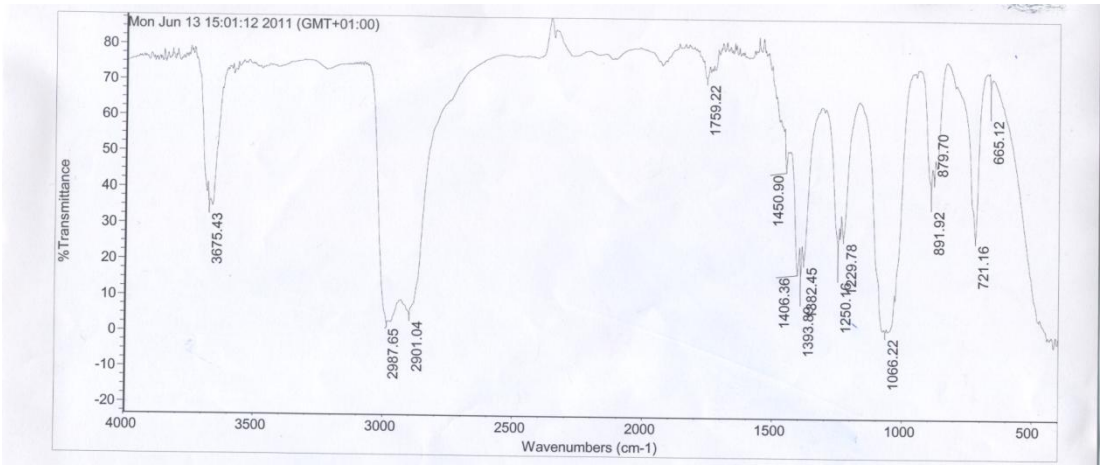

Figure 7.6. The gas phase IR spectra of the exhaust gas during the deposition of TiO_2 with TTIP in ethanol solvent.

Functional Group ethanol + TTIP	Characteristics Absorptions (cm^{-1})
Alcohol O-H sharp	3676
C-H	2988, 2901
C-O	1066, 1250
CH_2 rocking	721
CH_2 deformation	1340

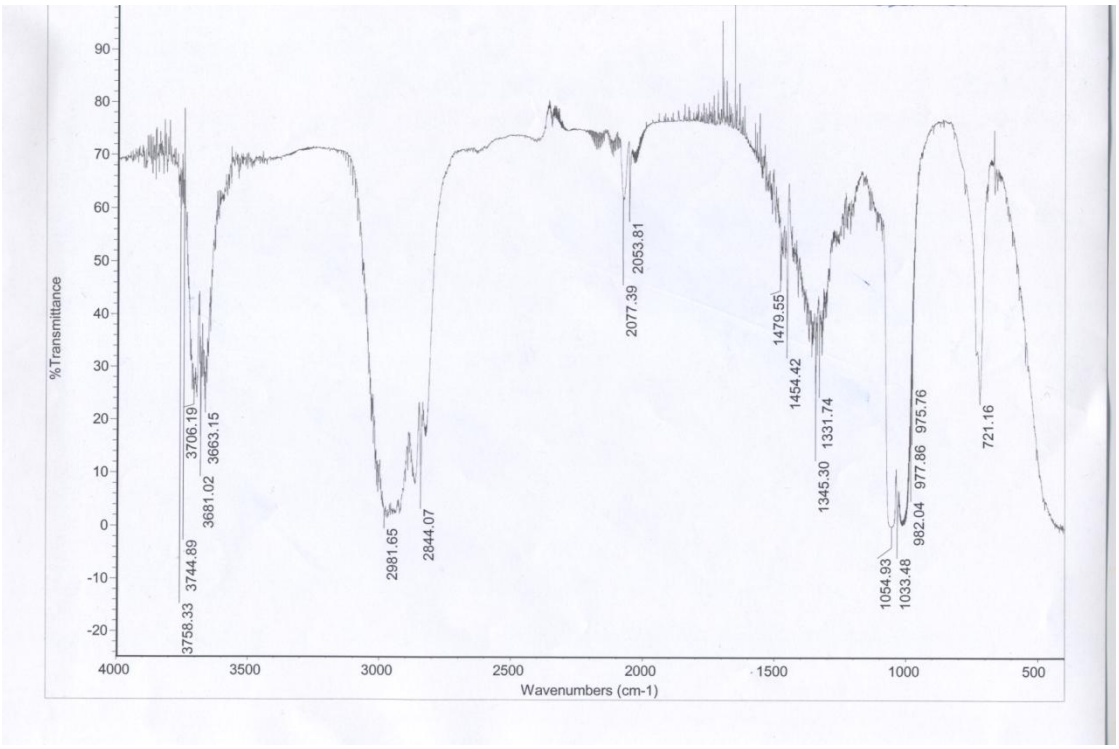

Figure 7.7. The gas phase of the exhaust gas during TiO_2 deposition with TTIP in methanol solvent.

Functional Group methanol	Characteristics Absorptions (cm^{-1})
Alcohol O-H sharp	3759
C-H	2982,2844
C-O	1065,
CH_2 deformation	1345
Weak CO_2	2077

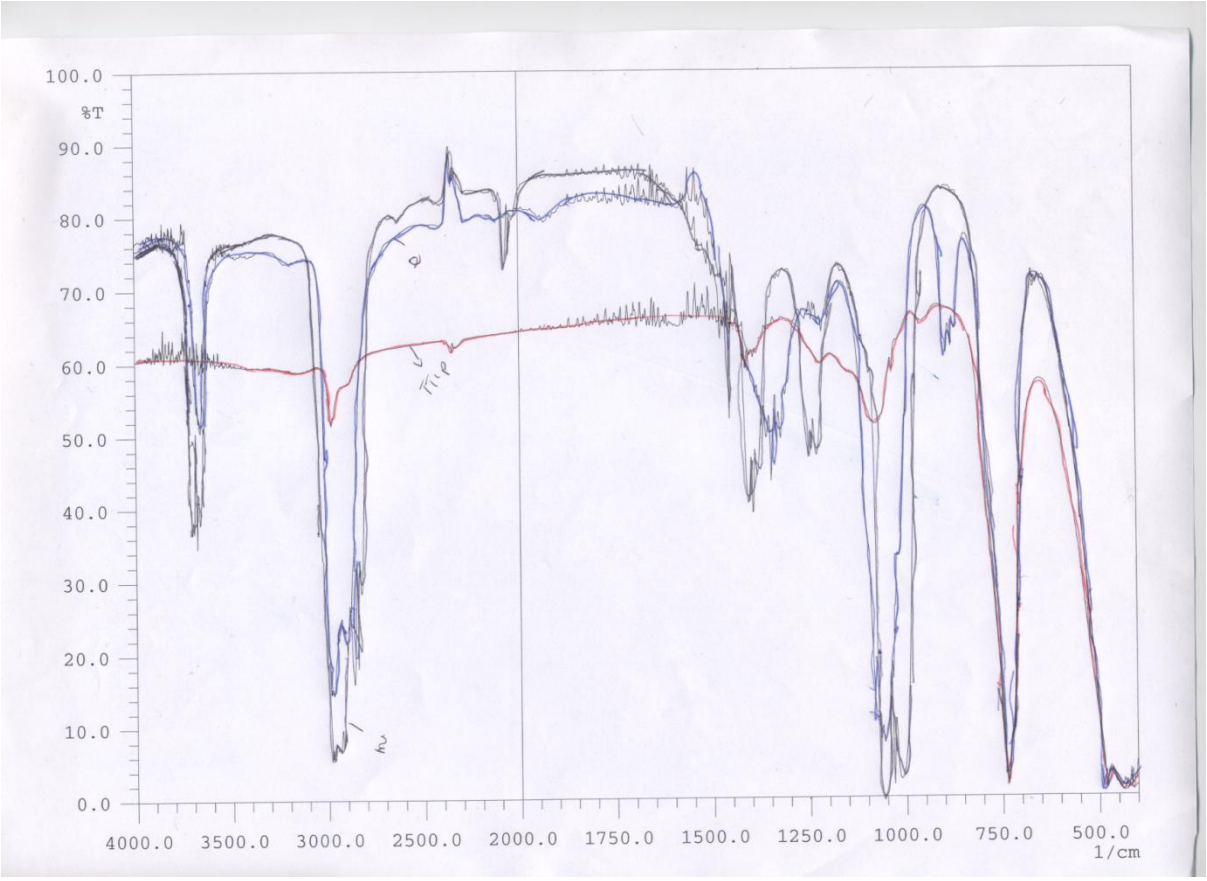

Figure 7.8. Showing the gas phase IR spectra of methanol in Black, ethanol in blue and TTIP in red layered together.

The results shown in the *in-situ* IR were not been able to shed light on the reaction mechanism of TTIP with methanol or ethanol as a carrier solvent but has shown that IR spectroscopy can be used to study AACVD processes and that the aerosol is fully evaporated in the reaction (as no broad O-H bands are seen). To our knowledge this is the first time this type of *in-situ* gas phase IR spectra has been reported for AACVD and the results shows that the involvement of the carrier solvent in the reaction can in principle be followed whether it dissociates or goes through the reaction unaffected using AACVD.

7.5. Insitu studies of titanium dioxide and tungsten oxide using X-ray Absorption Near Edge Structure (XANES)

7.5.1. Introduction

XANES is a type of X-ray absorption spectroscopy (XAS) which also includes Extended X-Ray Absorption Fine Structure (EXAFS). XAS data are collected using synchrotron radiation as described in chapter 2.

XAS has been increasingly useful in the study of active species in catalyst and has been used to determine the chemical state of important species mostly those with low concentration. XAS has been recognised as a powerful analytical technique due to the use of synchrotron radiation. XAS is concerned with excitation of atoms using radiation sources, when an atom is excited using a synchrotron radiation source the electronic state of the atom changes. In XANES the core level of an atom absorbs X-ray radiation; it ejects a photoelectron which can interact with the neighbouring atom causing interference. The XANES region focuses on the modulation of the absorption spectrum close to the absorption edge and is particularly useful in the determination of the oxidation state and coordination environment (octahedral, tetrahedral etc) of an element. The μXANES region is very sensitive to the symmetry that is around the absorbing atom and this can been observed in the pre-edge peak of the atom, indicating 4, 5 or 6 fold coordination. [10]

This *in-situ* study focuses on the deposition of titanium dioxide and tungsten oxide thin films. Several characterization methods have been used to derive structure-function relationships in these thin films, in particular SEM, XRD and Raman spectroscopy. It was found that, depending on the substrate, glass or metal (titanium, copper and stainless steel are used as metal substrates), deposition temperature and time at a specific temperature, different phases of

anatase or rutile and varying degree of their composition were obtained. Although diffraction and Raman spectroscopic studies were able to identify these phases, both these techniques are sensitive only to the crystalline part of the material present in the film. X-ray absorption spectroscopy can be used to determine the local structure of Ti(IV) across the film during deposition. To do so, it is important to use very small beam (preferably micro-beam) to map the film.

The *ex-situ* mapping of as deposited TiO_2 is reported in chapter 5. The *ex-situ* μXANES mapping shows that at 550^{o}C using methanol as the carrier solvent on steel substrate the rutile polymorph of titania was deposited and that on glass substrate there is a random mixture of anatase and rutile. Chapter 3 reported that using ethanol as the carrier solvent the ethanol phase is deposited on steel substrate. The motivation for studying the *in-situ* reaction is to follow the reaction process and to determine if the anatase phase is the initial phase deposited and then transforms to the rutile phase during the course of the deposition or if the rutile phase is initially deposited using methanol as the carrier solvent. This thesis also aims to investigate any changes in the coordination state of TiO_2 during deposition.

The *in-situ* and *ex-situ* μXANES on tungsten oxide film growth was also studied. The type of tungsten oxide produced whether WO_3 the fully oxidised form or WO_{3-x} the partially oxidised form is dependent on a number of factors, in particular temperature, substrate, solvent used during deposition. In a typical synthesis tungsten hexacarbonyl [$W(CO)_6$] was used as a single source precursor; [$W(CO)_6$] is one of the most researched precursor used in chemical vapour deposition of tungsten oxide films.[13] When [$W(CO)_6$] is used in CVD

deposition the structure and properties of the deposited films are highly dependent on the conditions used during the deposition, high deposition temperatures usually produces the yellow stoichiometric orthorhombic WO_3 films whilst low temperatures produces partially reduced blue WO_{3-x} (where x is usually equal to 0.02–0.1) thin films. SEM, XRD and Raman spectroscopy have been used to characterise and derive the structure-function relationships. Chapter 4 of this thesis reports the solvent and substrate effect on the type of tungsten oxide films deposited showing that the carrier solvent used during deposition and the substrate (glass or steel) has an effect on the orientation of the crystal and their surface morphology. This section aims to follow the deposition process of deposition of tungsten oxide thin films using X-ray absorption spectroscopy, at the W L3 edge. The allowed $2p_{3/2}$ to 5d transition will allow us to estimate the density of unoccupied states which can be correlated to oxygen deficiency.[14] The main objective of this work was to understand the process of formation of WO_3 thin films during deposition on glass and steel substrates at 550^oC.

7.5.2. Aerosol Assisted Chemical Vapour deposition (AACVD) insitu cell development

Thin film deposition in AACVD is generally carried out on a cold-wall horizontal-bed CVD reactor that contains a graphite block heated by a Whatman cartridge heater. The glass plate is placed on the carbon heater block and for the steel substrates the steel foil is placed on top of a glass substrate which in turn is placed on top of the carbon heater block. A glass top-plate is positioned parallel and the whole set up is contained within a quartz tube.

To carry out in-situ XANES a new cell was designed with a window that is X-ray transparent. The quartz cell typically used in AACVD deposition is not X-ray transparent. A material that can allow X-ray in and out of the cell needs to be cut in as a window and to reduce parasitic scattering. Beryllium windows have been reported to be most transparent and would have been best suitable but beryllium is toxic and expensive. The commonly used window in EXAFS is Kapton material because of its low cost and convenience.[6] Kapton is a polymer that is stable between -290 to 400^{o}C. Kapton is thermally and mechanically stable and has a high transmittance to X-rays. The maximum deposition temperature in this project was 550^{o}C and kapton is stable at a maximum temperature of 400^{o}C after which it will melt so this needs to be considered when designing the cell. To resolve this challenge a water cooling system was built around the kapton window and air was blown directly on the kapton window to keep the temperature low whilst the experiment was conducted.

A flat surface was also required to scan using synchrotron radiation so the cell needed to be able to rotate from the inside to allow X-ray in and out. In designing the cell heat loss was reduced by adjusting the contact area between the carbon heating block and the quart tube. The thickness of the carbon heating block was reduced and made of a flat base rather than the usual half-cylinder shape. The whole cell body was 80 mm and sample length at 60 mm. Figure 7.9 shows a schematic diagram of the rig setup and figures 7.10-7.13 show the features of the rig. The flat base of the carbon heater also enabled easy movement of the substrate on it to allow X-ray in and out at a perfect

angle. The weight of the new cell was 4.89 kg, the maximum weight the sample holder at diamond I18 beamline can hold is 5 kg.

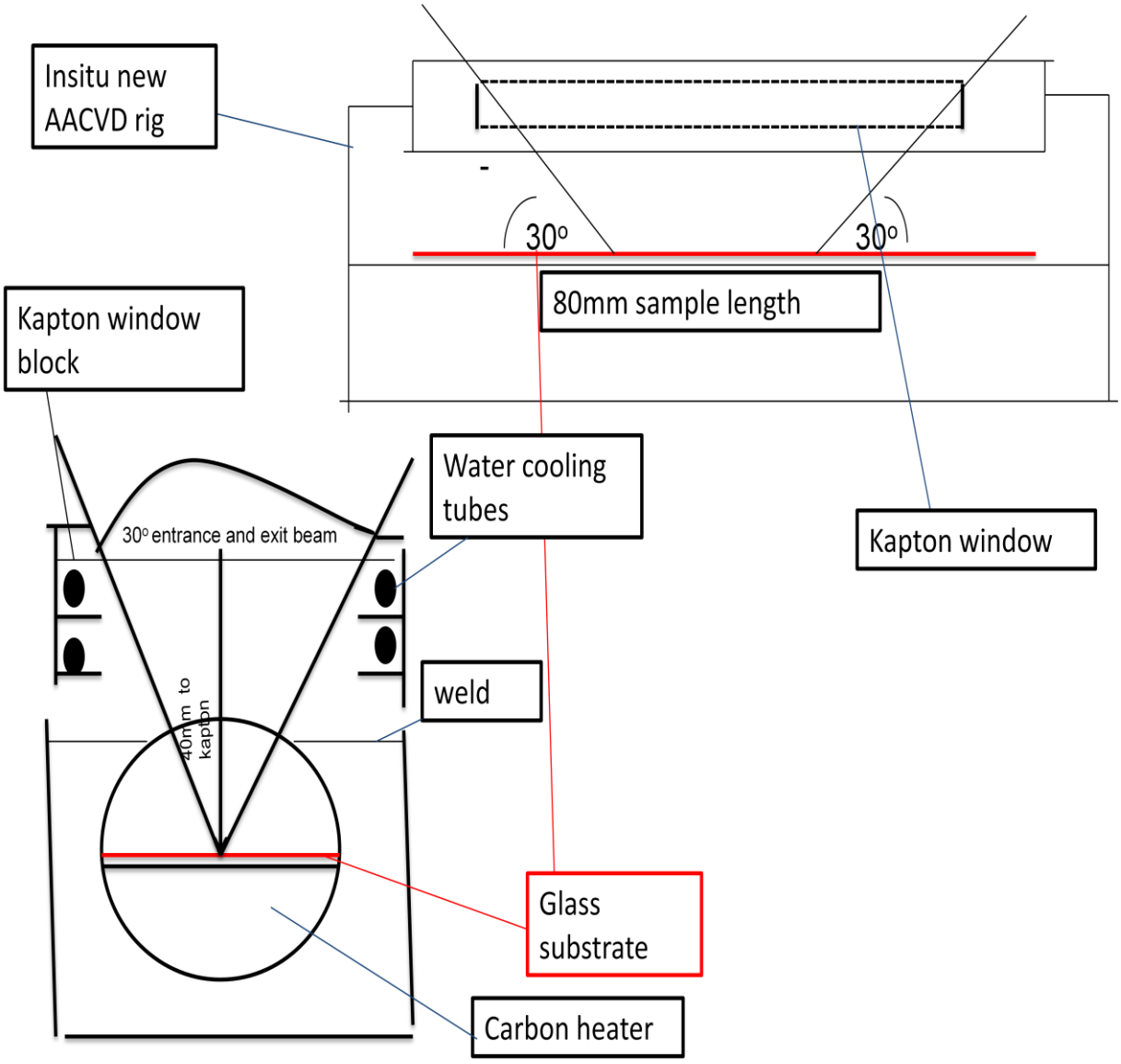

Figure 7.9. Schematic of the X-ray transparent AACVD rig.

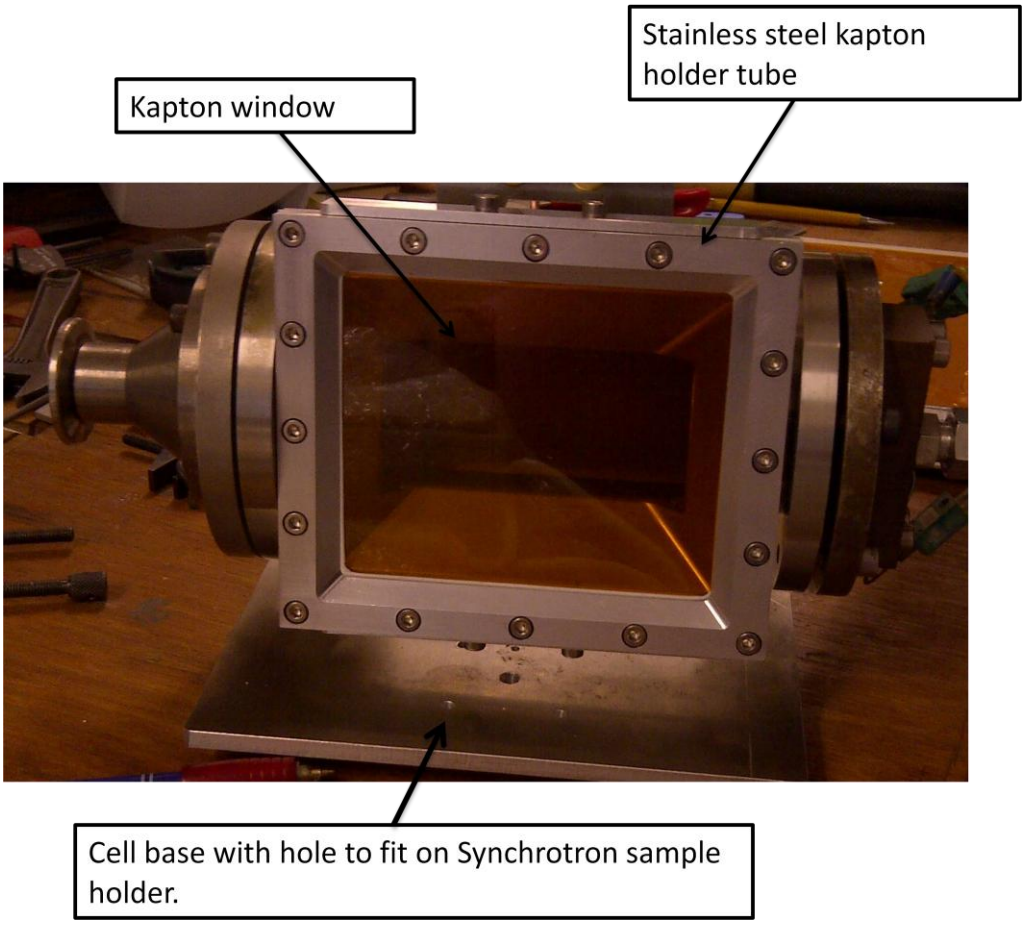

Figure 7.10. X-ray transparent AACVD rig

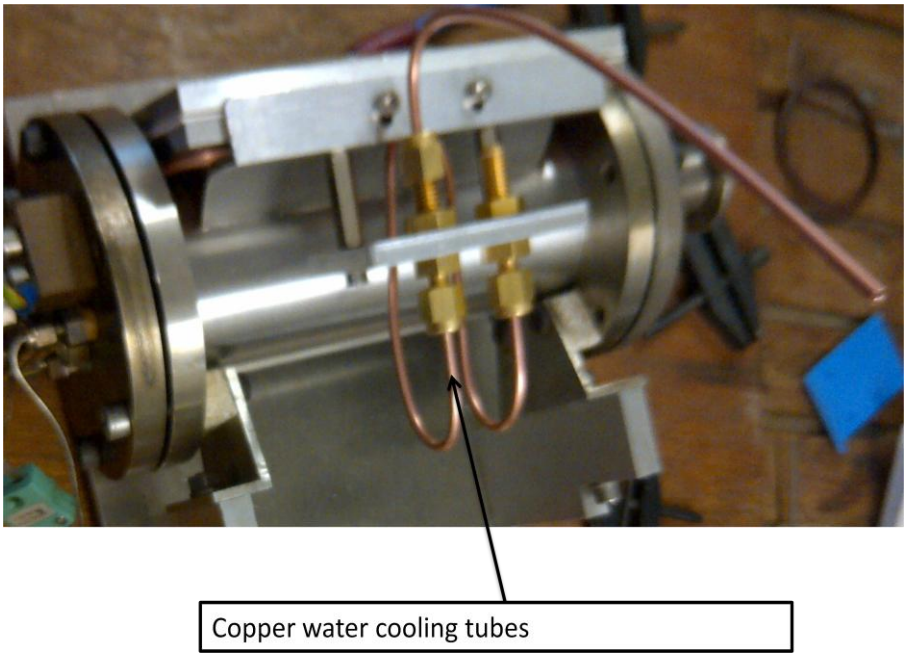

Figure 7.11. X-ray transparent AACVD rig showing copper water cooling tubes

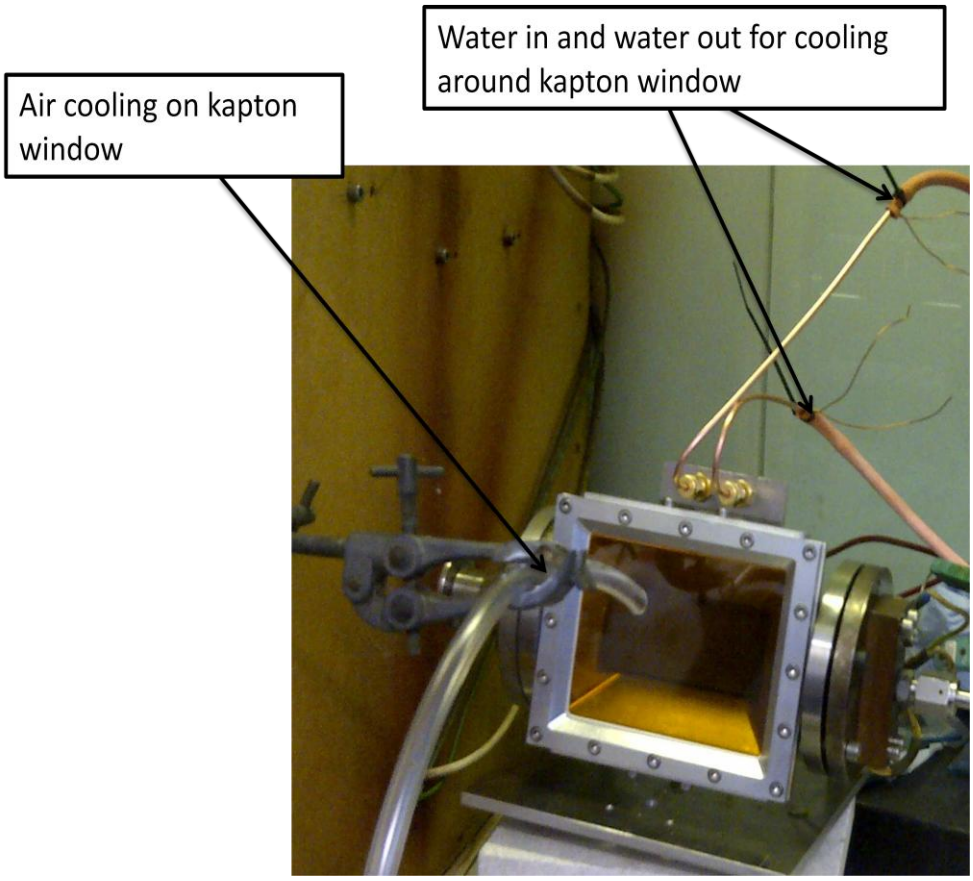

Figure 7.12. X-ray transparent AACVD rig showing how the kapton window was kept cool.

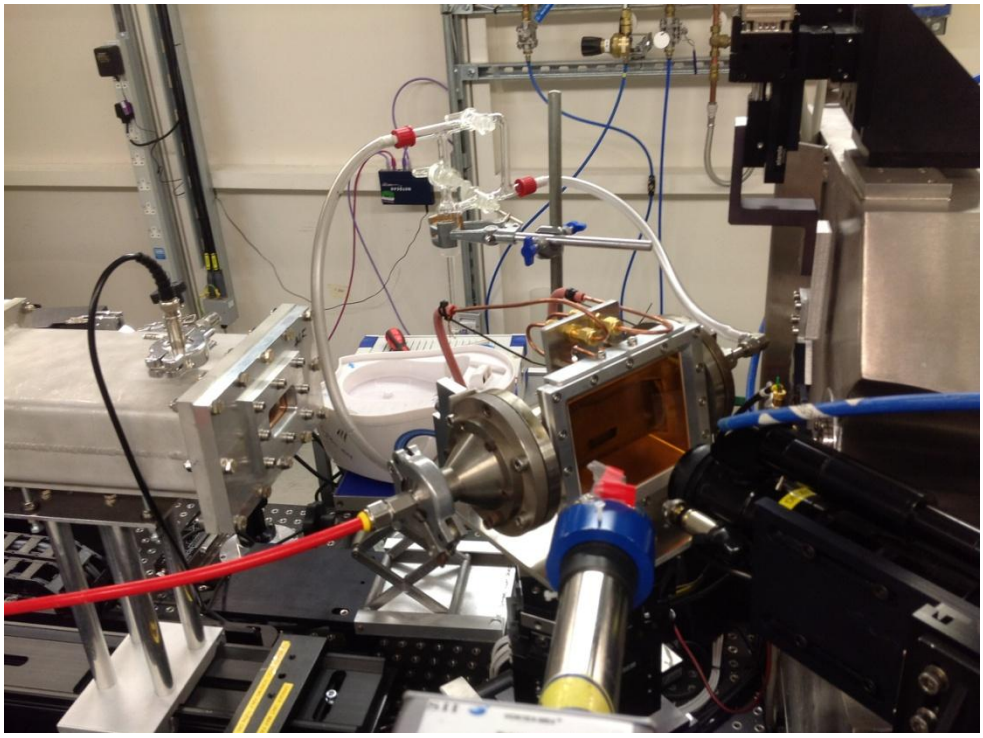

Figure 7.13. X-ray transparent AACVD rig showing how the beam focused on the substrate.

7.5.3. Experimental

All experiments were conducted at the I18 μX-ray absorption spectroscopy (XAS) beam line in the synchrotron radiation source at Diamond Light Source UK.

(1) *In-situ* AACVD of titanum (IV) isopropoxide (TTIP) (97% Aldrich) and methanol (Fisher, reagent grade) were used without any purification. The set up is the same as shown in chapter 3 except the glass top plate was replaced with a stainless steel top-plate with a hole in the middle to allow the beam in and out. The cell was mounted on the sample holder and the beam was focused on the steel substrate. AACVD reaction was carried out at 550^{o}C and μXANES scans were taken every 11 minutes during deposition at the center of the steel substrate. μXANES at the titanium K edge were recorded in fluorescence mode, in the energy range of 4.806 to 5.127 keV and using a beam size of ca 5 microns.

(2) *In-situ* deposition of thin films of tungsten oxide were carried out using aerosol assisted chemical vapour deposition (AACVD) on stainless steel substrates (Goodmans, 250 mm thickness) of dimension 25 x 25 mm. Tungsten hexacarbonyl [$W(CO)_6$] (97% Aldrich) and methanol (Fisher, reagent grade) were be used without any purification. The deposition procedure was the same as described above for TiO_2. [$W(CO)_6$] was used as a single source precursor (0.37 g, 0.5 mmol) and was added to methanol (50 ml) and an aerosol was generated at room temperature using a Pifco ultrasonic humidifier. AACVD reaction was carried out at 550^{o}C and μXANES scans were taken every 11 minutes during deposition at the center of the steel substrate. μXANES at the W L3 edge were recorded in

fluorescence mode, in the energy range of 10.050 to 10.400 keV and beam size of ca 10 microns was used.

(3) µXANES measurements were also carried out on as deposited *ex-situ* tungsten oxide thin films using either methanol or ethanol as carrier solvents using the same procedure as shown above.

7.5.4. Film characterisation and analysis using µXANES of tungsten oxide thin films deposited on steel substrates

7.5.4.1. µXANES *insitu* deposition of WO_3 thin films

WO_3 L-edge X-ray Absorption Near Edge Structure (µ*XANES*) was carried out on thin films deposited on steel plates *in-situ*. The *in-situ* deposition via AACVD was unsuccessful partly due to the limitations of AACVD reaction in producing a good flow of aerosol. There was little room to manoeuvre the humidifier to achieve a better mist of aerosol. The µ*XANES* data recorded during the deposition was very noisy and was not clear enough to solve the structure.

7.5.4.2. µXANES exsitu deposition of WO_3 thin films

WO_3 L edge X-ray Absorption Near Edge Structure (µ*XANES*) map was carried out on thin films deposited on steel plates. The mapping was done in an H shape fashion as described in chapter 5. The data was normalised following the procedure already described in chapter 5. Pure calcium tungstate $CaWO_4$ and tungsten hexaphenoxide [$W(OPh_6)$] were both used as standards and their µXANES spectra is shown in figure 7.14. The µXANES spectra shows a decrease in the white line intensity from [$W(OPh_6)$] to $CaWO_4$ because tungsten goes from been in the octahedral surrounding to tetrahedral

surrounding respectively. The W L_3-edge white line corresponds to electron transitions from the 2p3/2 state to a vacant 5d state.

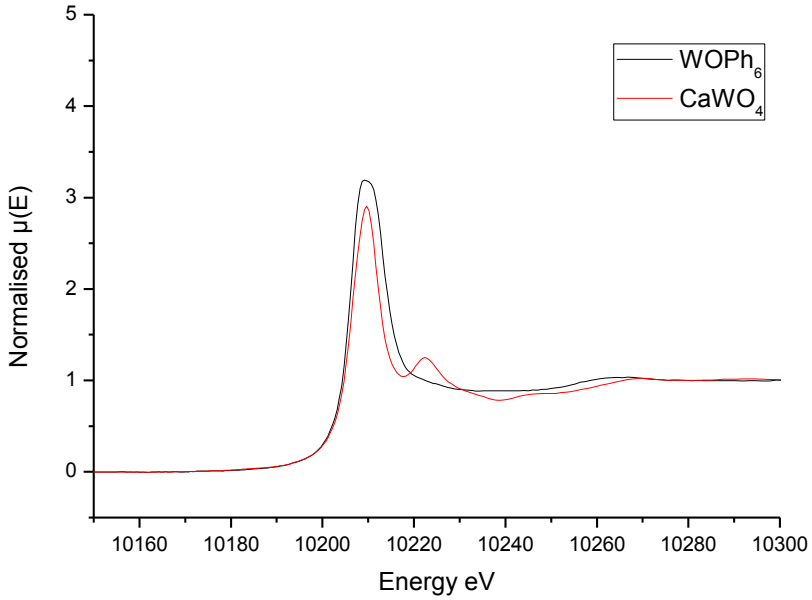

Figure 7.14. μXANES Pure calcium tungstate ($CaWO_4$) and tungsten hexaphenoxide [$W(OPh_6)$] recorder at the W L_3 edge.

The μXANES spectra map of as deposited tungsten oxide film on steel substrate using ethanol as the carrier solvent shown in figure 7.15. It shows that the tungsten in the as-deposited tungsten-oxide film is in the distorted octahedral coordination because only one peak is observed in the white line and the peak is broad. Whereas if the W was in the tetrahedral coordination a single sharp asymmetrical peak will be observed.

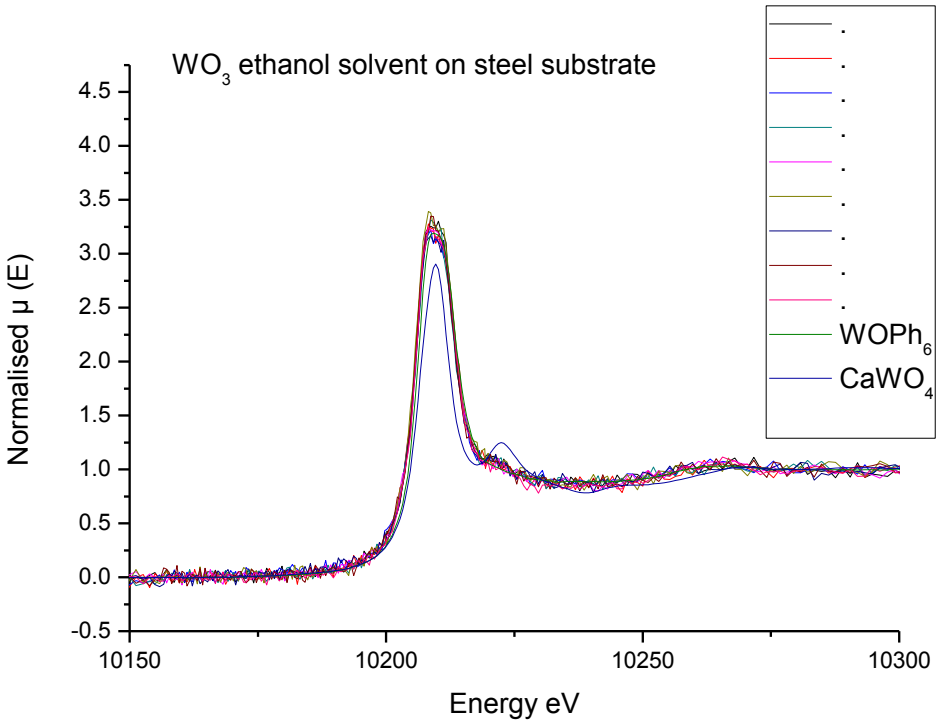

Figure 7.15. Ex-situ μXANES mapping of tungsten oxide thin film deposited from the AACVD reaction of [$W(CO)_6$*] in ethanol on glass at 550*^oC*.*

The μXANES spectra map of as deposited tungsten oxide film on steel substrate using methanol as the carrier solvent is shown in figure 7.16 and it also shows tungsten in the as deposited tungsten oxide film to be in distorted octahedral coordination.

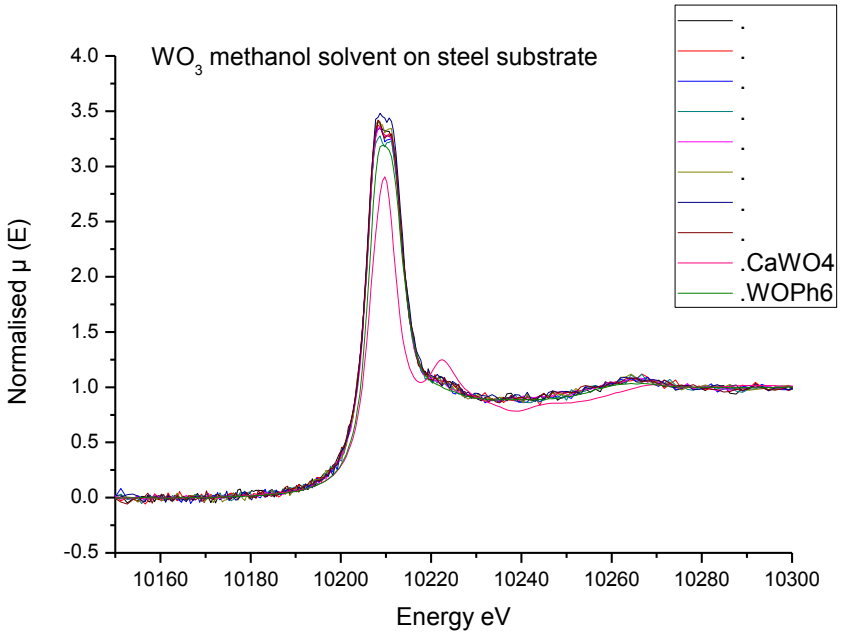

Figure 7.16. Ex-situ μXANES mapping of tungsten oxide thin film deposited from the AACVD reaction of [$W(CO)_6$] in methanol on glass at 550^oC.

An interesting observation is that the white line intensity of the as deposited tungsten oxide films are closer to the [$W(OPh_6)$] than to [$CaWO_4$] again this confirms tungsten in the octahedral coordination.

7.5.5. Film characterisation and analysis using μXANES of titanium dioxide film deposited *in-situ* on steel substrates

TiO_2 K edge X-ray Absorption Near Edge Structure (μXANES) was carried out on thin films deposited steel plates as already described in the experimental section. The normalised standard spectrum of pure anatase and rutile phase is shown in chapter 5 (Figure 5.3). One of the observations made during the *in-situ* deposition was that the kapton window was cloudy indicating deposition on the window. The *in-situ* deposition was repeated

twice to improve the data quality recorded using methanol as a carrier solvent. An attempt was also made using ethanol as the carrier solvent but the *in-situ* reaction was unsuccessful. Figure 7.17 shows the µXANES spectra during deposition. It can be observed that the initial data collected was very noisy due to the very thin nature of the film and also due to the cloud of mist present in the reactor during deposition. The observed pre-edge is very different to the expected pre-edge in T K-edge. We see a sharp pre-edge rather than a split pre-edge. We were unable to identify the pre-edge observed.

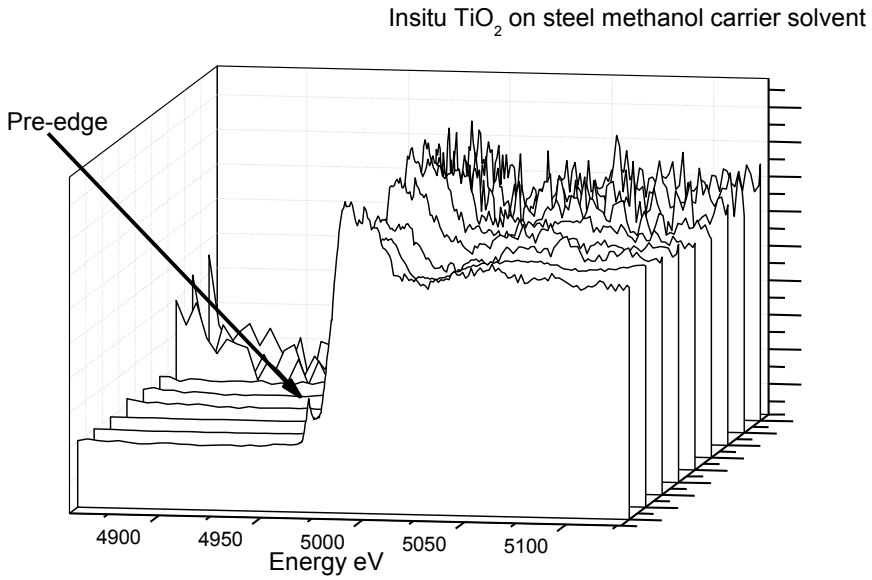

Figure 7.17. In-situ µXANES of TiO_2 thin film deposited from the AACVD reaction of TTIP in methanol on substrate at 550^oC.

The µXANES spectra of the deposition on the kapton window was also recorded and the spectra matches exactly with the spectra recorded *in-situ* (figure 7.18). These results show that the µXANES data recorded was the deposition on the kapton window.

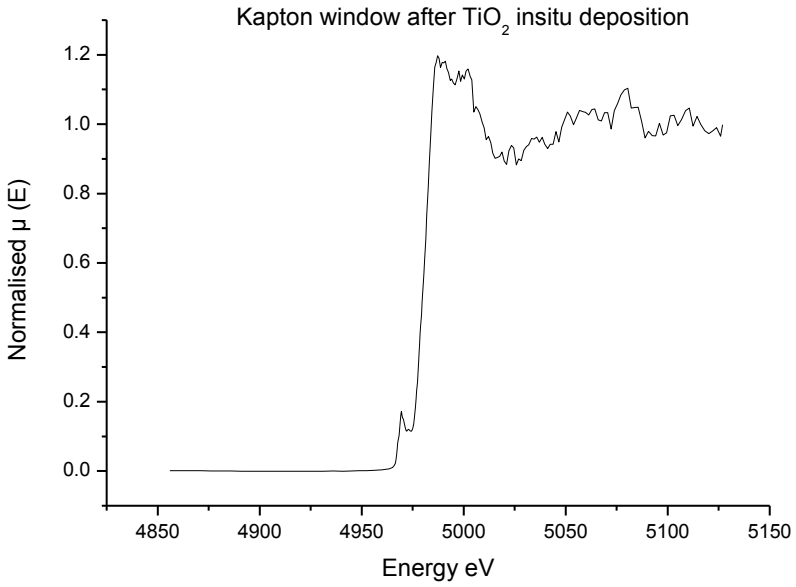

Figure 7.18. μXANES spectra of the kapton window from AACVD deposition of TiO_2 from the reaction of TTIP in methanol on steel at 550^oC.

This method of following reaction process of thin films via AACVD by recording the μXANES data *in-situ* not successful however this experiment has opened a new area of research to develop a cell that can allow the effective recording of data insitu.

7.6. Conclusion

In this chapter an attempt was made using IR, NMR and μXANES characterisation techniques to understand the deposition process of titanium dioxide and tungsten oxide films formed by aerosol assisted chemical vapour deposition. The IR spectra recorded did not show the production of CO_2 or CO using either ethanol or methanol as the carrier solvent and the ^{1}H NMR NMR spectra showed no exchange reaction between the isopropyl group on the TTIP

and the methanol solvent at room temperature. *In-situ* µXANES data collected for titanium oxide was the same as the µXANES spectra recorded from the kapton window and the Ti K-edge was very different from what has been previously observed (see chapter 5). This section reports the first application of *in-situ* µXANES technique for the study of AACVD depositions of both WO_3 and TiO_2 *in-situ*. Although the results obtained was not able to resolve the phases of TiO_2 present during deposition, this new chemical vapour deposition reactor vessel can be further modified to overcome the challenges faced during this attempt. For future work the cell could be modified by creating a layer of nitrogen flow under the kapton window which will help to overcome the challenge of depositing on the kapton window. To our knowledge this is the first attempt of *in-situ* µXANES data collection in CVD reactions.

7.7. References

1. H.M. Yates, P. Evans, D.W. Sheel, Z. Remes, M. Vanecek, *Thin Solid Films*, **2010**, 519, 1334.
2. V. Hopfe, W. Graehlert, O.throl, *J. Phys. IV*, **1999**, 9, 995.
3. V. Hopfe, D. W. Sheel, W. Graehlert, O.throl, *Surf. Coat. Tech.*, **2001**, 142, 328.
4. D. C. Koeningsberger, R. Prins, John Wiley & Sons, New York, **1988**.
5. R. I. Walton, R. I. Smith and D. O'Hare, *Microporous Mesoporous Mater*., **2001**, 48, 79.
6. C. Kongmark, V. Martis, A. Rubbens, C. Pirovano, A. Lofberg, G. Sankar, E. Bordes-Richard, R.-N. Vannier and W. Vaneek, *Chem. Commun.***, 2009**, 4850.

7. G. Sankar, J. M. Thomas, F. Rey and G. N. Greaves, *J. Chem. Soc, Chem. Commun.*, **1995**, 2549.
8. K. Simmance, G. Sankar, R. G. Bell, C. Prestipino, W. Beek, *Phys. Chem. Chem. Phys.*, **2010**, 12, 559.
9. S. D. Jackson, D.S. Anderson, G. J. Kelly, T. Lear, D. Lennon, S. R. Segal, *Top. Catal.*, **2003**, 22, 173.
10. P. Schnurrenberger, M.F. Zuger, D. Seebach, *Helvetica Chemical Acta*., **1982**, 65, 1197.
11. P.C. Angelomé., *J. Phys. Chem. B*, JP069020Z, in press.
12. D. Davazoglou, K. Geougouleas, *J. Electrochem. Soc.*, **1998**, 145, 1346.
13. S.Yamazoe, Y. Hitomi, T. Shishido, T. Tanaka**,** *J. Phys. Chem. C.*, **2008,** *112*, 6869.
14. S. J. Henderson, *Appl. Cryst.*,**1995**, 28, 820.

8.Conclusion and Future work

This thesis focused on the deposition of titanium dioxide and tungsten oxide using aerosol assisted chemical vapour deposition (AACVD). Titanium dioxide is one of the most researched metal oxides in the past few years and this is because of its distinct ability to act as a photocatalyst.[1] TiO_2 based self-cleaning glasses are already commercialised, the thin films are deposited by atmospheric pressure chemical vapour deposition (APCVD).[2,3] Aerosol assisted chemical deposition is a unique technique in depositing thin films as it allows for non-volatile precursors to be used and this allows for films with a range of morphology and properties to be produced. At the start of this work there had not been any commercial use for AACVD but this has since changed. Beneq has commercialised the use of AACVD for the deposition of films on different substrates (glass, ceramic, plastics). [4]

AACVD has been used in this thesis to produce TiO_2 films with very interesting surface morphology. As described in chapter 2, needle like particles were observed when methanol is used as a carrier solvent on steel substrates and this surface were also found to exhibit a Wenzel-type surface that are hydrobic in nature. This is somewhat surprising as TiO_2 films are usually observed to be hydrophillic. The use of AACVD resulted in rutile films rather than the anatase phase deposited using APCVD (Chapter 2). Further using AACVD was able to change the surface morphology and this changes the hydrophillicity of the surface.

The as-deposited TiO_2 films were also photoactive, tested with methylene blue. The films produced using ethanol as a carrier solvent were more photo-active (anatase), whilst the film deposited using methanol were less photo-

active (rutile). The films also were also reported to be able to photo-split water using a sacrificial solution and the values recorded are amongst some on the highest values reported.

Research into hydrogen fuel cells has increased in the last few years as the need for alternative fuel has increased.[5-7] Using AACVD for the deposition of TiO_2 produced films that were able to photo-split water producing hydrogen. This work can be further researched to optimise the properties of the films deposited on steel substrates to improve their ability to photo-split water.

This thesis also reports the solvent and substrate effect on TiO_2 films deposited by AACVD. It was reported that the rutile phase is favoured on steel substrates at high temperatures and a mixture of anatase and rutile is observed at the same temperature. This observation suggests that the steel substrate affects the deposited phase. Methanol as a carrier solvent was also reported to direct the formation of the rutile phase on steel compared to ethanol and other solvents used as a carrier solvent where the anatase phase is observed.

AACVD deposition of tungsten oxide was studied to further investigate the solvent effect on films deposited using methanol or ethanol as carrier solvent. The films deposited had different preferred orientation and therefore different morphology when either ethanol or methanol is used. The phase directing effect of films deposited particularly when methanol is used as a carrier solvent lead to the investigation of the reaction path of the solvents during AACVD deposition.

A number of experiments were conducted to explain the solvent directing effect displayed when methanol is used as the carrier solvent. NMR was used

to try and observe any exchange reaction between the isopropyl group and the methoxyl group but no exchange was recorded at room temperature. IR was also used to record the gases coming out of the exhaust; this was done to monitor the ligand break down process. The IR was unable to detect the production of CO_2 or CO form the exhaust gas. IR spectra was not able to report any reaction between the TTIP and the solvent.

XAS was successfully used to map the as-deposited TiO_2 thin films. µXANES data was recorded for TiO_2 deposited on glass and steel at using different solvents. Linear combination fitting (LCF) analysis of the µXANES data showed the exact percentage of anatase and rutile present at each point on the substrate. LCF of the data showed almost 100% of rutile was deposited on steel substrate using methanol as the carrier solvent and shows a mixture of anatase and rutile deposited on glass substrates. The µXANES map also showed that the phase of TiO_2 deposited is not in the flow direction but it is random as shown from the data recorded using glass substrates. The anatase and rutile phase observed are randomly distributed across the film. Mapping across a µXANES has proven to be a very useful technique for determining the composition across a film.

In the final chapter of this thesis an X-ray transparent AACVD rig was built. This rig to our knowledge is the first of its kind. A few challenges were faced including deposition on the kapton window and space limitation on the beam line. This was however a successful attempt in following film deposition *in-situ* and gaining an insight into the phase deposited with time. The rig can be improved by designing a smaller cell to allow for better movement to improve the flow of aerosol during deposition and as already suggested in chapter 7 the

deposition on the kapton window could also be reduced by allowing a flow of nitrogen gas just under the kapton window.

The work carried out in this thesis has opened a new door into the understanding of the process of thin film deposition and can be used to modify the properties and uses of films deposited by AACVD.

8.1. References

1. A. Mills, N. Elliot, S. Bhopal, I. P. Parkin, S. A. O'Neill, R.J Clark, *J. Photochem. Photobiol, A. Chem.*, **2002**, *151*, 171.
2. Mills, A. Lepre, N. Elliott, S. Bhopal, I. P. Parkin and S. A. O'Neill, *J. Photochem, Photobiol A Chem.*, **2003**, *160*, 213.
3. P. Parkin, R. G. Palgrave, *J. Mater. Chem.*, **2005**, *15*, 1689.
4. Joonas, R. Markku, V. Tomi, A. Kai. Device for forming aerosol, and method and apparatus for coating glass. Beneq OY, **2011**. CN20101051610.
5. Fujishima, K. Honda, *Nat.*, **1972**, 238, 37.
6. Kudo, Y. Miseki, *Chem. Soc. Rev*., **2009**, 38, 253.
7. F. E. Osterloh, *Chem. Mater*., **2008**, 20, 35.

8.2. List of Papers Published/Submitted

1. C. Edusi, G. Hyett, G. Sankar, I. P. Parkin, Aerosol-Assisted CVD of Titanium Dioxide Thin Films from Methanolic Solutions of Titanium Tetraisopropoxide; Substrate and Aerosol-Selective Deposition of Rutile or Anatase, *Chem. Vap. Deposition*, **2011**, 17, 30-36.

2. C. Edusi, G. Sankar and I. P. Parkin, The Effect of Solvent on the Phase of Titanium Dioxide Deposited by Aerosol-assisted CVD, Chem. Vap. Deposition, **2012**, 18, 126–132.

3. C. Edusi, F. Mosselmans G. Sankar and I. P. Parkin, X-ray absorption spectroscopy mapping of titanium dioxide thin films deposited on glass and steel using aerosol assisted chemical vapour deposition, *PCCP*, **2014** (submitted).

4. C. Edusi, T. Daley, S. Sathasivam, D. Bhachu, G. Sankar and I. P. Parkin, Design of an X-ray transparent AACVD reactor vessel and *in-situ* studies of titanium dioxide using X-ray Absorption Near Edge Structure (XANES). (Manuscript in preparation).